The Dissertation Committee for Steven Adam Scheer Certifies that this is the approved version of the following dissertation:

Segregation and Stability in Ultra-Thin Film Polymer-Polymer Blends

Committee:

Peter F. Green, Supervisor

Donald Paul

Roger Bonnecaze

Brian Korgel

David Vanden Bout

Segregation and Stability in Ultra-Thin Film Polymer-Polymer Blends

by

Steven Adam Scheer, BS, MS

Dissertation

Presented to the Faculty of the Graduate School of

The University of Texas at Austin

in Partial Fulfillment

of the Requirements

for the Degree of

Doctor of Philosophy

The University of Texas at Austin

December 2002

Dedication

To Mr. Albin and Mr. Miller for recognizing that a student is not a vessel to be filled, but a fire to be lit.

Acknowledgements

I would like to express my gratitude to the numerous people who have made my experiences in graduate school a rewarding one. First I would like to thank all of the members of the Green group. In particular I would like to thank Karl Putz for numerous hours of input on many topics. Our conversations always helped me to stay focused, and push the bounds of my research. I would like to thank Joseph Pham, for his assistance and advice. I would also like to thank Luciana and Abraham, your support and encouragement will always be appreciated.

I would like to express my gratitude to my advisor Peter Green. He has always strived to push me further than I thought I was capable. Without his assistance I am sure that I would not have grown as much during my graduate school experience.

I would also like to thank the many friends that I have made in graduate school: Colin, Paul, Brian, Joel, Tina, and many others have acted as my support when I needed most, and for that I am truly grateful.

Finally, I would like to thank my wife Kristen. She has always been there to help, encourage, and assist me when I really needed it.

Segregation and Stability in Ultra-Thin Film Polymer-Polymer Blends

Publication No._____

Steven Adam Scheer, PhD

The University of Texas at Austin, 2002

Supervisor: Peter F. Green

It is well known that the phase behavior of thin film polymer-polymer blends differs appreciably from bulk analogs. This difference is due largely to the influence of interfacial interactions (polymer-substrate and polymer free surface) and to entropic effects associated with confinement. Interfacial interactions, for example, "drive" preferential segregation of the constituents of the mixture to the interfaces. This influences the symmetry of the phase diagram.

Beginning with the work of Schmidt and Binder in the late 1980s, a number of authors examined the influence of a single interface (the so-called semi-infinite case) on the "local" concentration profiles of polymer-polymer mixtures. The most complete work to date involve simulations of Flebbe and Binder, who examined a situation in which one component of the mixture preferentially segregated to both interfaces, the so-called symmetrically adsorbing

case. They showed how the phase diagram would be altered under varying degrees of confinement.

Polymer-polymer thin film blends of poly(styrene-co-acrylonitrile) (SAN) and Poly(methylmethacrylate) (PMMA) in the thickness range $h<5R_g$, where R_g is the radius of gyration of one component, were examined. The phase behavior of this system was observed to phase separate over temperature ranges where the bulk mixtures were miscible. In fact, the PMMA component segregated to both interfaces (symmetric adsorption). Structural instabilities were observed to accompany phase segregation. Specifically, surface patterns (topographies), nucleation and growth and spinodal patterns, were observed over a range of film thicknesses. Such patterns are usually due to the antagonistic action of long and short-range intermolecular forces that influence stability of films in the thickness range of $h<10$ nm. We observed similar patterns over a wider range of film thickness, depending on the composition of the SAN copolymer. These observations can not be rationalized in terms of the current theory.

A series of numerical calculations were performed to explain these observations. It was shown that in this thickness range, segmental asymmetry effects (entropic), not accounted for by Binder and coworkers, have a strong influence on the phase behavior of these systems. These numerical calculations further enable a calculation of the interfacial free energy of the system as a function of film thickness. This is significant since the topographical instabilities that we observe in these films can now be rationalized.

Table of Contents

List of Tables

List of Figures

Chapter 1: Overview of the Thermodynamics of Bulk Polymer-Polymer Mixtures

1.1 INTRODUCTION

It was recognized approximately 5000 years ago (3000 BC) that processing (mixing) dissimilar metals could create new materials, alloys, with properties that were different, and often superior, to those of the constituents. This practice proved to be very effective with other materials, such as polymers. Today polymer-polymer mixtures are an important class of engineering materials. Blending can be a cost effective way of "tailoring" certain properties compared to synthesizing entirely new polymers for the same application.

The thermodynamics of bulk polymer-polymer mixtures is reasonably well understood, experimentally and theoretically [1.1-1.7]. One drawback associated with the mixing of polymers is that the entropy of mixing is very small, hence miscibility typically occurs when favorable, specific, enthalpic interactions exist between the components. Currently, the important challenges in this area are associated with the continued development of effective strategies for controlling the microstructural features of polymer-polymer mixtures for different applications.

More recently there has been considerable interest in understanding the physical and thermodynamic properties of thin films because of their potential applications as photoresists, membranes, adhesive coatings, lubricants, and

biopatterned surfaces [1.8-1.24]. It is currently understood that the phase behavior of thin film polymer-polymer blends differ appreciably from their bulk analogs [1.21, 1.24-1.29]. This deviation from bulk behavior is largely due to the increasing importance of the interfacial interactions and confinement as the surface to volume ratio increases.

The influence of an interface on the homogeneity of a polymer-polymer mixture is manifested in several ways. It has been shown that even when small surface energy differences (less than 0.2 dyne/cm) exist between the polymers in a mixture, the lower surface energy component could preferentially segregate to the free surface [1.21]. Specific interactions (e.g.: hydrogen bonding) between one blend constituent and a substrate will also determine the "local" concentration profile in the vicinity of the substrate. Moreover, the presence of a solid substrate also introduces entropic effects. The polymer chains near the wall experience a loss of conformational entropy. This loss of conformational freedom can produce an "entropic repulsion" [1.27]. The combination of interfacial interactions, segment-segment (A/B) interactions, and entropic effects (combinatorial and conformational) lead to complicated phase behavior in thin film mixtures. These effects are not well understood.

Sufficiently thin films experience additional complications. Long range Van der Waals intermolecular forces can influence the structural homogeneity and stability of films in the nanometer thickness range. If the long range Van der Waals forces between the free interface and the substrate are attractive, the excess free energy of the system can be reduced by locally reducing the film thickness,

resulting in instability and subsequent dewetting of the thin polymer film from the underlying substrate [1.30-1.38].

Two important questions are addressed in this thesis. I first consider the effects of confinement on the thermodynamics of mixing in thin film polymer-polymer blends. Secondly, an attempt is made to reconcile effects associated with the thermodynamics of mixing and those associated with potentially destabilizing long-range van der Waals interactions and with interfacial capillarity on the structure of blends during various stages of miscibility. I begin with an overview of the thermodynamics of mixing in bulk polymer-polymer mixtures. Chapter 2 of this dissertation summarizes the current understanding of the effects of confinement on the thermodynamics of mixtures. In Chapter 3, I discuss the influence of long-range van der Waals interactions on the structure, long range stability and lateral homogeneity of thin films. Together, these first three chapters provide a context for the remainder of the dissertation, which reconciles the connection between thermodynamics of mixing in thin films and affects associated with capillarity and destabilizing long-range van der Waals interactions.

1.2 BULK PHASE SEPERATION

The Flory-Huggins analysis provides a mean field description of free energy of mixing in bulk polymer$^{(A)}$-polymer$^{(B)}$ mixtures:

$$\Delta G_{mix} = \frac{cRT}{\tilde{\nu}_c} f_A f_B + RT\left[\frac{r_A f_A \ln f_A}{M_A} + \frac{r_B f_B \ln f_B}{M_B}\right]. \qquad (1.1)$$

In Equation 1.1, ΔG_{mix} is the Gibbs free energy change for mixing per unit volume of polymers A and B, M_i is the molecular weight of species i, ρ_i is the density of species i, ϕ_i is the volume fraction of species i, χ is the energetic Flory-Huggins interaction parameter, and $\tilde{\nu}_c$ is the molar volume of a reference unit common to both polymers. The first term on the right hand side of Equation 1.1 accounts for enthalpic interactions between the species and is assumed to arise from random, pair-wise contact between monomers. The enthalpic term can be either positive or negative depending on the sign of χ. The second term is the entropy of mixing. The entropic contributions are always negative and the magnitude of its contribution to the free energy decreases with increasing M_i. This means that, in general, favorable interactions must exist between the A and B monomers for a polymer blend to be miscible.

Equation 1.1 is simplified if one considers a symmetric case, whereby

$$\frac{\rho_A}{M_A} = \frac{\rho_A}{M_A} = \frac{1}{\tilde{V}}. \tag{1.2}$$

leading to

$$\frac{\Delta G_{mix}}{RT} = \chi f_A f_B + \frac{f_A}{N} \ln f_A + \frac{f_B}{N} \ln f_B. \tag{1.3}$$

Equation 1.3 is plotted in Figure 1.1 illustrating the effect of the term χN on the stability of the mixture. It is obvious from Figure 1.1 that there is a critical value at:

$$(\chi N)_{Crit} = 2. \tag{1.4}$$

For values of χN less than the critical value the Gibbs free energy of mixing exhibits a minimum at $\phi_A = 0.5$, with the free energy increasing as the

composition of the mixture approaches either pure polymer components. These mixtures will be miscible at all compositions for $\chi N<2$.

As the value of χN is increased above the critical point at $\chi N = 2$ a maximum in the free energy occurs at $\phi_A = 0.5$, the critical composition. A mixture with the critical composition can decrease its overall free energy by separating into two separate phases. The new phases possess compositions indicated by the crosses in Figure 1.1 for various values of $\chi N>2$.

All mixtures located between the minimum free energies on a given curve in Figure 1.1 are not at thermodynamic equilibrium. The nature of a mixture's instability and the mechanism by which it reaches the thermodynamic equilibrium can clearly be separated into two different regions. The locus of the points located at the inflection point between the maximum and the minimum define the spinodal curve. Mixtures that exist within the spinodal are inherently unstable and will spontaneously phase separate via the spinodal decomposition mechanism. The second curve, the binodal, is defined by the minima in the free energy function. Mixtures located between the binodal and the spinodal curves are metastable and will phase separate via nucleation and subsequent growth.

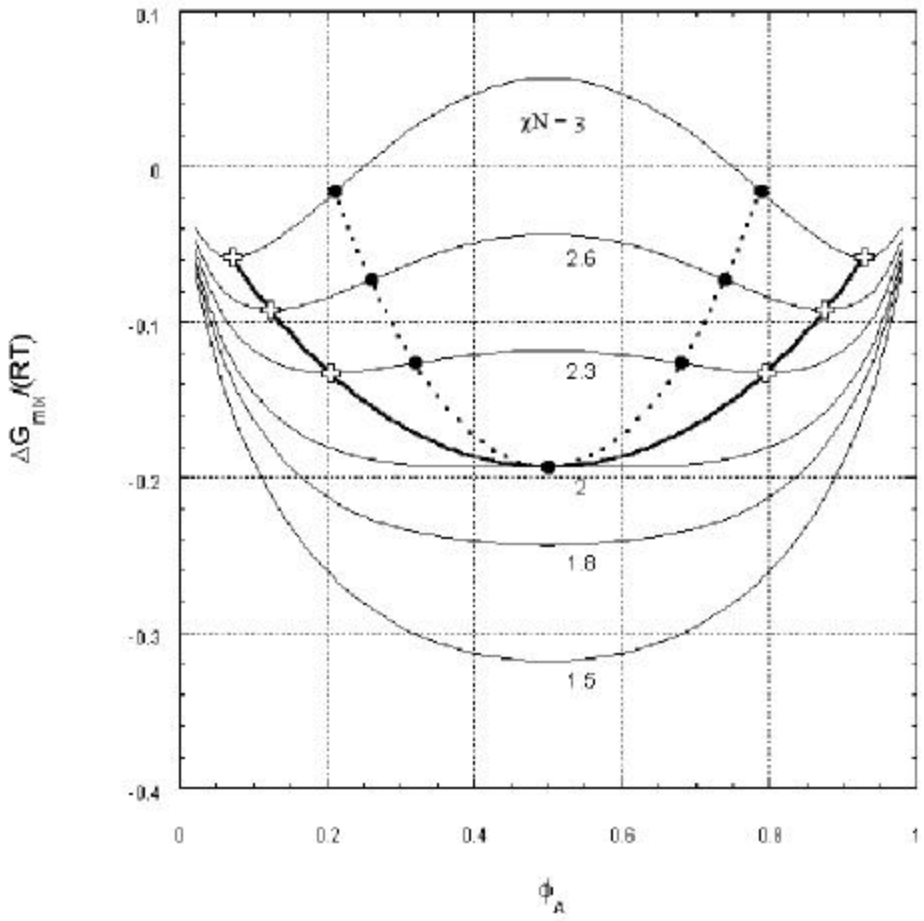

Figure 1.1: Gibbs free energy change of a symmetric binary polymer mixture as described by Equation 1.3. The solid circles indicate the inflection points in the free energy curves and mark the transition from the unstable to the metastable region. The crosses indicate the minimum free energies and the composition of the equilibrium phases. The dashed line indicates the spinodal and the solid line connecting the minimum free energies is the binodal.

Flory-Huggins theory, as described in Equation 1.1 and Figure 1.1, predicts that mixtures should exhibit an upper critical solution temperature (UCST) as shown in Figure 1.2. The UCST results when a polymer mixture is immicible at some composition below a critical temperature, but forms a homogeneous mixture at all compositions above the critical point.

A second type of behavior is also possible in polymer blends, as shown in Figure 1.3. In these polymer systems, the blend is miscible below the critical temperature, but phase separates at temperatures above the critical temperature. This behavior is known as a lower critical solution temperature (LCST). It can easily be seen in Equation 1.1 that a LCST cannot be predicted by classical Flory-Huggins theory without the inclusion of an empirical temperature dependent function for the binary interaction parameter χ. While this approach may be used to fit the data from polymer mixtures that exhibit LCST behavior, the empirical nature of the approach does not provide fundamental insight into the nature of the phase separation process. A more rigorous analysis was proposed by Sanchez and Lacombe [1.6, 1.7]. This theory includes compressibility effects in the equation of state. Briefly, the Sanchez-Lacombe (SL) equation of state [1.6, 1.7] is shown to be:

$$\tilde{\rho}+\tilde{P}+\tilde{T}\left[\ln\left(1-\tilde{\rho}\right)+\left(1-\frac{1}{r}\right)\tilde{\rho}\right]=0 \tag{1.5}$$

where:

$$\tilde{P}=\frac{P}{P^{*}}, \tag{1.6}$$

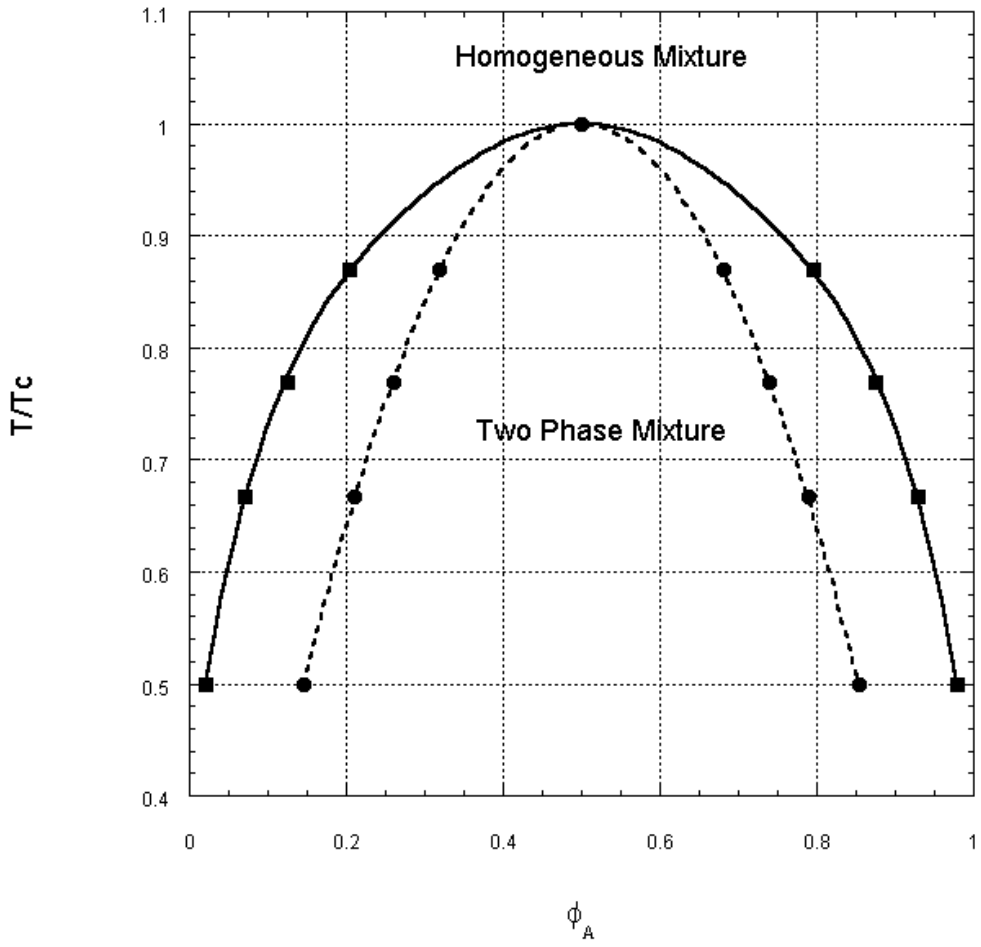

Figure 1.2: A typical a phase diagram of a binary polymer mixture that exhibits an upper critical solution temperature, UCST. The dashed line is the spinodal and the solid line is the binodal.

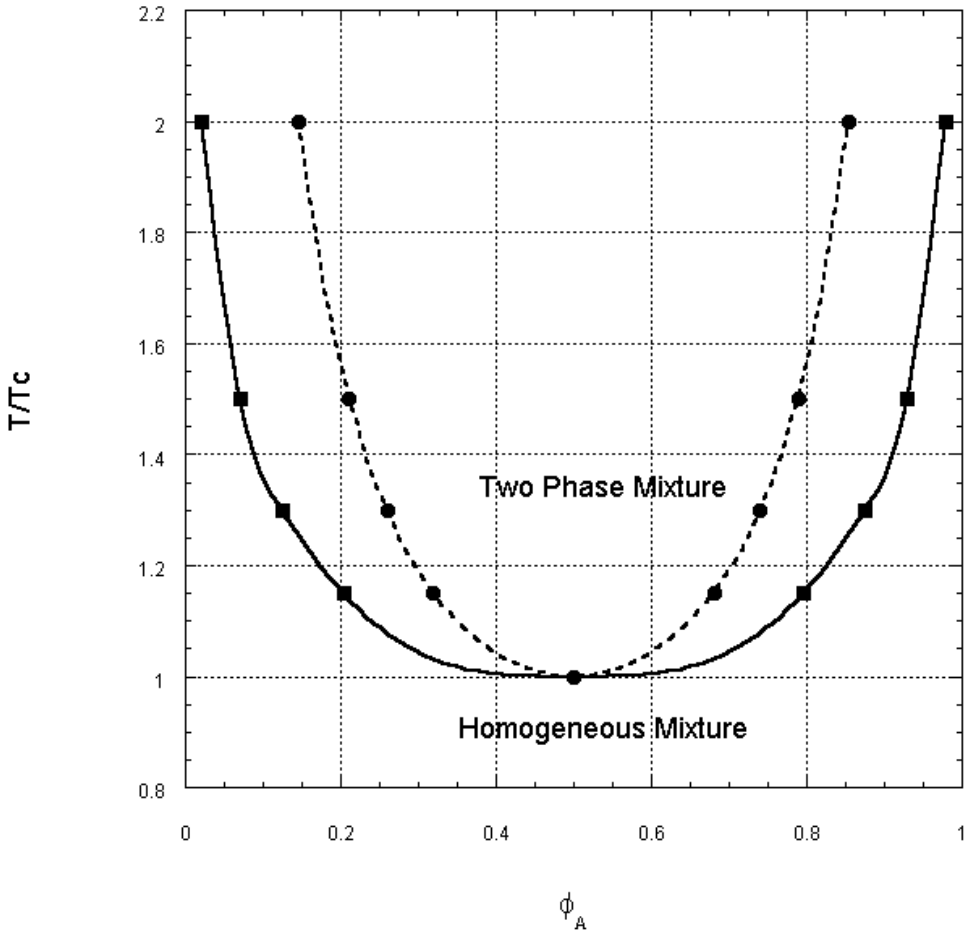

Figure 1.3: Example of a phase diagram of a binary polymer mixture exhibiting thermally induced phase separation or a lower critical solution temperature, or LCST. The dashed line is the spinodal, and the solid line is the binodal.

$$\tilde{T} = \frac{T}{T^*}, \tag{1.7}$$

$$\tilde{\rho} = \frac{\rho}{\rho^*} = \frac{v^*}{v}, \tag{1.8}$$

and

$$r = \frac{MP^*}{kT^*\rho^*} = \frac{M}{v^*\rho^*}. \tag{1.9}$$

In the above equations, P is pressure, v is specific volume, and r is the polymer chain length. Reduced variables are denoted by a ~.

Now that the compressibility effects are accounted for, it can be shown thermodynamically that LCST behavior is driven by the entropic (equation-of-state) effects of the polymer- polymer blend [1.1]. It can be shown that:

$$\left.\frac{\partial g_{\phi\phi}}{\partial T}\right)_{P,\phi} = -\left.\frac{\partial^2 s}{\partial \phi^2}\right)_{T,P} \equiv -s_{\phi\phi}. \tag{1.10}$$

As shown in Figure 1.1, when $\Delta g_{\phi\phi} < 0$ the mixture is unstable and when $\Delta g_{\phi\phi} > 0$ then mixture is stable, with the transition occurring at $\Delta g_{\phi\phi} = 0$ or the spinodal line. For a system that exhibits a USCT, the transition from $\Delta g_{\phi\phi} < 0$ to $\Delta g_{\phi\phi} > 0$ occurs as the temperature is increased, so if

$$\left.\frac{\partial g_{\phi\phi}}{\partial T}\right)_{P,\phi} > 0 \tag{1.11}$$

then the solution exhibits a UCST. Using Equations 1.10 and 1.11, one can see that if $\Delta s_{\phi\phi} < 0$ then the system will have an UCST. The same logic can be used to show that if $\Delta s\phi\phi > 0$ then the system will exhibit a LCST. These results are illustrated in Figure 1.4.

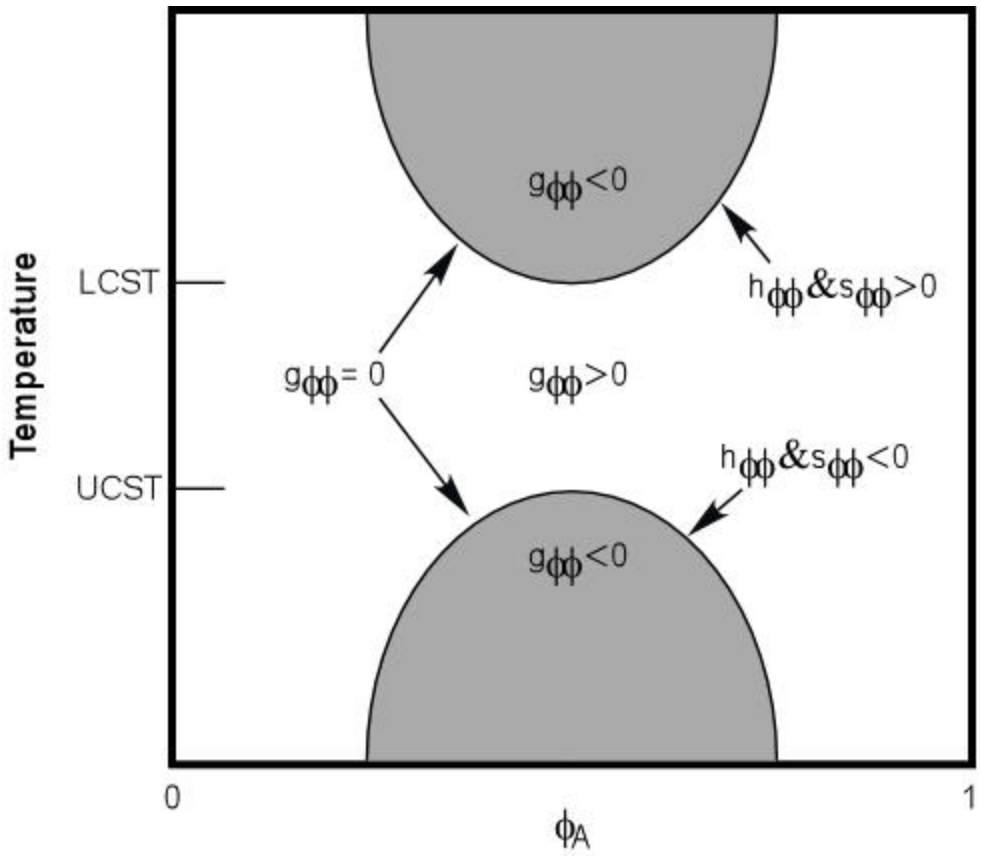

Figure 1.4: Demonstration of relationship between the $\Delta g_{\phi\phi}$ change with temperature and UCST and LCST behavior. Reproduced from with permission from [1.1].

The implications of this analysis are that unfavorable entropic effects drive phase separation of polymer blends in LCST systems rather than unfavorable energetic effects as seen in UCST systems. As shown in Figure 1.5, the LCST occurs because the total entropy of the system is increased when the mixture separates into two phases.

1.3 CONCLUSION

The Flory-Huggins description of the free energy of mixing was shown to describe USCT phase behavior, whereas it fails to describe LCST phase behavior in polymer-polymer mixtures. The prediction of LCST behavior requires the inclusion of compressibility effects through the use of an equation of state model, as shown by Sanchez and Lacombe [1.6, 1.7]. The foregoing analysis provides a context for the discussion of wetting and phase separation in thin films in Chapter 2.

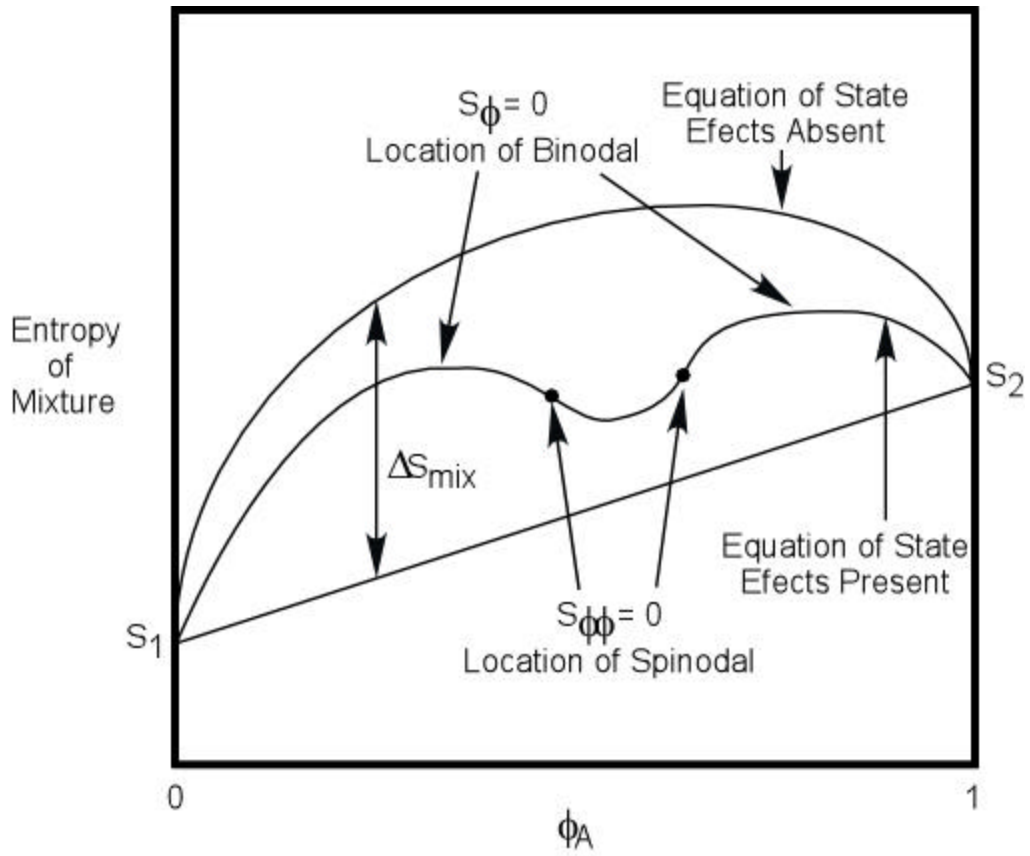

Figure 1.5: Entropy of mixing as a function of composition. It can be seen that when equation of state effects are not present, the entropy of a mixture is always maximized in the mixed state. When the equation of state effects are present, however, there is a region where the entropy can be maximized by forming a two phase mixture. Reproduced with permission from [1.1].

1.4 REFERENCES

1.1 Paul, D.R. and C.B. Bucknall, *Polymer Blends Volume 1: Formulation*. 2000: John Wiley and Sons, Inc. 600.

1.2 Scott, R.L., *J. Polym. Sci.*, 9 1952 p. 423.

1.3 Huggins, M.L., *J. Chem. Phys*, 9 1941 p. 440.

1.4 Flory, P.J., *J. Chem. Phys.*, 9 1941 p. 660.

1.5 Binder, K., "Phase Transitions in Polymer Blends and Block Copolymer Melts: Some Recent Developments," *Advances in Polymer Science*, 112 1994 p. 181-299.

1.6 Sanchez, I.C. and R.H. Lacombe, "An elementary molecular theory of classical fluids. Pure fluids," *J. Phys. Chem.*, 80(21) 1976 p. 2352-62.

1.7 Lacombe, R.H. and I.C. Sanchez, "Statistical thermodynamics of fluid mixtures," *J. Phys. Chem.*, 80(23) 1976 p. 2568-80.

1.8 Zhao, X., *et al.*, "Determination of the concentration profile at the surface of deuterated polystyrene/hydrogenated polystyrene blends using high-resolution ion scattering techniques," *Macromolecules*, 24(22) 1991 p. 5991-6.

1.9 Slep, D., *et al.*, "Phase Separation of Polystyrene and Bromo-Polystyrene Mixtures in Equilibrium Structures in Thin Films," *Langmuir*, 14(17) 1998 p. 4860-4864.

1.10 Walheim, S., *et al.*, "Nanophase-separated polymer films as high-performance antireflection coatings," *Science (Washington, D. C.)*, 283(5401) 1999 p. 520-522.

1.11 Boltau, M., *et al.*, "Surface-induced structure formation of polymer blends on patterned substrates," *Nature (London)*, 391(6670) 1998 p. 877-879.

1.12 Krausch, G., *et al.*, "Interference of spinodal waves in thin polymer films," *Macromolecules*, 26(21) 1993 p. 5566-71.

1.13 Karim, A., *et al.*, "Phase-separation-induced surface patterns in thin polymer blend films," *Macromolecules*, 31(3) 1998 p. 857-862.

1.14 Sung, L., *et al.*, "Dimensional crossover in the phase separation kinetics of thin polymer blend films," *Phys. Rev. Lett.*, 76(23) 1996 p. 4368-4371.

1.15 Newby, B.-m.Z. and R.J. Composto, "Influence of Lateral Confinement on Phase Separation in Thin Film Polymer Blends," *Macromolecules*, 33(9) 2000 p. 3274-3282.

1.16 Wang, H. and R.J. Composto, "Thin film polymer blends undergoing phase separation and wetting: Identification of early, intermediate, and late stages," *J. Chem. Phys.*, 113(22) 2000 p. 10386-10397.

1.17 Zhu, S., *et al.*, "Confinement-induced miscibility in polymer blends," *Nature (London)*, 400(6739) 1999 p. 49-51.

1.18 Gutmann, J.S., *et al.*, "Influence of the blend compatibility on the morphology of thin polymer blend films," *J. Macromol. Sci., Phys.*, B38(5 & 6) 1999 p. 563-576.

1.19 Steiner, U. and J. Klein, "Growth of wetting layers from liquid mixtures," *Phys. Rev. Lett.*, 77(12) 1996 p. 2526-2529.

1.20 Steiner, U., J. Klein, and LJ. Fetters, "Surface phase inversion in finite-sized binary mixtures," *Phys. Rev. Lett.*, 72(10) 1994 p. 1498-501.

1.21 Jones, R.A.L., *et al.*, "Surface enrichment in polymer blends: simple theory and an experimental test," *Mater. Res. Soc. Symp. Proc.*, 153(Interfaces Polym., Met., Ceram.) 1989 p. 133-41.

1.22 Jones, R.A.L., *et al.*, "The form of the enriched surface layer in polymer blends," *Europhys. Lett.*, 12(1) 1990 p. 41-6.

1.23 Jones, R.A.L., *et al.*, "Surface-directed spinodal decomposition," *Phys. Rev. Lett.*, 66(10) 1991 p. 1326-9.

1.24 Binder, K., "Surface effects on polymer blends and block copolymer melts: theoretical concepts of surface enrichment, surface induced phase separation and ordering," *Acta Polym.*, 46(3) 1995 p. 204-25.

1.25 Schmidt, I. and K. Binder, "Model calculations for wetting transitions in polymer mixtures," *J. Phys. (Les Ulis, Fr.)*, 46(10) 1985 p. 1631-44.

1.26 Binder, K., P. Nielaba, and V. Pereyra, "Phase coexistence in binary mixtures in thin films with symmetric walls: model calculations for two- and three-dimensional Ising lattices," *Z. Phys. B: Condens. Matter*, 104(1) 1997 p. 81-98.

1.27 Brazhnik, P.K., K.F. Freed, and H. Tang, "Polymer melt near a solid wall," *J. Chem. Phys.*, 101(10) 1994 p. 9143-54.

1.28 Tang, H., I. Szleifer, and S.K. Kumar, "Critical temperature shifts in thin polymer blend films," *J. Chem. Phys.*, 100(7) 1994 p. 5367-71.

1.29 Budkowski, A., U. Steiner, and J. Klein, "The effects of confinement and surface interactions on coexistence in a binary polymer mixture," *J. Chem. Phys.*, 97(7) 1992 p. 5229-38.

1.30 Reiter, G., *et al.*, "Thin Film Instability Induced by Long-Range Forces," *Langmuir*, 15(7) 1999 p. 2551-2558.

1.31 Reiter, G., "Dewetting of thin polymer films," *Phys. Rev. Lett.*, 68(1) 1992 p. 75-8.

1.32 Seemann, R., S. Herminghaus, and K. Jacobs, "Dewetting Patterns and Molecular Forces: A Reconciliation," *Physical Review Letters*, 86(24) 2001 p. 5534-5537.

1.33 Seemann, R., S. Herminghaus, and K. Jacobs, "Gaining control of pattern formation of dewetting liquid films," *Journal of Physics: Condensed Matter*, 13(21) 2001 p. 4925-4938.

1.34 Muller, M., *et al.*, "Nano-dewetting: Interplay between van der Waals- and short-ranged interactions," *Journal of Chemical Physics*, 115(21) 2001 p. 9960-9969.

1.35 Sharma, A. and R. Khanna, "Pattern Formation in Unstable Thin Liquid Films," *Phys. Rev. Lett.*, 81(16) 1998 p. 3463-3466.

1.36 Masson, J.-L., O. Olufokunbi, and P.F. Green, "Flow instabilities in entangled polymer thin films," *Macromolecules*, 35 2002 p. 6992.

1.37 Masson, J.L. and P.F. Green, "Hole Formation in Thin Films: A two stage process," *Phys Rev. Lett.*, 88 2002 p. 205504.

1.38 Masson, J.L. and P.F. Green, "Pattern Formation in a Thin Random Copolymer Film: Evolution of an Intermediate Morphology," *Journal of Chemical Physics*, 112 2000 p. 349.

Chapter 2: Effect of Interfaces on the Composition Profiles in Polymer-Polymer Mixtures

2.1 INTRODUCTION

This chapter is divided into two sections. In the first, I consider the effect of a free surface on the local composition profile of an A-B mixture in a film of semi-infinite thickness. The work of Schmidt and Binder, who to date have performed the most complete theoretical study in polymer-polymer mixtures, is summarized. It is shown that depending on the proximity of the mixture to the critical point, various situations of partial and complete wetting of the lower surface energy component can occur.

The thermodynamics of a mixture of finite thickness, D, is considered in the second section. Through a series of simulations, Flebbe and Binder have shown how the stability of a mixture, bounded by two interfaces, would be affected. This work, however, fails to describe a range of experimental observations. Limitations of the model, discussed at the end of the chapter, provide a rationale for the research in this dissertation.

2.2 SEGREGATION IN A SEMI-INFINITE POLYMER FILM

The local composition of a polymer blend at an interface is generally different from the composition in the bulk. Near a free surface, the overall free energy is decreased by increasing the concentration of the component with the lower surface energy at the surface [2.1-2.3]. This is an important area of

research because the surface composition influences properties such as wetting, adhesion, friction, and wear resistance. For these reasons, interfacial effects on polymer blends have been of interest, theoretically [2.4-2.23] and experimentally [2.2, 2.24-2.34].

The first attempts to model the segregation of polymers in thin films [2.4] involved extensions of theory used to describe the wetting of small molecule liquids at interfaces [2.35-2.38]. The theory of wetting proposed by Cahn is described by the following extension of Young's equation:

$$\sigma_{AB} \geq \left|\sigma_{AX} - \sigma_{BX}\right|, \tag{2.1}$$

where σ_{AB} is the interfacial energy between phase A and B, σ_{AX} is the surface free energy of phase A at the interface, and σ_{BX} is the free energy of phase B at the interface. If the inequality is satisfied, then the free energy penalty associated with creating an A-B interface between the phases is greater than the free energy gain of phase B completely wetting the surface. If the equality is satisfied, then the surface energy of the non-wetting layer must be equal to the sum of the surface energy of the wetting layer and the surface interfacial energy between the two phases,

$$\sigma_{AX} = \sigma_{BX} + \sigma_{AB}\,. \tag{2.2}$$

In this situation, the B phase completely wets the interface to the exclusion of phase A, otherwise known as perfect wetting. Equation 2.2 is commonly represented by the "spreading coefficient", which is defined as

$$S = \sigma_{AX} - \sigma_{BX} - \sigma_{AB}\,. \tag{2.3}$$

When S is positive, then B will perfectly wet the surface of the substrate.

It can be seen from Equation 2.2 that complete wetting will occur when the interfacial energy between phases A and B is small. Thus, the model predicts that for mixtures of small molecule liquids, perfect wetting usually occurs close to the critical point. Even so, Schmidt and Binder [2.4] demonstrated that complete wetting can occur far from the critical point in polymer-polymer mixtures. This effect can be explained by two factors. First, the interfacial energy between components of partially compatible polymer blends is typically much smaller than the surface energy difference between the components and the free interface [2.39, 2.40]. Second, the large molecular weight of polymers also decreases the translational entropy penalty associated with increasing the concentration of one species at an interface.

A description of the free energy of a small molecule liquid mixture at an interface using mean field theory was first developed by Cahn [2.35] and later extended to polymers by Schmidt and Binder [2.4, 2.7]. For a semi-infinite system with a boundary at a wall at z=0, the free energy per unit area of surface is given by

$$\frac{\Delta F}{k_B T} = \int_0^\infty dz \left\{ f_{FH}[\boldsymbol{f}(z)] - \Delta \boldsymbol{m} \boldsymbol{f}(z) + \boldsymbol{k} \left[\frac{d\boldsymbol{f}(z)}{dz} \right]^2 \right\} + \frac{f_s^{(b)}}{k_B T}, \qquad (2.4)$$

where $\phi(z)$ is the volume fraction of one component, A, at distance z from the wall, $\Delta\mu$ is the chemical potential difference between the two components, f_{FH} is the Flory-Huggins free energy of mixing per effective monomer as described in Equation 1.3, κ describes the free energy cost of having a concentration gradient, described below by Equation 2.5, at the wall, and $f_s^{(b)}$ is the "bare" surface free energy per unit area at the wall described below by Equation 2.6.

The free energy cost associated with having a concentration gradient, κ, is

$$\kappa = \frac{r_o^{\,2}}{6}\chi_{eff} + \frac{a^2}{36\phi(1-\phi)}. \qquad (2.5)$$

The first term on the right side of Equation 2.5 is related to enthalpic contributions, with r_o being the effective range of interactions. This term can be ignored for polymer systems, because $\chi_{eff} \approx \frac{2}{N}$ at the critical point and N is large, thus $\chi_{eff} << 1$. The second term in Equation 2.5 is related to the configurational entropy of the Gaussian coils, where *a* is the effective length of a segment. The surface free energy, $f_s^{(b)}$, was defined by Schmidt and Binder [2.4] as

$$f_s^{(b)}(\phi_s) = -\mu_s \phi_s - \frac{1}{2} g \phi_s^{\,2}. \qquad (2.6)$$

Equation 2.6 is a function of the volume fraction at the interface, $\phi_s \equiv \phi(z = 0)$, μ_s is the chemical potential difference favoring one species at a surface, and g is the change of interactions near the surface, including effects due to "missing neighbors".

Solving for the concentration profile of the film as a function of film thickness requires the minimization of Equation 2.4,

$$\frac{d}{d\phi}\left[\frac{\Delta F}{k_B T}\right] = 0, \qquad (2.7)$$

which yields Equation 2.8 [2.37, 2.38]:

$$\frac{a^2}{36\phi(1-\phi)}\left(\frac{d\phi}{dz'}\right)^2\Bigg|_{z'=0}^{z'=z} = \left\{\frac{1}{N}\left[\phi \ln \phi + (1-\phi)\ln(1-\phi)\right] + \chi\phi(1-\phi) - \Delta\mu\phi\right\}\Bigg|_{\phi_s}^{\phi(z)}. \qquad (2.8)$$

Using the treatment of Cahn [2.35], it can be shown that the excess free energy at the surface F_s is

$$\frac{F_s}{k_B T} = \int_{f_s}^{f_\infty} d\phi \left\{ \frac{a^2}{18\phi(1-\phi)} \frac{d\phi}{dz} + \mu_s + g\phi \right\} - \mu_s \phi_\infty - \frac{1}{2} g \phi_\infty , \tag{2.9}$$

where ϕ_∞ is the equilibrium concentration of the polymer in the bulk, far away from the interface. If this equation is minimized with respect to ϕ_s then the following boundary condition must be met [2.4, 2.7]:

$$\frac{a^2}{18\phi_s(1-\phi_s)} \left. \frac{d\phi}{dz} \right|_{z=0} = -\mu_s - g\phi_s = \left(\frac{\partial f_s^{(b)}}{\partial \phi_s} \right). \tag{2.10}$$

Combining Equation 2.10 with Equation 2.8 yields the following expression for ϕ_s [2.4, 2.7]:

$$\frac{\partial f_s^{(b)}}{\partial \phi_s} = -\mu_s - g\phi_s = \pm f_1(\phi_s) \tag{2.11}$$

where

$$f_1(\phi_s) = \left[\frac{a}{3} \frac{f_{FH}(\phi_s) - f_{FH}(\phi_\infty) - \Delta\mu(\phi_s - \phi_\infty)}{\phi_s(1-\phi_s)} \right]^{\frac{1}{2}}. \tag{2.12}$$

Equation 2.9 can be written as [2.4, 2.7, 2.35]:

$$\frac{F_s}{k_B T} = \int_{f_s}^{f_\infty} d\phi \left[f_1(\phi) - \frac{\partial f_s^{(b)}(\phi)}{\partial \phi} \right] \tag{2.13}$$

Finally, the following solution for Equation 2.8 yields $\phi(z)$:

$$\frac{6z}{a} = \int_{f_s}^{f(z)} \frac{d\phi}{\{\phi(1-\phi)[f_{FH}(\phi) - f_{FH}(\phi_\infty) - \Delta\mu(\phi - \phi_\infty)]\}^{\frac{1}{2}}}. \tag{2.14}$$

From Equation 2.14, the concentration profile of the polymer mixture from the wall into the bulk of the film can be determined, if the concentration of the polymers at the wall and in the bulk are specified.

As mentioned earlier, the difference between the surface energies of two components leads to the preferential attraction of one to the interface. The penalty associated with creating the composition gradient in the film from the wall into the bulk mixture acts to counterbalance this preferential attraction. This balance is described by Equations 2.11 and 2.12 and is represented graphically in Figure 2.1. As seen in Figure 2.1, the area under the line defined by the equation $\mu_s+\phi_s g$ is the decrease in free energy associated with the concentration ϕ_s existing at the interface. The area under the $f_1(\phi_s)$ curve is related to the increase in free energy associated with creating unfavorable contact between polymers A and B. There exists solutions for ϕ_s in Equation 2.11 each time the two lines cross each other in Figure 2.1. In fact, there are four solutions to Equation 2.11 in Figure 2.1. In this example, the bulk polymer mixture is rich in B, but polymer A preferentially wets the surface. If the bulk polymer mixture starts at concentration ϕ_∞, the first solution, at about $\phi = 0.05$ is not possible, because the total energy saved by this solution, represented by area A_1 is less than the total energy saved by the second solution at ϕ_s, represented by A_2. The third solution is again a maximum due to the increase in free energy represented by the area associated with S_2. The final solution is another minimum due the subtraction of the S_1 term

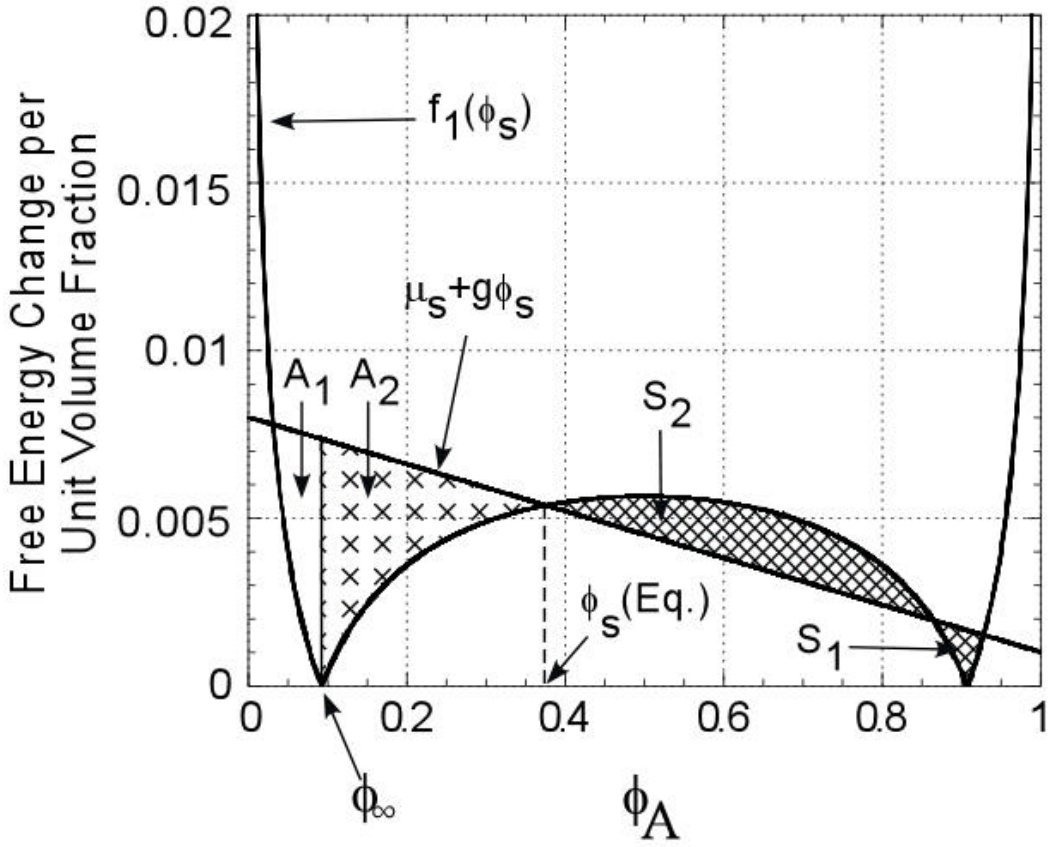

Figure 2.1: Free energy diagram for a semi infinite film, where species A is preferentially attracted to the substrate. The area under $\mu_s+\phi_s g$ is the total energy saved by having a surface concentration ϕ_s equal to the value of ϕ_A on the x axis. The area under $f_1(\phi_s)$ is the energetic penalty associated with creating a mixture composition with the value of ϕ_A at the interface. Summing all of the areas under these curves (A_1, A_2, S_2, and S_1) determines which of the four possible solutions to Equation 2.12 is stable.

from the total free energy. If all of the areas A_1, A_2, S_1, S_2 are summed to any given solution, then it can be seen that the global minimum in free energy for this system occurs for the second solution and is labeled as ϕ_s(Eq.).

If we go back to the "spreading coefficient" as defined by Equation 2.3, we can see that for Figure 2.1

$$S = S_1 - S_2 , \tag{2.15}$$

where

$$S_1 = \sigma_{AX} - \sigma_{BX} \tag{2.16}$$

and

$$S_2 = \sigma_{AB} . \tag{2.17}$$

If S = 0, or the area under $S_1 = S_2$, then perfect wetting of a phase rich in B will occur on the substrate, and the fourth solution for ϕ_s is correct. If $S_2 > S_1$, then the B rich phase does not completely wet the interface.

It is useful to investigate the relationship between the location of the bulk composition of the polymer mixture on the phase diagram and the wetting of the preferential species at an interface. The model polymer system exhibits an upper critical solution temperature and is shown in Figure 2.2. In this example, as before, the bulk polymer mixture is rich in B, but polymer A preferentially wets the surface. Three situations are demonstrated in Figure 2.2.

(1) First, as the temperature, or distance from the critical point, is changed and the composition of the mixture remains on the binomal, related changes in the free energy are shown in Figure 2.3.

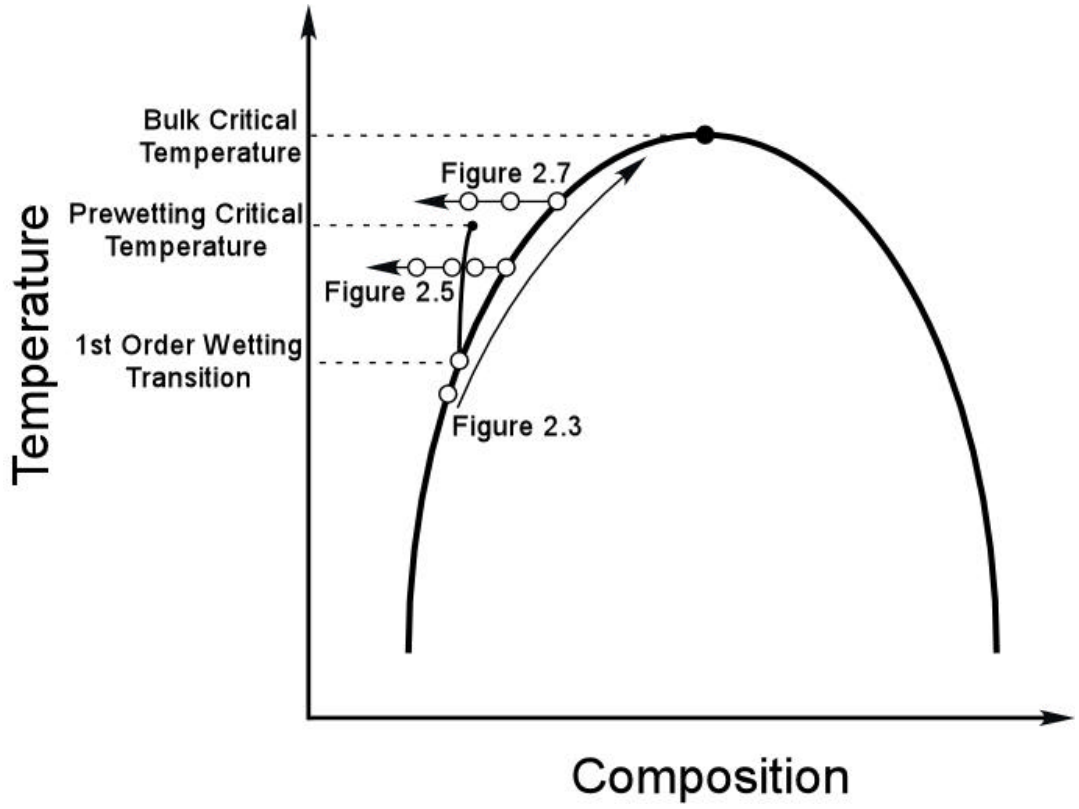

Figure 2.2: Phase diagram of a polymer mixture exhibiting a UCST. The labeled arrows indicate three different possibilities for wetting transitions. The first arrow labeled as Figure 2.3, indicates a first order wetting transition on the coexistence curve. The second arrow, labeled as Figure 2.5, indicates a first order wetting transition off of the coexistence curve, but below the prewetting critical temperature. The final arrow, labeled as Figure 2.7, indicates a second order wetting transition off of the coexistence curve, above the prewetting critical temperature.

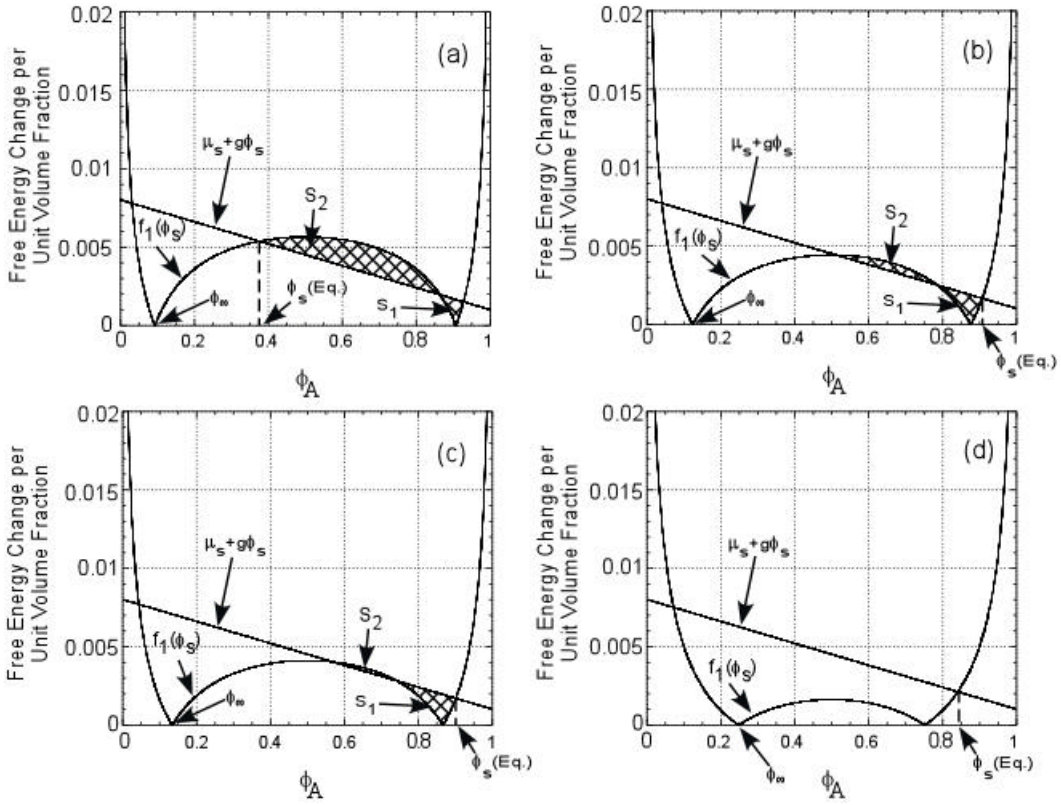

Figure 2.3: First order wetting transition on the coexistence line. (a) illustrates the solution to Equation 2.12 well below the 1st order wetting transition. The surface is partially wet by polymer A, but the energetic penalty associated with creating a fully wetted surface (indicated by S_2) is still much larger than the benefit of fully wetting the surface (indicated by S_1). In (b) the area S_2 is the same as the area S_1 and the surface goes through a first order wetting transition from a partially wet surface to a completely wet one. This corresponds to a rapid change of the composition of A at the surface from a value of $\phi_s \sim 0.5$ to $\phi_s \sim 0.9$. As the temperature is increased further, the value of S_1 is larger than S_2, and the surface is still completely wet. As seen in (c) and (d), ϕ_s continues to increase a small amount.

(2) Second, the composition of the mixture is changed at a constant temperature below the prewetting critical temperature and the results are displayed in Figure 2.5.

(3) Finally, the composition of the mixture is also changed at a constant temperature, but this time above the prewetting critical temperature, with the results presented in Figure 2.7.

Increasing the temperature of the mixture has the effect of decreasing the value of χ, or, in other words, decreasing the magnitude of the unfavorable interactions between polymer A and B. If we start with the temperature furthest away from the bulk critical point, as represented by Figure 2.3(a), we can see that $S_2 > S_1$, or $S < 0$ indicating a state of partial wetting. In this case, there is enrichment of A at the interface, but the concentration of A returns to the equilibrium state on the phase diagram $\phi_\infty = \phi_{\beta(Coex)}$. The resulting value of the surface excess of polymer A will be finite and the composition profile will appear similar to Figure 2.4(a). If the coexistence curve is followed as the temperature of the mixture is increased, the value of S_2 will decrease as the value of S_1 increases, due to a decrease in the energetic penalty associated with bringing A and B monomers into contact as the critical point is approached. Eventually, S_1 equals S_2 and the wetting transition has been reached. The composition of the bulk mixture at infinite distance from the interface is still $\phi_\infty = \phi_{\beta(Coex)}$, but now the interface is completely wet by an A rich phase. As seen in Figure 2.3(b), the composition at the interface is greater than the composition of the A rich phase on

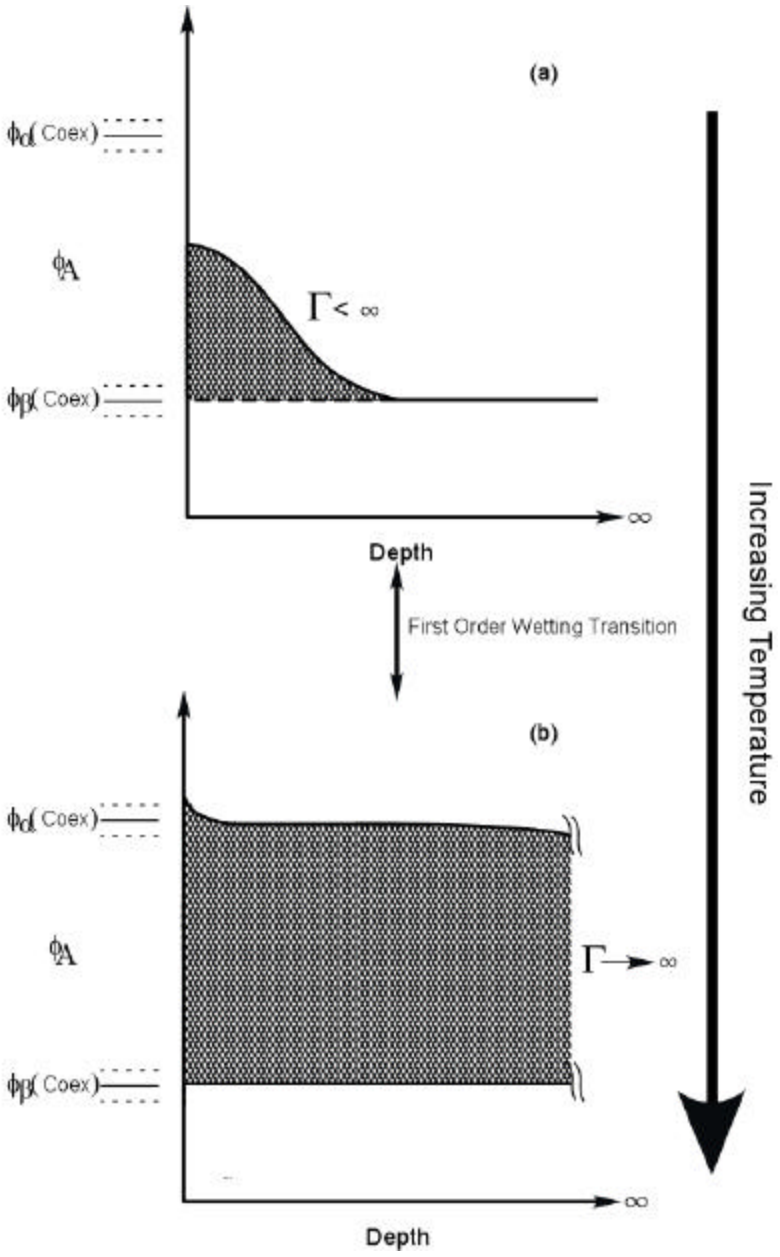

Figure 2.4: Concentration profile for first order transition from partial (a) to complete wetting (b) in a semi-infinite system.

the coexistence line ($\phi_{\alpha(Coex)}$), but the concentration of A will quickly decrease to from ϕ_s to $\phi_{\alpha(Coex)}$. The resulting mixture, since it assumed to be infinitely thick, will have an infinite value of the surface excess of A, and appear similar to Figure 2.4(b). The transition from the value of $\phi_s \sim 0.5$ to a value $\phi_s \sim 0.9$ occurs with very little change in temperature and is not smooth. This transition is first order and occurs at the "wetting point". As the temperature is further decreased, the value of S_2 will continue to decrease and S_1 will continue to increase, as seen in Figure 2.3(c), which results in a positive value for S. The positive value of S only that the fourth solution continues to be the global minimum, as was the situation as Figure 2.2(b). As before, the interface is perfectly wet by an A rich layer with composition ϕ_s that decays to the coexistence value $\phi_{\alpha(Coex)}$. Finally, a temperature is reached where the reduction in free energy associated with creating the wetting layer at the interface is always greater than the increase in free energy necessary to create the concentration gradient, as seen in Figure 2.3(d). Now there are only two solutions to Equation 2.11, one at a value of ϕ_A lower than ϕ_∞ and one where ϕ_A is greater than ϕ_∞. As described earlier, enriching the interface in polymer A reduces the total free energy of the system more than reducing the amount of A at the interface. The interface is completely wet by an A rich phase with composition ϕ_s, which decays to the coexistence value of $\phi_{\alpha(Coex)}$.

The extent of wetting of a polymer at an interface is commonly measured by the surface excess Γ, which is given by

$$\Gamma = \int_0^{z(\phi_\infty)} [\phi(z) - \phi_\infty] dz \,. \qquad (2.18)$$

In a semi-infinite system that has perfectly wet the interface, the thickness of the wetting layer is infinite, so $\Gamma = \infty$, as shown in Figure 2.4(b). In all physically obtainable systems, the thickness of the wetting layer is, of course, finite, even if the substrate is perfectly wet. If $S < 0$, then the B rich phase only partially wets the interface, as seen in Figure 2.4(a) and Γ has a finite value.

The starting point for the next series of free energy diagrams is on the coexistence line at a temperature above the 1st order wetting transition, but below the prewetting critical transition temperature, as seen in Figure 2.2. Figure 2.5(a) is the same as diagram 2.3(c), with $S_2 < S_1$ and the A rich phase completely wetting the interface. If the value of ϕ_∞ is decreased such that it is no longer on the coexistence line, but the temperature of the mixture remains the same, the value of S_2 will increase and S_1 will decrease, as seen in Figure 2.5(b). In this case, the interface will still be completely wet by a B rich phase $\phi_s > \phi_{\alpha(Coex)}$, but the composition of the polymer will decay back into the film until the bulk composition ϕ_∞ is reached, Figure 2.6(b). Eventually, as the bulk concentration of polymer A is reduced, the first order wetting transition is again reached, where $S_2 > S_1$ and there is a discontinuous jump in ϕ_s from a high concentration of polymer A to a low concentration of polymer A, as seen in Figure 2.5(c). Since the value of $S > 0$, the interface is no longer perfectly wet with an A rich layer and the composition at the interface ϕ_s decays to the bulk polymer composition ϕ_∞, Figure 2.6(c). Finally, as seen in Figure 2.5(d), as the composition of polymer A in the bulk is reduced further, the composition of polymer A at the interface continues to decrease, and the state of partial wetting continues with ϕ_s decaying to ϕ_∞.

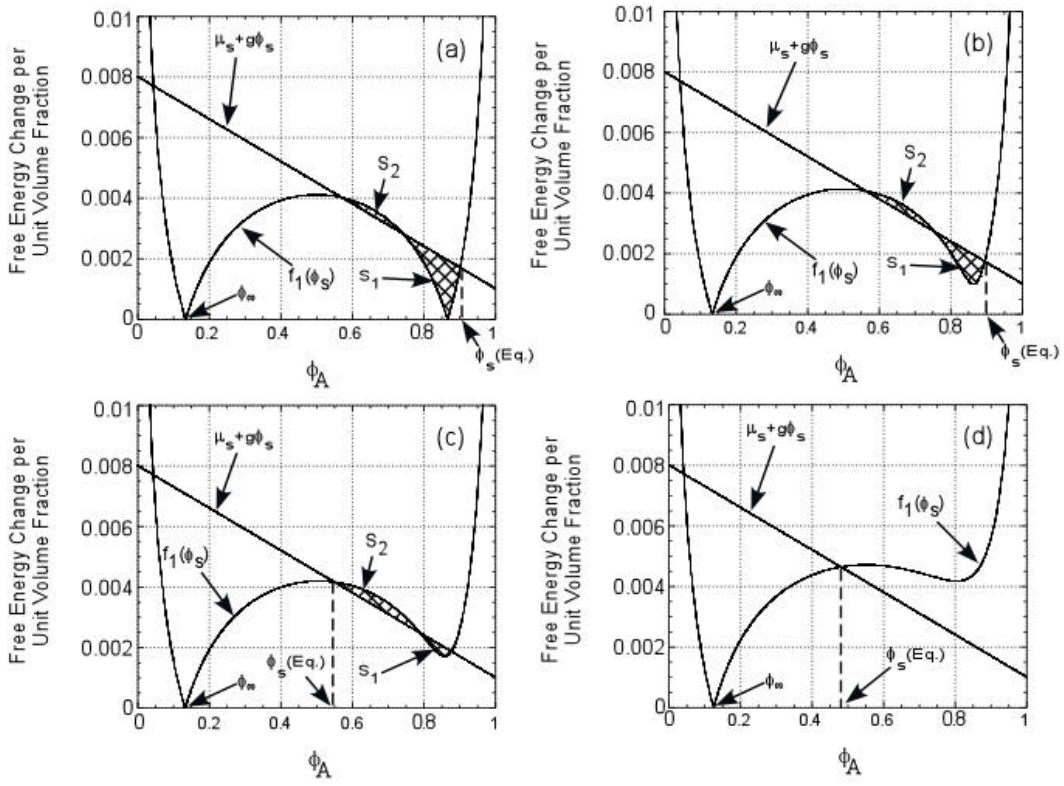

Figure 2.5: First order wetting transition off the coexistence line. (a) illustrates the same solution as Figure 2.3(c). The surface is completely wet by polymer A. In (b), the bulk polymer composition ϕ_∞ is decreased, resulting in a reduction of ϕ_s. The area S_2, however, is still less than the area S_1 and the surface is still wet by an A rich layer. The composition from this surface rapidly dies off to the bulk value ϕ_∞. As ϕ_∞ is decreased further, as seen in (c) the area S_1 becomes less than the area S_2. When this occurs, the film undergoes a first order transition from a wet state to a partially wet state. The concentration of A at the surface ϕ_s rapidly decreases. (d) demonstrates that as the composition of the bulk mixture ϕ_∞ is decreased further, the film is still partially wet and the value of ϕ_s decreases smoothly.

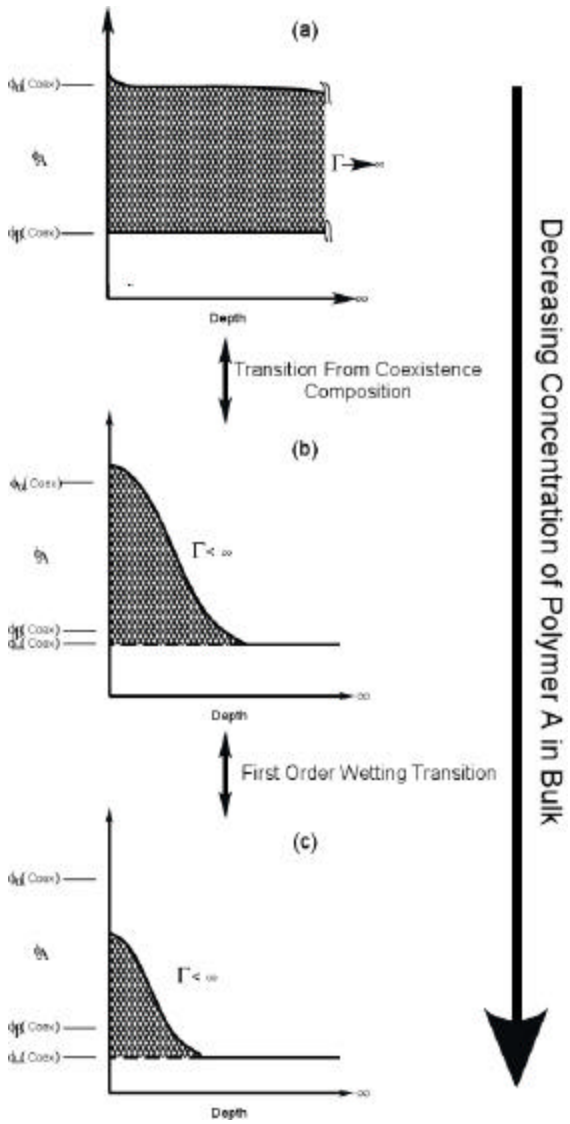

Figure 2.6: Concentration profile for first order transition from complete (a) to partial wetting (c) in a semi infinite system. The system passes through an intermediate point (b) where the surface is wet by a highly A rich layer, but it is not macroscopically thick as in the completely wet case.

If the temperature at which the free energy diagrams in Figure 2.5 was continuously increased, the energetic penalty associated with the contact between A and B monomers would decrease. Consequently the difference in the composition at the interface for the complete and partial wet sides of the first order transition will decrease smoothly. Eventually, the first order transition no longer occurs and only a smooth transition from a complete to partial wetting occurs. This results in a series of free energy diagrams, Figure 2.7, which have only two solutions for Equation 2.12, indicating that a second order transition is occurring. The highest temperature at which a first order transition still occurs is known as the precritical wetting temperature. Initially while the composition of the mixture is still on the coexistence line, as seen in the free energy diagram Figure 2.7 (a), the interface will be completely wet with the A rich phase $\phi_{\alpha(Coex)}$. This wetting layer will be infinitely thick for the semi-infinite system as seen in Figure 2.8 (a). As ϕ_∞ is decreased and moves off the coexistence value, $\phi_{\beta(Coex)}$, $f_1(\phi_s)$ continues to be below $\mu_s+\phi_s g$ for the entire range of values between the two solutions to Equation 2.12. As discussed before, the free energy is minimized when ϕ_s remains rich in polymer A, but the composition decays to ϕ_∞ in the bulk polymer, as seen in Figure 2.8(b). As ϕ_∞ continues to decrease there is a smooth transition to smaller values of ϕ_s, as seen in Figures 2.7(c), 2.8(c), and 2.8(d).

The final situation to be considered for a semi-infinite polymer interface is a change in the values of μ_s and g, which determine the "bare" surface free energy per unit area, $f_s^{(b)}$. Changing these values can make it more

energetically favorable for the polymer A to be at the interface. The free energy diagrams

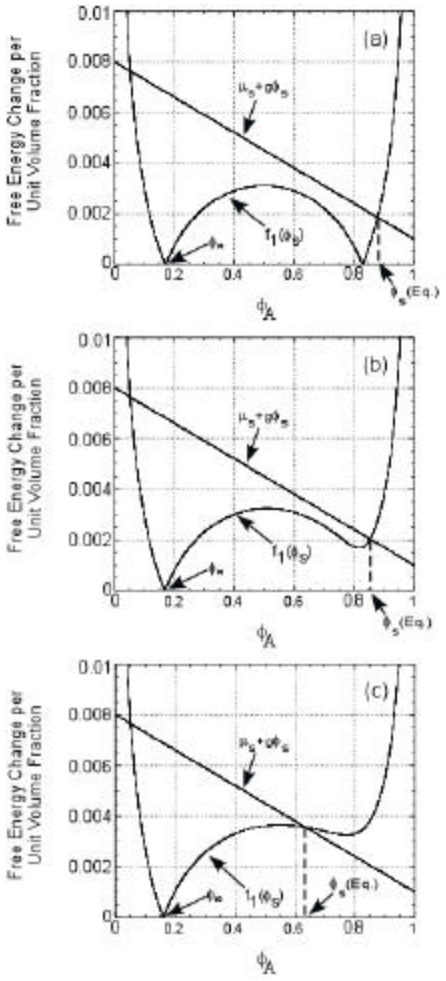

Figure 2.7 Second order wetting transition off the coexistence line. (a) illustrates a solution similar to Figure 2.3(d). The surface is completely wet by polymer A. In (b) the bulk polymer composition ϕ_∞ is decreased, resulting in a reduction of ϕ_s and a change from a completely wet state, with a thick A rich layer, to one where there is a microscopic A rich layer at the surface. As ϕ_∞ is decreased further, as seen in (c), there is a smooth transition of $\phi_s \sim 0.9$ to $\phi_s \sim 0.65$. This transition is said to be second order because there is no sudden jump in ϕ_s.

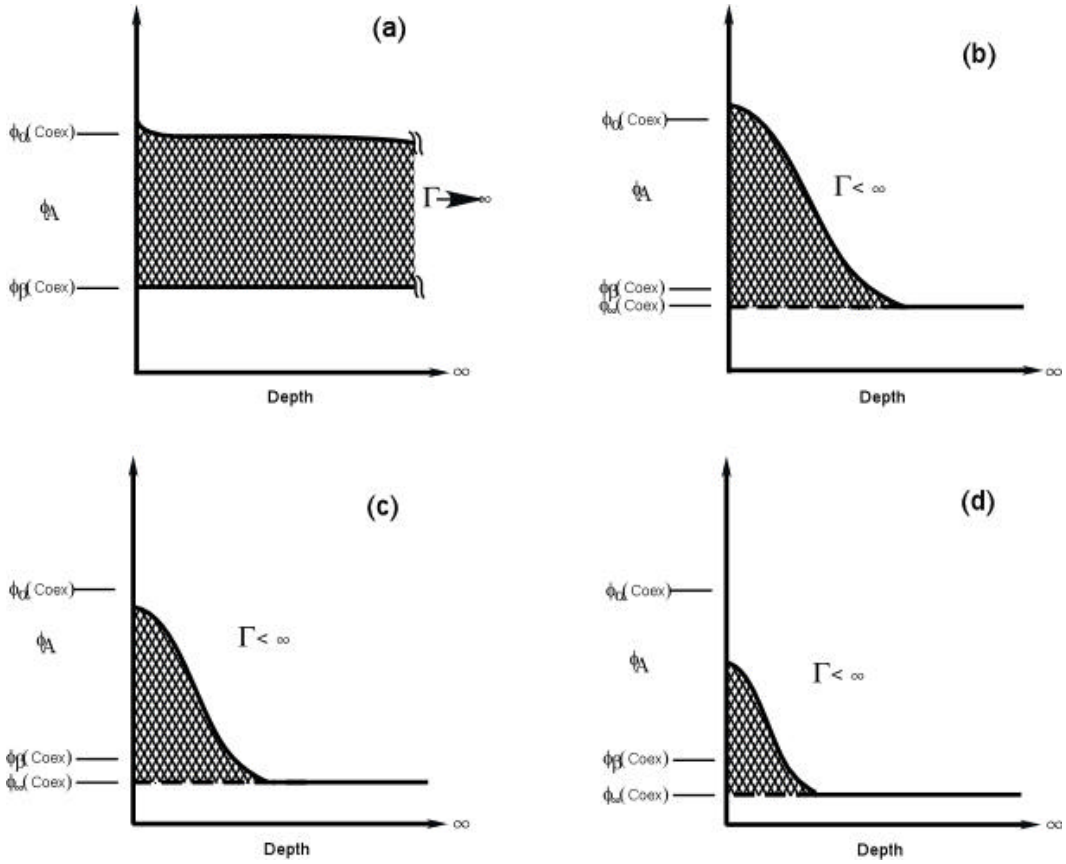

Figure 2.8: Concentration profile for the wetting transition above prewetting critical point. This system smoothly passes from a completely wet state (a) to a partially wet state (d).

describing these changes are displayed in Figure 2.8. It can be seen from these graphs that since it is now highly favorable for A to be at the interface, there is effectively only one solution to Equation 2.13. There could potentially be a second solution at very small values of ϕ_A but, as discussed previously, these would not be energetically favorable. Consequently, the system will only exhibit second order transitions as the temperature approaches the critical point and the composition of the mixture is moved off of the coexistence curve. If the system was at a temperature far from the critical point, then ϕ_s is less than the coexistence value $\phi_{\alpha(Coex)}$, as shown in Figure 2.9(a) and the system is only partially wet as shown in Figure 2.10(a). As the temperature increases, there is a smooth transition to partial wetting where $\phi_s = \phi_{\alpha(Coex)}$, seen in Figure 2.9(b), and complete wetting occurs. This situation, where $\phi_s = \phi_{\alpha(Coex)}$, is unique to this type of second order transition that occurs at surfaces that strongly attract the segregating species and is seen in Figure 2.9(b). Finally, as the temperature approaches the critical point, the value of $\phi_s > \phi_{\alpha(Coex)}$ and again decays to an equilibrium value of $\phi_{\alpha(Coex)}$ as seen in previous systems, Figure 2.8(c) and Figure 2.9(c).

2.3 SEGREGATION IN THIN FILMS

As the thickness of a polymer film is reduced, the effect of the second interface must be taken into account when determining the segregation of polymers. Flebbe *et al.* found that when D < 100*Rg, that finite film thickness effects become significant [2.41], where D is the thickness of the film and Rg is the radius of gyration. In contrast to the semi-infinite geometry already discussed,

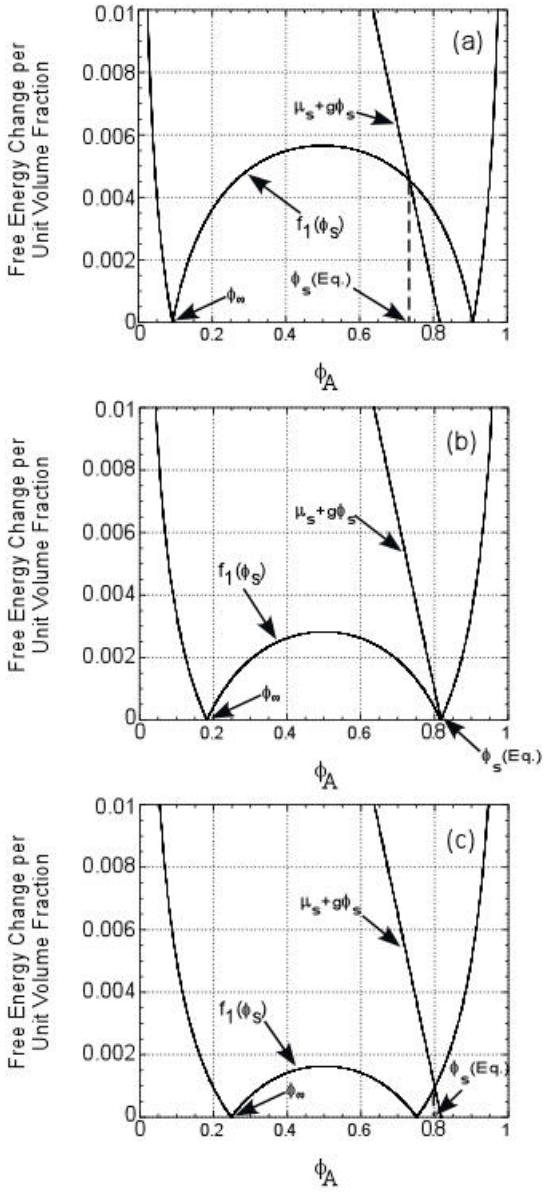

Figure 2.9: Second order wetting transition on the coexistence line. The value of g and μ_s have been changed to increase the attraction of A to the interface. This has the effect of eliminating the possibility of a first order wetting transition. The concentration of A at the interface ϕ_s smoothly increases from partial, (a), to complete wetting, (b) and (c), as the temperature is increased.

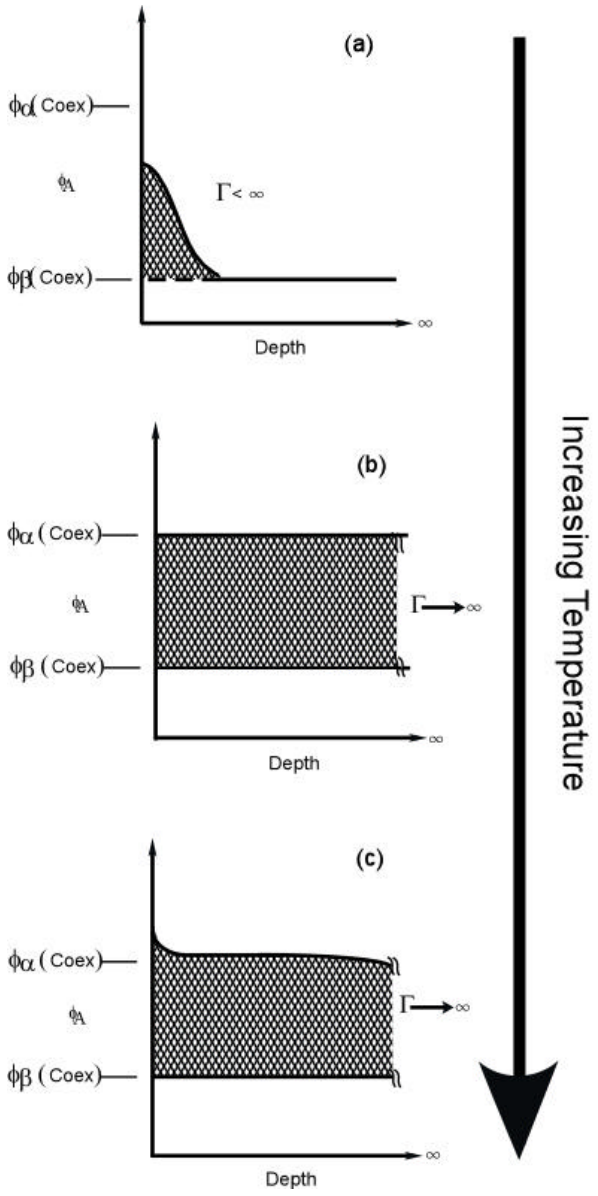

Figure 2.10: Concentration profile for the second order wetting transition on the coexistence curve. The concentration profile smoothly transitions from partially wet, (a), to completely wet, (b) and (c). There is direct correspondence between (a), (b), and (c) and Figure 2.9(a), (b), and (c).

where the bulk polymer properties are not effected by the interface, the effect of both interfaces must be accounted for in thin films. It will become obvious from this discussion that finite film thickness effects are significant not only to the wetting of polymer mixtures at interfaces, but that they significantly effect the location of the critical point and the shape of the phase diagram.

The derivation of the equations describing segregation in thin films will start in essentially the same way as the derivation in the semi-infinite geometry, discussed in section 2.1. First, a description of the free energy of the polymer mixture may be written as

$$\frac{\Delta F}{k_B T} = \int_0^D dz \left\{ f_{FH}[\phi(z)] - \Delta\mu\phi(z) + \kappa\left[\frac{d\phi(z)}{dz}\right]^2 \right\} + \frac{f_s(\phi_0)^{(b)}}{k_B T} + \frac{f_s(\phi_D)^{(b)}}{k_B T} \quad (2.19)$$

All of the terms of Equation 2.19 are defined in the same way as those in Equation 2.3. In this equation, however, the limits of integration are finite and bound by the thickness of the film. There is also one free energy term for each interface, $f_s(\phi_0)^{(b)}$ and $f_s(\phi_D)^{(b)}$. In this example, we will assume that the attraction at both interfaces is for the same polymer species and of the same magnitude. We also assume that the film is thick enough that configurational entropy contributions are not significant, an assumption that is generally made for films where D > 5*Rg [2.11, 2.41-2.45]. The surface potential at each interface will be described as:

$$f_s(f_0)^{(b)} = f_s(f_D)^{(b)} = -m_s f_s - \frac{1}{2} g f_s^2 \quad (2.20)$$

where, as before, μ_s is the chemical potential difference favoring one species at a surface, g is the change of interactions near the surface including effects due to "missing neighbors", and ϕ_s is the composition at either interface.

To solve Equation 2.19, it is more convenient to make the film thickness symmetric about the center of the film, such that the interfaces are at $\pm\frac{D}{2}$. Under this assumption, the standard Euler-Lagrange solution for the following equation [2.41] can be utilized:

$$\frac{\partial f(\phi)}{\partial \phi} - \frac{\partial k(\phi)}{\partial \phi}\left(\frac{d\phi}{dz}\right)^2 - 2k(\phi)\frac{d^2\phi}{dz} = 0 \tag{2.21}$$

where

$$f(\phi) = f_{FH}[\phi(z)] - \Delta m\phi(z) \tag{2.22}$$

with the following boundary conditions:

$$2k(\phi)\left.\frac{d\phi}{dz}\right|_{z=-D/2} = -m_s - g\phi(z = -D/2) \tag{2.23}$$

and

$$2k(\phi)\left.\frac{d\phi}{dz}\right|_{z=D/2} = m_s + g\phi(z = D/2). \tag{2.24}$$

If it can also be assumed for a symmetric system that

$$\left.\frac{d\phi}{dz}\right|_{z=0} = 0, \tag{2.25}$$

then the following equation for the profile of the thin film can be derived [2.41]:

$$z(\phi) = \pm\int_{\phi^*}^{\phi} \sqrt{\frac{k(\phi')}{[G(\phi') - G(\phi^*)]}}\, d\phi' \tag{2.26}$$

where

$$G(\phi) = f(\phi) - f(\phi_b), \tag{2.27}$$

ϕ_b is the bulk concentration of the polymer mixture, and ϕ^* is the concentration of the polymer in the center of the film. With the boundary condition above being rewritten as

$$m_s = -g f_s \pm 2\sqrt{k(f_0)[G(f_0) - G(f^*)}\,, \tag{2.28}$$

where ϕ_s is the concentration of the polymer at both interfaces.

The solution of the Equations 2.26 and 2.28 is nontrivial, since the concentration in the center of the film is important in determining not only the shape of the profile, but the value of the boundary condition. The technique for solving these equations is described in detail elsewhere [2.41] and will be described briefly here. The profile of the film is calculated using Equation 2.26 for all values ϕ^* between 0 and 1, as seen in Figure 2.11. The value of ϕ at $\frac{D}{2}$ is equal to ϕ_s, allowing the use of Equation 2.28 to calculate values of μ_s explicitly, as seen in Figure 2.12. Multiple solutions for μ_s may be possible, as seen in Figure 2.12 where μ_s crosses 0.2 three times. The three profiles corresponding to the solutions in Figure 2.12 are given in Figure 2.13 (Note that unlike the previous example, B is the surface preferred phase in this example). Each profile can then be used to determine a free energy change using Equation 2.19. The profile that results in the minimum free energy is the profile that is most likely to occur for a given composition.

The above technique was utilized to design a FORTRAN program that can be used to calculate the phase diagram of thin films confined in a substrate that exhibits symmetric surface potentials. The program is attached in

Appendix A. The results of the simulation for a system that exhibits preferential segregation of

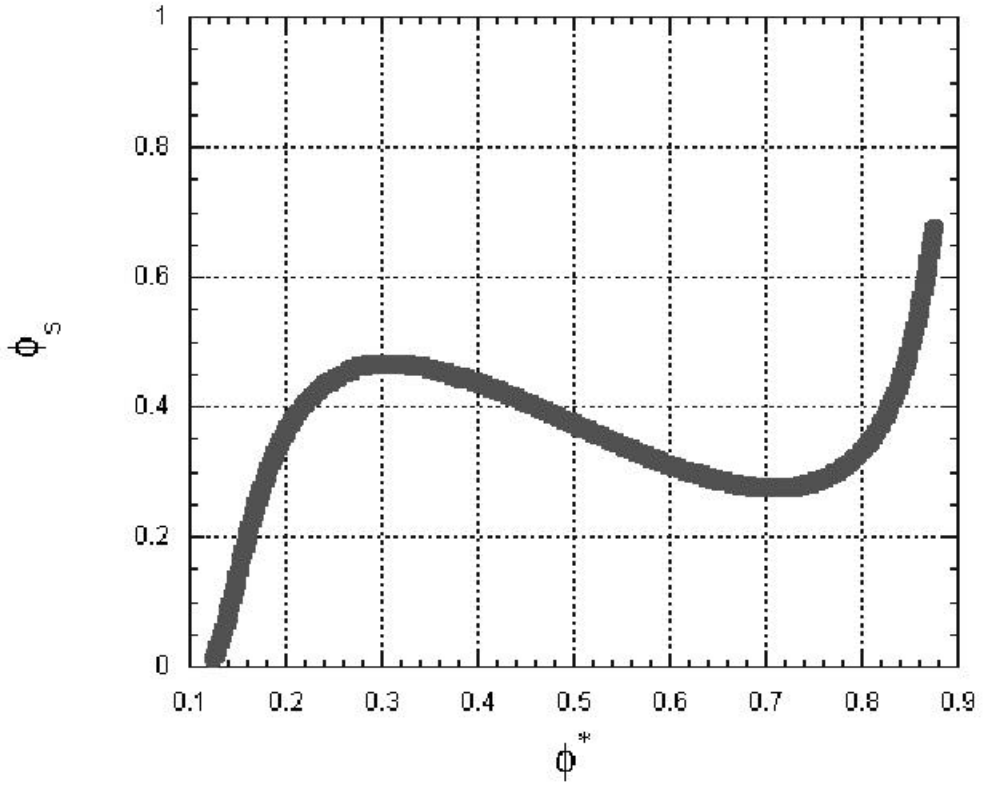

Figure 2.11: Surface concentration (ϕ_s) versus center concentration (ϕ^*) calculated using Equation 2.27. The parameters used for this calculation are χ = 0.026, N = 100, D = 20, a = 1, μ_s = 0.2, and g = -0.5. $\Delta\phi$ = 0.019, where $\Delta\phi$ is the distance mixture composition from the bulk coexistence curve.

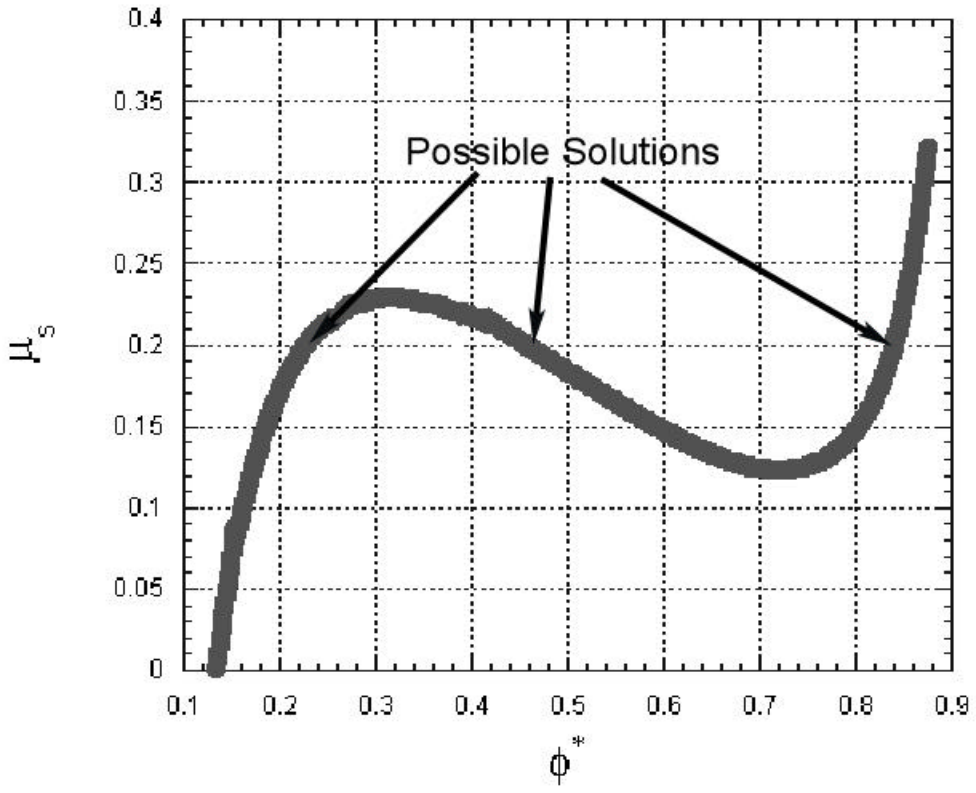

Figure 2.12: Energetic favorablity of species B (μ_s) versus center concentration (ϕ^*) calculated using Equation 2.29, resulting in three potential solutions for the center concentration. The parameters used for this calculation are χ = 0.026, N = 100, D = 20 (nm), a = 1 (nm), μ_s = 0.2, and g = -0.5. $\Delta\phi$ = 0.019, where $\Delta\phi$ is the distance mixture composition from the bulk coexistence curve.

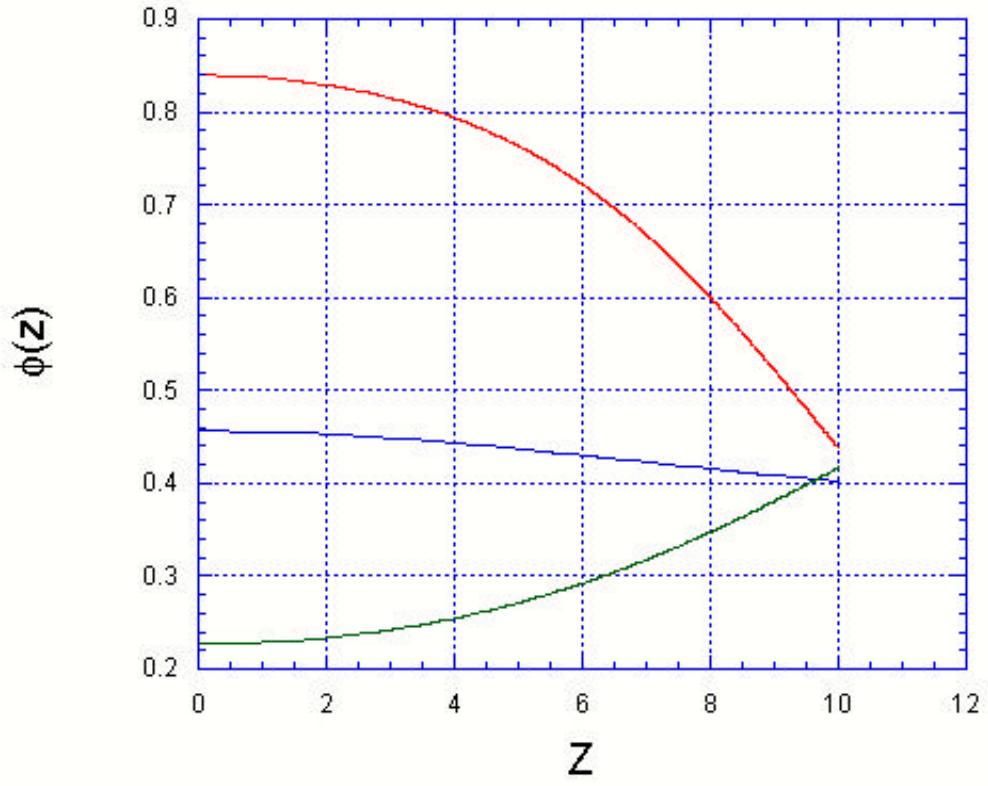

Figure 2.13: Composition profiles for the three solutions in Figure 2.12. Each of these solutions is possible, but only one of them is a free energy minimum as defined by Equation 2.20. For the curve starting at $\phi^* = 0.840$, $\Delta F/k_BT = -0.100$. For the curve starting at $\phi^* = 0.457$, $\Delta F/k_BT = -0.0968$. . For the curve starting at $\phi^* = 0.227$, $\Delta F/k_BT = -0.0973$. Consequently, in this situation the curve starting at $\phi^* = 0.840$ is the most stable solution.

polymer A to the substrate is given in Figure 2.14. The following values were used as the parameters of the simulation: N = 100, D = 20, a = 1 , μ_s = -0.2, and g = 0.5, The simulation results show that as the thickness of the film is reduced, the confinement induces stability in phase separation in the x-y plane parallel to the substrate. The significance of these results will be discussed further in Chapter 4.

2.4 CONCLUSIONS

The technique developed by Flebbe is adequate for the determination of phase diagrams for thin films when h > 5Rg. It does, however, have many limitations. First, the technique assumes that the surface potentials are symmetric and is not easily modified to account for asymmetric potentials. Second, the technique, as designed, finds only the binodal and does not provide any information about the spinodal. Third, determining the profile for films thinner than 5Rg is not possible, because conformational entropy is not taken into account. Finally, this technique provides no convenient way to account for long range effects on the segregation of polymers to the interface. A new technique for calculating the phase diagram and composition profiles in thin and ultra thin films, which addresses these issues, is presented in Chapter 4.

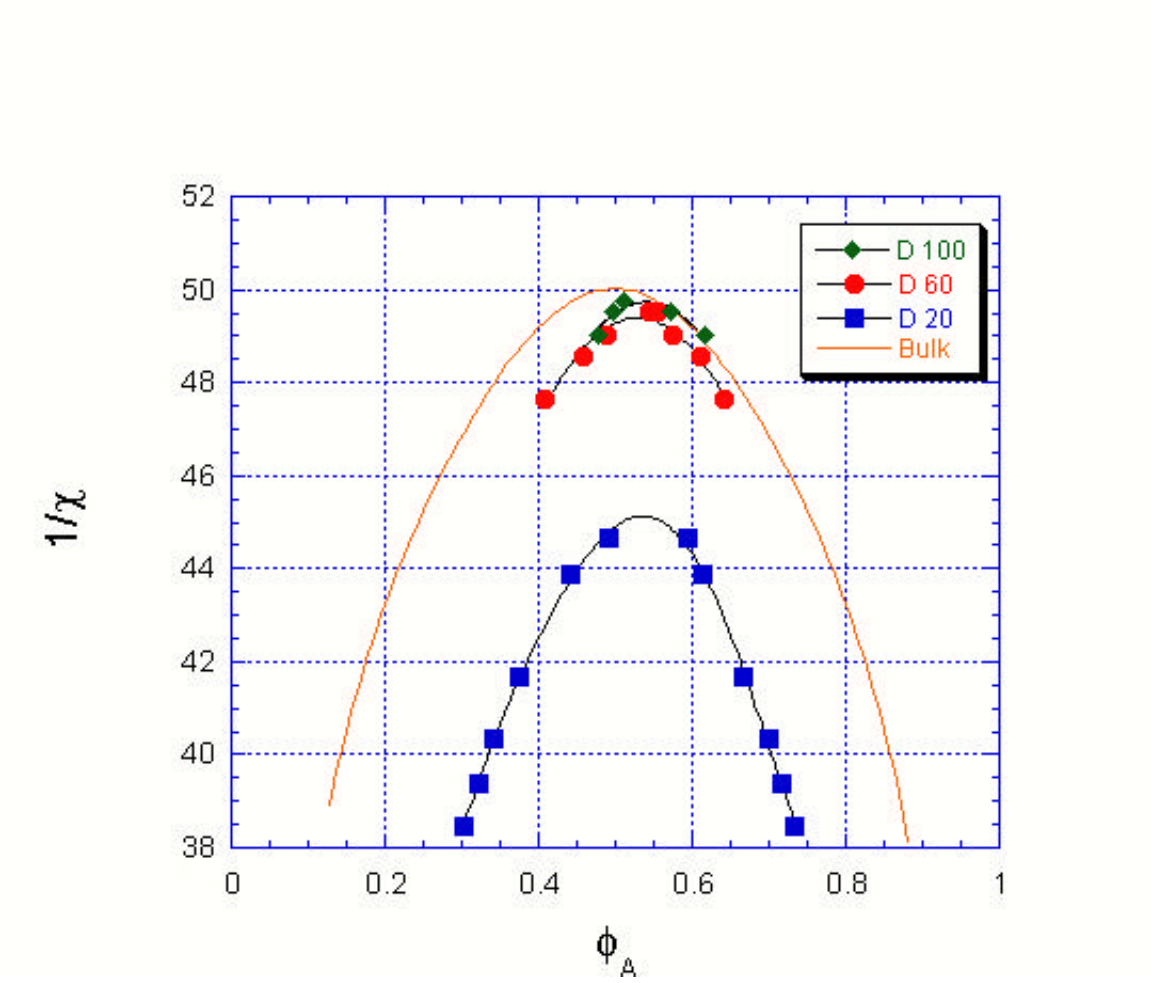

Figure 2.14: Phase diagrams calculated using the FORTRAN program. Simulation input parameters are N = 100, a = 1 (nm), μ_s = -0.2, and g = 0.5. This simulation shows that as the thickness of the film is reduced, the confinement induces stability in phase separation in the x-y plane parallel to the substrate.

2.5 REFERENCES

2.1 Jones, R.A.L., *et al.*, "Surface enrichment in an isotopic polymer blend," *Phys. Rev. Lett.*, 62(3) 1989 p. 280-3.

2.2 Jones, R.A.L., *et al.*, "Surface enrichment in polymer blends: simple theory and an experimental test," *Mater. Res. Soc. Symp. Proc.*, 153(Interfaces Polym., Met., Ceram.) 1989 p. 133-41.

2.3 Jones, R.A.L., *et al.*, "The form of the enriched surface layer in polymer blends," *Europhys. Lett.*, 12(1) 1990 p. 41-6.

2.4 Schmidt, I. and K. Binder, "Model calculations for wetting transitions in polymer mixtures," *J. Phys. (Les Ulis, Fr.)*, 46(10) 1985 p. 1631-44.

2.5 Genzer, J. and R.J. Composto, "A self-consistent field study of the wetting transition in binary polymer blends," *J. Chem. Phys.*, 106(3) 1997 p. 1257-1263.

2.6 Binder, K., "Phase Transitions in Polymer Blends and Block Copolymer Melts: Some Recent Developments," *Advances in Polymer Science*, 112 1994 p. 181-299.

2.7 Binder, K., "Surface effects on polymer blends and block copolymer melts: theoretical concepts of surface enrichment, surface induced phase separation and ordering," *Acta Polym.*, 46(3) 1995 p. 204-25.

2.8 Binder, K., D.P. Landau, and A.M. Ferrenberg, "Thin Ising films with competing walls: A Monte Carlo study," *Phys. Rev. E: Stat. Phys., Plasmas, Fluids, Relat. Interdiscip. Top.*, 51(4-A) 1995 p. 2823-38.

2.9 Binder, K., *et al.*, "Interface localization transition in Ising films with competing walls: Ginzburg criterion and crossover scaling," *Phys. Rev. E: Stat. Phys., Plasmas, Fluids, Relat. Interdiscip. Top.*, 53(5-B) 1996 p. 5023-5034.

2.10 Binder, K., P. Nielaba, and V. Pereyra, "Phase coexistence in binary mixtures in thin films with symmetric walls: model calculations for two- and three-dimensional Ising lattices," *Z. Phys. B: Condens. Matter*, 104(1) 1997 p. 81-98.

2.11 Binder, K., "Phase Transitions of Polymer Blends and Block Copolymer Melts in Thin Films," *Avances in Polymer Science*, 138 1999 p. 1-89.

2.12 Binder, K., M Muller, and E.V. Albano, "Symmetric binary polymer blends confined in thin films between competing walls: Interplay between finite size and wetting behavior," *Physical Chemistry Chemical Physics*, 3(7) 2001 p. 1160-1168.

2.13 Brazhnik, P.K., K.F. Freed, and H. Tang, "Polymer melt near a solid wall," *J. Chem. Phys.*, 101(10) 1994 p. 9143-54.

2.14 Muller, M., K. Binder, and E.V. Albano, "Non-monotonous crossover between capillary condensation and interface localisation/delocalisation transition in binary polymer blends," *Europhysics Letters*, 50(6) 2000 p. 724-730.

2.15 Muller, M., K. Binder, and E.V. Albano, "Finite size effects on the phase diagram of a binary mixture confined between competing walls," *Los*

Alamos National Laboratory, Preprint Archive, Condensed Matter, 2000 p. 1-6, arXiv:cond-mat/0005060.

2.16 Muller, M., K. Binder, and E.V. Albano, "Phase diagram of polymer blends in confined geometry," *Journal of Molecular Liquids*, 92(1-2) 2001 p. 41-52.

2.17 Muller, M., K. Binder, and E.V. Albano, "Phase equilibria in thin polymer films," *International Journal of Modern Physics B*, 15(13) 2001 p. 1867-1903.

2.18 Muller-Buschbaum, P. and M. Stamm, "Film thickness dependence of the domain size in weakly incompatible thin polymer blend films," *Colloid and Polymer Science*, 279(4) 2001 p. 376-381.

2.19 Cserhati, C., I.A. Szabo, and D.L. Beke, "Segregation and phase separation in thin films," *Nanostructured Materials*, 10(2) 1998 p. 195-204.

2.20 Cherrabi, R., A. Saout-Elhak, and M. Benhamou, "Phase separation of polymer blends in solution near adsorbing surface," *European Physical Journal E: Soft Matter*, 2(1) 2000 p. 91-101.

2.21 Cherrabi, R., *et al.*, "Phase separation in confined polymer blends," *Journal of Chemical Physics*, 111(17) 1999 p. 8174-8181.

2.22 Hariharan, A., *et al.*, "The effect of finite film thickness on the surface segregation in symmetric binary polymer mixtures," *J. Chem. Phys.*, 99(1) 1993 p. 656-63.

2.23 Saout-Elhak, A., M. Benhamou, and M. Daoud, "Phase separation in polymer blends near a surface," *J. Phys. II*, 7(3) 1997 p. 503-516.

2.24 Genzer, J. and R.J. Composto, "Surface segregation amplification in miscible polymer blends near criticality," *Europhys. Lett.*, 38(3) 1997 p. 171-176.

2.25 Zhu, S., *et al.*, "Confinement-induced miscibility in polymer blends," *Nature (London)*, 400(6739) 1999 p. 49-51.

2.26 Zhao, W., *et al.*, "Neutron and x-ray reflectivity measurements of polystyrene/poly(bromostyrene) (PS/PBrS) interfaces," *Physica B (Amsterdam)*, 173(1-2) 1991 p. 43-6.

2.27 Wang, H. and R.J. Composto, "Thin film polymer blends undergoing phase separation and wetting: Identification of early, intermediate, and late stages," *J. Chem. Phys.*, 113(22) 2000 p. 10386-10397.

2.28 Tang, H., I. Szleifer, and S.K. Kumar, "Critical temperature shifts in thin polymer blend films," *J. Chem. Phys.*, 100(7) 1994 p. 5367-71.

2.29 Tanaka, K., A. Takahara, and T. Kajiyama, "Film Thickness Dependence of the Surface Structure of Immiscible Polystyrene/Poly(methyl methacrylate) Blends," *Macromolecules*, 29(9) 1996 p. 3232-9.

2.30 Tanaka, K., *et al.*, "Ultrathinning-Induced Surface Phase Separation of Polystyrene/Poly(vinyl methyl ether) Blend Film," *Macromolecules*, 28(4) 1995 p. 934-8.

2.31 Scheffold, F., *et al.*, "Surface phase behavior in binary polymer mixtures. I. Miscibility, phase coexistence, and interactions in polyolefin blends," *J. Chem. Phys.*, 104(21) 1996 p. 8786-8794.

2.32 Scheffold, F., *et al.*, "Surface phase behavior in binary polymer mixtures. II. Surface enrichment from polyolefin blends," *J. Chem. Phys.*, 104(21) 1996 p. 8795-8806.

2.33 Slep, D., *et al.*, "Phase Separation of Polystyrene and Bromo-Polystyrene Mixtures in Equilibrium Structures in Thin Films," *Langmuir*, 14(17) 1998 p. 4860-4864.

2.34 Budkowski, A., *et al.*, "Surface phase behavior in binary polymer mixtures. III. Temperature dependence of surface enrichment and of wetting," *J. Chem. Phys.*, 106(2) 1997 p. 719-727.

2.35 Cahn, J.W., "Critical point wetting," *J. Chem. Phys.*, 66(8) 1977 p. 3667-72.

2.36 De Gennes, P.G., "Wetting: statics and dynamics," *Rev. Mod. Phys.*, 57(3, Pt. 1) 1985 p. 827-63.

2.37 Pandit, R., M. Schick, and M. Wortis, "Systematics of multilayer adsorption phenomena on attractive substrates," *Phys. Rev. B: Condens. Matter*, 26(9) 1982 p. 5112-40.

2.38 Pandit, R. and M. Wortis, "Surfaces and interfaces of lattice models: Mean-field theory as an area-preserving map," *Physical Review B*, 25(5) 1982 p. 3226-3241.

2.39 Joanny, J.F. and L. Leibler, *J. Phys. (Paris)*, 39 1978 p. 951.

2.40 Helfand, E. and Y. Tagami, *J. Chem. Phys.*, 56 1971 p. 3592.

2.41 Flebbe, T., B. Duenweg, and K. Binder, "Phase separation versus wetting: a mean field theory for symmetrical polymer mixtures confined between selectively attractive walls," *J. Phys. II (France)*, 6(5) 1996 p. 667-695.

2.42 Rouault, Y., J. Baschnagel, and K. Binder, "Phase Separation of Symmetrical Polymer Mixtures in Thin-Film Geometry," *Journal of Statistical Physics*, 80(5/6) 1995 p. 1995.

2.43 Cohen, S.M. and M. Muthukumar, "Critical wetting in two-component polymer blends," *J. Chem. Phys.*, 90(10) 1989 p. 5749-55.

2.44 Fredrickson, G.H. and J.P. Donley, "Influence of broken conformational symmetry on the surface enrichment of polymer blends," *J. Chem. Phys.*, 97(12) 1992 p. 8941-6.

2.45 Donley, J.P. and G.H. Fredrickson, "Influence of conformational asymmetry on the surface enrichment of polymer blends. II," *J. Polym. Sci., Part B: Polym. Phys.*, 33(9) 1995 p. 1343-51.

Chapter 3: Thin Film Wetting and Stability

3.1 INTRODUCTION

Thus far, I have discussed the effect of interfacial interactions on the local composition profile of an A-B polymer-polymer mixture of semi-infinite thickness. In addition, I have shown that if the mixture is a film of thickness h, and h is less than 100 R_g, then the composition profile for the entire sample differs from the bulk composition profile. In fact, for the symmetric wetting case the UCST shifts to lower temperatures as h decreases, indicating that the mixture becomes more stable. There is an additional factor that influences the structure of the sample that becomes important when h is on the order of many nanometers. Long-range van der Waals forces can destabilize the structure of the film. This phenomenon is well known in thin non-polar homopolymer films.

Most of this chapter will be devoted to a discussion of the role of long and short-range intermolecular forces on the stability, lateral homogeneity, and uniformity of thin films. The chapter is concluded with experimental results showing how phase separation, destabilizing long-range forces, and attractive short-range interfacial interactions affect the structure of a thin film polymer-polymer mixture. The results in this chapter provide a rationale for Chapter 4, which addresses limitations of the Flebbe and Binder calculations and provide a backdrop for the topics addressed in future chapters.

3.2 WETTING

The surface free energy per molecule can be thought of as the difference between the energy of interaction between a molecule in contact with like molecules and the same molecule in contact with an interface of a free surface. Alternatively, one may consider the work, δw, needed to increase the area, δA, of contact between two phases [3.1],

$$dw = \gamma dA \tag{3.1}$$

where γ is a proportionality constant known as the surface energy or equivalently, the surface tension (force per unit length).

The spreading coefficient can be then be used to understand the tendency of a drop of polymer to wet or not wet a substrate. Figure 3.1(a) illustrates a sessile drop on a solid surface, where both the drop and the solid surface are in contact with the vapor phase. The interfacial forces acting on the three phase contact line are the liquid-vapor surface tension (γ_{LV}), the solid-liquid surface tension (γ_{SL}), and the solid-vapor surface tension (γ_{SV}). The surface tension is determined by short-range (< 1 nm) interactions between the phases. These forces define the spreading coefficient (S),

$$S = \gamma_{SV} - \gamma_{LV} - \gamma_{SL}. \tag{3.2}$$

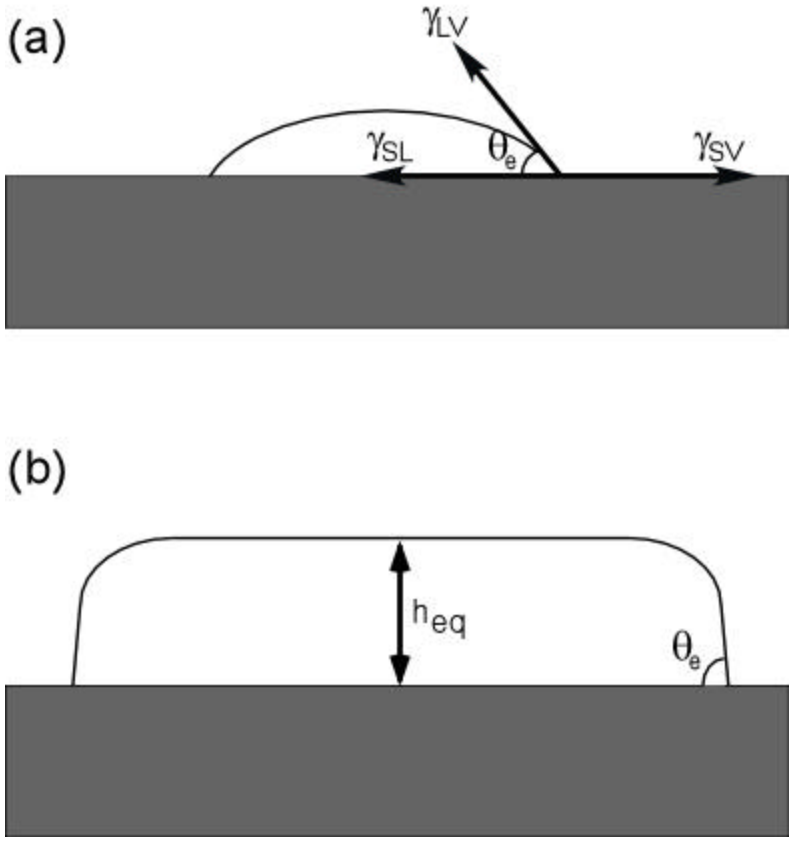

Figure 3.1: (a) A sessile liquid drop in contact with a solid surface and vapor phase. The contact angle θ_e is determined using Young's equation, and is dependant on the balance of the three surface energies at the triple line of contact. (b) A drop for which the effects of gravity are not negligible. h_{eq} is the equilibrium drop height and is determined using Equation 3.4. (Pictures are not drawn in the same scale).

When the spreading coefficient S < 0 the liquid will not wet the substrate. The energy per unit area required to create both the liquid-vapor and solid-liquid interfaces exceeds γ_{SV}, on the other hand, when S ≥ 0 the liquid will spread on the substrate. The equilibrium angle of contact, θ_e, at the three phase line of contact is described by Young's equation [3.2],

$$g_{SV} = g_{SL} + g_{LV}\cos(q_e). \tag{3.3}$$

Sufficiently large droplets can spread under the influence of gravity. This effect is illustrated in Figure 3.1(b), where a large droplet is flattened due to gravity. The equilibrium height of this flattened droplet is [3.3]

$$h_{eq} = 2\left(\frac{g_{LV}}{rg}\right)^{\frac{1}{2}}\sin\left(\frac{q_e}{2}\right) \tag{3.4}$$

where g is the gravitational constant and ρ is the density.

For non-polar films of $h << h_{eq}$, gravitational effects are not important.

Moreover, the spreading coefficient alone is not sufficient to describe the wetting characteristics of the film. This effect is discussed further in the following section.

3.3 LONG-RANGE FORCES AND STABILITY OF THIN FILMS

Short-range interactions between molecules are significant for distances of d < 1 nanometer ($Force_{(SR)} \propto d^{-8}$), while long-range between macroscopic bodies act over distances on the order of many nanometers. In the case of two non-polar surfaces separated by a distance d in a vacuum, the force is attractive and the

interaction energy per unit area $\propto d^{-2}$. These interactions in non-polar polymers are due to ubiquitous apolar van der Waals forces. The strength of the interaction can be expressed in terms of a Hamaker constant $A_{11} > 0$.

A slightly more complicated case involves a thin liquid film of thickness h on a substrate. The effective Hamaker constant can be determined from the Hamaker constants, A_{ii}, of the three media, i = 1 (substrate), 2 (vapor), 3 (liquid) using the following equation:

$$A_{132} = \left(\sqrt{A_{11}} - \sqrt{A_{33}}\right)\left(\sqrt{A_{22}} - \sqrt{A_{33}}\right). \tag{3.5}$$

A_{132} can be approximated using the dispersive part of the individual surface tensions [3.4],

$$A_{132} \approx 24\pi\delta_o^{\,2}\left(\sqrt{\gamma_1^{\,D}} - \sqrt{\gamma_3^{\,D}}\right)\left(\sqrt{\gamma_2^{\,D}} - \sqrt{\gamma_3^{\,D}}\right) \tag{3.6}$$

where δ_o is the atomic cut-off distance and γ_i^D is the dispersive part of the surface tension.

The total excess free energy (ΔG) of interaction per unit area or equivalently, the effective interface potential (Φ) is given by [3.5, 3.6]

$$\Delta G(h) = \Phi(h) = \frac{-A_{132}}{12\pi h^2} \tag{3.7}$$

where h is the thickness. The sign associated with the effective Hamaker constant A_{132} determines if materials 1 and 2 attract or repel each other through medium 3. If $A_{132} < 0$ then the there is repulsion between material 1 and 2 and the film will be stable since thinning the intermediate layer 3 increases the free energy of the system. On the other hand if $A_{132} > 0$ then the system is unstable due to the decrease in free energy as layers 1 and 2 attract each other through thinning layer 3.

The stability of thin films is commonly discussed in terms of the disjoining pressure, Π, the negative of the derivative of the total excess free energy described in Equation 3.7,

$$\Pi(h) = -\frac{\partial \Delta G}{\partial h} = -\frac{A_{132}}{6\pi h^3}. \tag{3.8}$$

If $A_{132} > 0$, then a fluctuation in the thickness of a polymer film, as seen in Figure 3.2, will become amplified. Hence a larger pressure exists in thinner regions of the film resulting in a net flow of polymer from the thinner regions to the thicker regions, causing the instability to grow. However, as the instability grows, the area of contact between the polymer and the vapor increases. This increase in surface area thereby increases the free energy. The Laplace pressure, which is defined as the ratio of γ_{LV} to the local radius of curvature of the film, attempts to flatten the film surface. It is the balance between the destabilizing disjoining pressure and the stabilizing Laplace pressure that determines the critical wavelength beyond which the instabilities will grow.

The growth of capillary waves at an interface has be modeled using linear stability [3.7]. The fluctuations in the surface of the polymer film z(x,t), as seen in Figure 3.2, are modeled using the following expression [3.7]:

$$z(x,t) = h + \delta h \exp(iqx) \tag{3.9}$$

where

$$\delta h = \delta h_o \exp\left(\frac{t}{\tau}\right), \tag{3.10}$$

h is the initial film thickness, q is the wave vector (where q is related to wavelength by the relationship $q=2\pi/\lambda$), δh_o is the magnitude of the disturbance, t is time, τ is relaxation time, and x is a coordinate parallel to the surface.

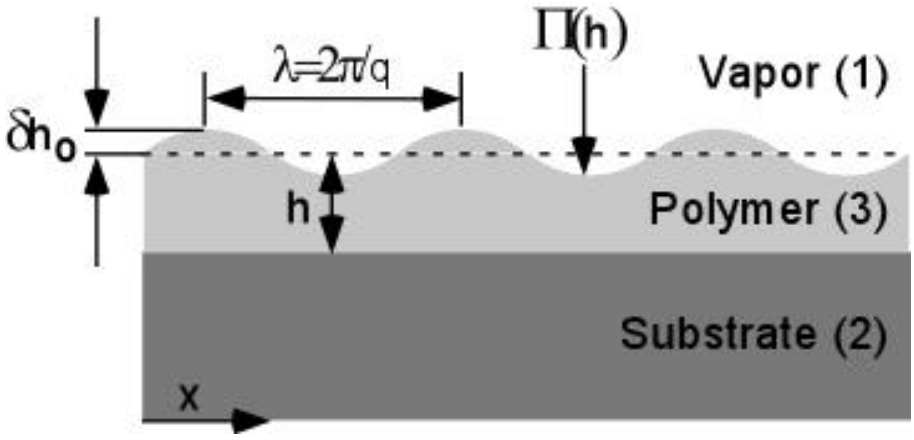

Figure 3.2: Capillary wave instability at an interface are amplified by attractive van der Waals forces between the vapor (1) and the substrate (2) through the polymer. The linear stability analysis of capillary instabilities assumes an initial film of thickness (h) is subject to a sinusoidal disturbance characterized by magnitude of the disturbance δh_o and a wavelength of the disturbance λ.

The modulation described by Equation 3.9 creates a pressure gradient, which induces a Poiseuille flow J in the film [3.7]:

$$J = \frac{z^3}{3\eta}\left[g\frac{\partial^3 z}{\partial x^3} - \frac{\partial \Pi}{\partial x} \right] \tag{3.11}$$

where γ is the surface tension at the film-vapor interface and η is the viscosity of the liquid. The first term in the brackets of Equation 3.11 represents the Laplace pressure and the second term represents the disjoining pressure. Conservation of mass gives

$$\nabla J + \frac{\partial z}{\partial t} = 0 . \tag{3.12}$$

By linearizing Equations 3.11 and 3.12, and looking for the solution given by Equation 3.9, the following dispersion relation is obtained [3.7]:

$$\frac{1}{\tau} = \frac{h^3}{3\eta}\left[-gq^4 + \frac{A_{132}q^2}{2\pi h^4} \right]. \tag{3.13}$$

The fluctuations will only grow if $1/\tau > 0$, so as stated previously, A_{132} must be positive. It can be seen from Equation 3.13 that if A_{132} is positive then $1/\tau$ will only be positive if q is below a critical value q_c:

$$q_c = \sqrt{\frac{3A_{132}}{2\pi\gamma}}\frac{1}{h^2} . \tag{3.14}$$

There are many values of q below which the instabilities grow, but there is one value of q that is the fastest growing mode, q_m. The fastest growing mode is associated with the value of q for which τ is smallest τ_m:

$$q_m = \sqrt{\frac{3A_{132}}{4\pi\gamma}}\frac{1}{h^2} \tag{3.15}$$

$$\tau_m = \frac{48\pi^2 \eta_0 h_0^5}{A_{132}} \tag{3.16}$$

When the instabilities reach the surface of substrate, the undulations will no longer be characterized by $q_{m.}$

3.4 FREE ENERGY DIAGRAMS AND DEWETTING PATTERNS

Spontaneous amplification of fluctuations, otherwise known as "spinodal dewetting", can occur in sufficiently thin films. In thicker films, dewetting can also occur by nucleation and growth of holes on the substrate. An AFM image of spinodal dewetting of a polymer film is shown in Figure 3.3(a) and nucleation and growth of holes is shown in Figure 3.3(b). In order to understand the mechanism by which dewetting will occur, the free energy (ΔG), or effective interface potential (Φ), must be investigated as a function of film thickness. Stability of a film can easily be recognized by plotting Φ'' as a function of film thickness. The film will seek to minimize its free energy, so if decreasing the film thickness increases the free energy, as seen in Figure 3.4, then the film will tend to maximize its film thickness, $\Phi'' > 0$. Consequently the film is stable and will not dewet. On the other hand, if the free energy decreases with film thickness as seen in Figure 3.5(a) then a film will seek to minimize its free energy by thinning and the film will become unstable. The mechanism by which the film will become unstable is related to the derivative of the disjoining pressure with respect to thickness $\frac{d\Pi}{dh}$. It was shown that for spinodal dewetting the fastest growing mode is given by Equation 3.13, from which it can be shown that:

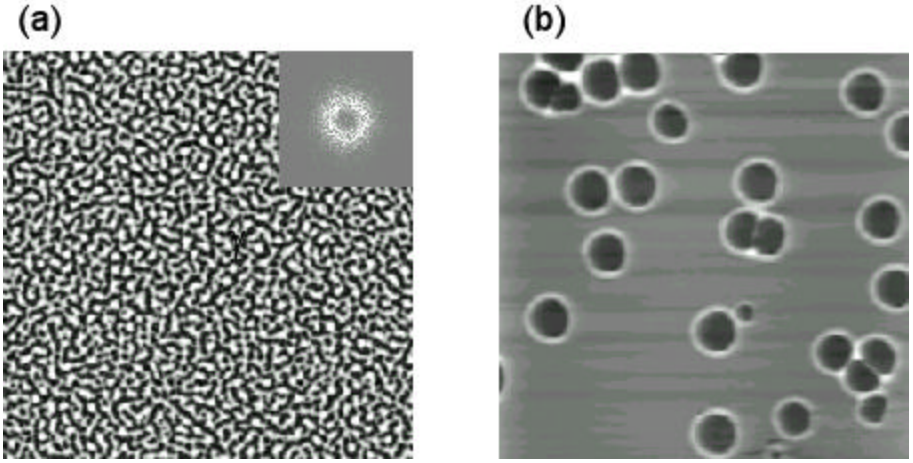

Figure 3.3: (a) AFM image of a polymer film exhibiting spinodal dewetting. The insert contains a 2-D fft of the image. The ring indicates that there is a characteristic wave vector for the undulations, as would be expected for spontaneous amplification of capillary wave fluctuations. (b) AFM image of a polymer film exhibiting dewetting via nucleation and growth of holes. The image illustrates that the holes build up material at their edges forming rims.

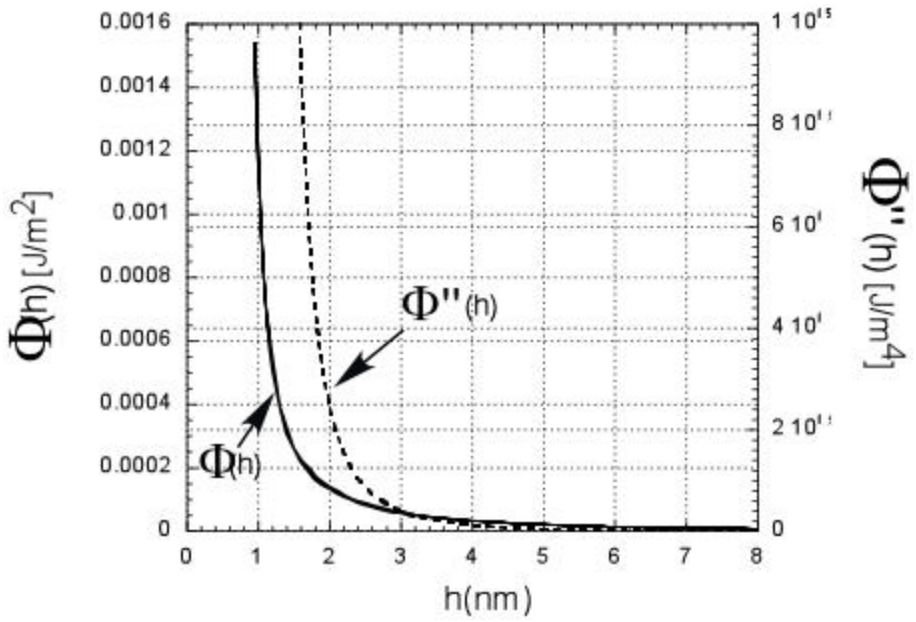

Figure 3.4: The left Y axis is the effective interface potential of a film as a function of film thickness for A_{132} = -2E10^{-20} J/m^2. The potential increases with decreasing film thickness indicating that the film is stable. The right Y axis is the second derivative of the effective interface potential with respect to h and is positive for all values of h indicating that spinodal dewetting is not preferred (as would be expected for a stable film).

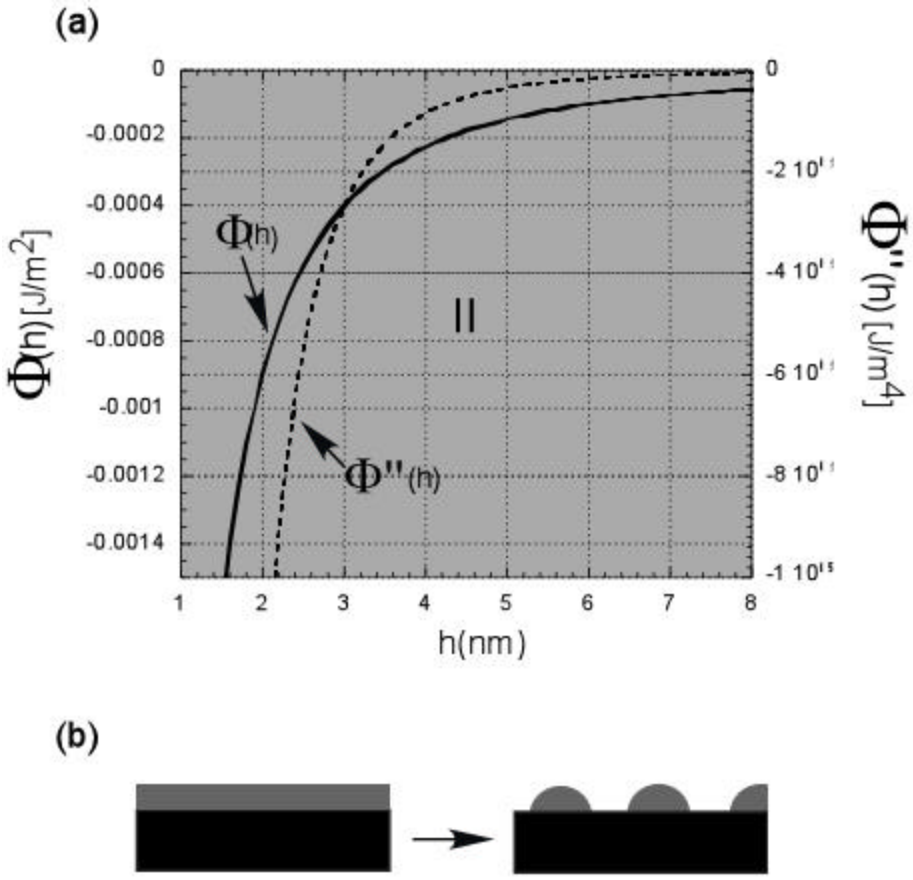

Figure 3.5: (a) The left Y axis is the effective interface potential of a film as a function of film thickness for $A_{132} = 2E10^{-20}$ J/m^2. The potential decreases with decreasing film thickness indicating that the film is unstable. The right Y axis is the second derivative of the effective interface potential with respect to h and is negative for all values of h indicating that spinodal dewetting will occur for this film at these thicknesses (labeled by the roman numeral II). (b) A graphic indicating that a film that exhibited this effective interface potential would become unstable and dewet.

$$q_m = \sqrt{\frac{-\frac{d^2\Phi}{dh^2}}{2}} \tag{3.17}$$

where

$$\frac{d^2\Phi}{dh^2} = \frac{-A_{132}}{2\pi h^4}. \tag{3.18}$$

In order for q_m to be a real value, then $\frac{d^2\Phi}{dh^2}$ must be negative. Therefore spinodal dewetting will only occur in systems where $\frac{d^2\Phi}{dh^2} < 0$, as in Figure 3.5(a). If $\frac{d^2\Phi}{dh^2} \geq 0$ and the film seeks to minimize its free energy, it must do so by nucleation and growth of holes. This is generally observed for thicker films.

An additional phenomenon, autophobic dewetting, may also occur. Autophobic dewetting arises when a liquid does not wet itself. The effective interface potential can be modeled by including a term describing the short-range interactions [3.8, 3.9],

$$\Phi(h) = \frac{c}{h^8} + \Phi_{vdW}(h) \tag{3.19}$$

where c is a short-range interaction strength and Φ_{vdw} is the long range van der Waals potential. Equation 3.19 was used to calculate the curve shown in Figure 3.6(a). The free energy minimum is not at zero thickness, but at h = 1.3 nm. In this example, a film where h > 1.3 nm will seek to minimize its free energy by reducing its thickness and will become unstable. So the film will autophobically dewet, leaving behind a thin layer of polymer of thickness h = 1.3 nm. Films that are thinner than 1.3 nm will seek to minimize there free energy by

increasing the film thickness. Figure 3.6(b) shows that $\frac{d^2\Phi}{dh^2} < 0$ for all thicknesses greater than

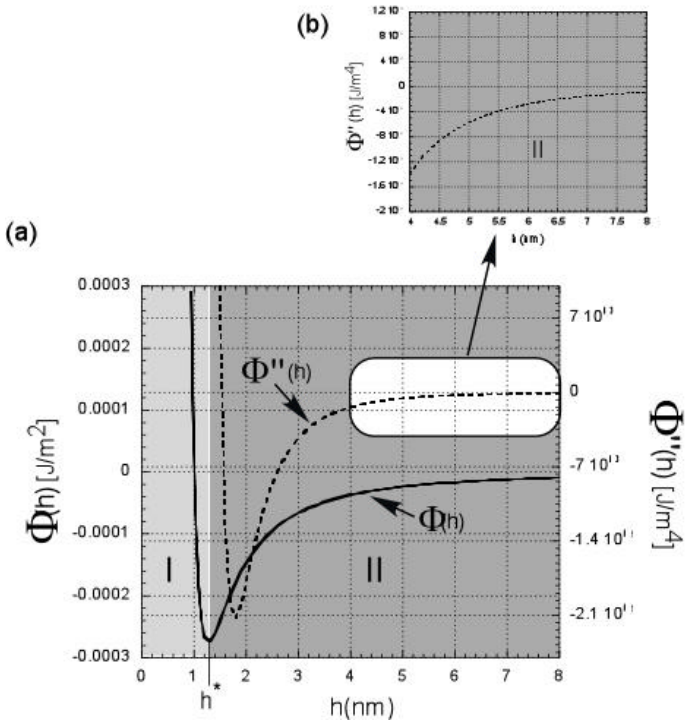

Figure 3.6: (a) The left Y axis is the effective interface potential of a film as a function of film thickness for $A_{132} = 2E10^{-20}$ J and $c = 6.3E10^{-76}$ $J*m^6$. The potential decreases with decreasing film thickness indicating that the film is unstable and has a minimum at h = 1.3 nm. Thus, an equilibrium film will have a wetting layer of 1.3nm. Films thinner than 1.3 nm will attempt to form this wetting layer (shown by the region with roman numeral I). The right Y axis is the second derivative of the effective interface potential with respect to h and is negative for all values of h. Thus, spinodal dewetting will occur for this film at these thicknesses (shown by the roman numeral II). (b) A blow up of graph a showing that $\Phi'' < 0$ at all thicknesses.

1.3 nm, so all of these films will dewet spinodally. Films that exhibit spinodal dewetting and nucleation and growth of holes will have a different effective interface potential as shown in Figure 3.7(a). In this example, the film also seeks to minimize its free energy, but the minimum thickness is at h $\approx$ 1 nm. Figure 3.7(b) shows that $\frac{d^2\Phi}{dh^2} < 0$ for thicknesses above 1 nm, but that $\frac{d^2\Phi}{dh^2} > 0$ for films with thicknesses above 3.8 nm, indicating that these films will dewet via nucleation and growth of holes, rather than a spinodal process.

3.5 CONCLUSIONS

This chapter discussed the effects of both wetting and stability of thin polymer films. Short-range forces affect wetting of thin films directly and the ability of a film to wet a surface can be measured using the spreading coefficient (S). For non-wetting films, the equilibrium contact angle can be determined using Young's equation. Stability of thin polymer films was also discussed. It is the balance between the destabilizing disjoining pressure and the stabilizing Laplace pressure that determines the critical wavelength beyond which the instabilities will grow. Linear stability analysis of capillary wave instabilities was performed to determine the critical wavelength and fastest growing mode of the instabilities. The use of free energy diagrams to predict the stability of thin films was discussed. These free energy diagrams are used to determine if an unstable film will dewet via spinodal instabilities or nucleation and growth of holes.

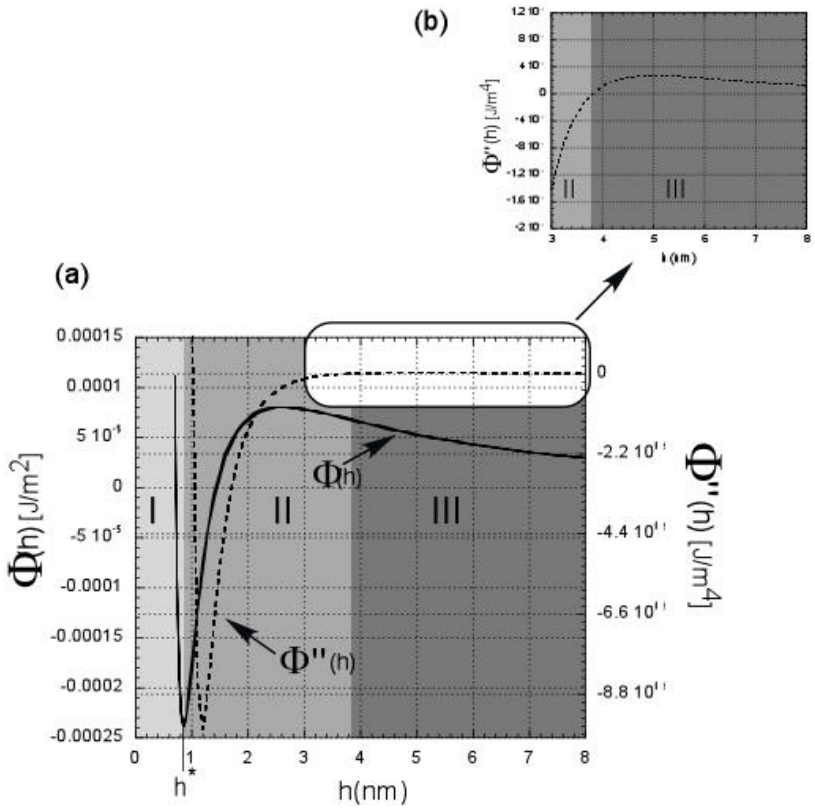

Figure 3.7: (a) The left Y axis is the effective interface potential of a film as a function of film thickness for A_{132} = 2E10^{-20} J and c = 5,11E10^{-77} J*m^6. The potential decreases with decreasing film thickness indicating that the film is unstable and has a minimum at h ≈ 1 nm. Thus, an equilibrium film will have a wetting layer of about 1 nm. Films thinner than 1 nm will attempt to form this wetting layer (shown by the region with roman numeral I). The right Y axis is the second derivative of the effective interface potential with respect to h and is negative for h < 3.8 nm indicating that spinodal dewetting will occur for this film at these thicknesses (shown by the roman numeral II). (b) A blow up of graph a showing that Φ" > 0 at h > 3.8 nm, implying that nucleation and growth of holes will cause dewetting of these films.

3.6 SUMMARY OF INTRODUCTORY CHAPTERS AND DISSERTATION OUTLINE

The first three chapters have covered three topics in relation to my research problem. The first chapter discussed bulk polymer phase separation. The second chapter covered segregation in confined geometeries, including semi-infinite, thin films, and ultra-thin films. Finally, the effect of long and short-range forces on the stability of thin polymer films was discussed.

I am interested in understanding ultra-thin film mixtures of styrene-acrylonitryle random co-polymers with poly-methylmethacrylate. These blends were coated on the surface of various substrates and annealed above their glass transition temperatures. The results of some of these experiments can be seen in Figures 3.8 and 3.9. The films have begun to dewet the surface of the substrate, but the type of dewetting is dependant on the copolymer composition. From Figure 3.10 it is obvious that the droplets of dewetting polymer are not homogeneous in composition. Such patterns are usually due to the antagonistic action of long and short-range intermolecular forces that influence stability of films in the thickness range of $h < 10$ nm. I observed similar patterns over a wider range of film thickness, depending on the composition of the SAN copolymer. These observations can not be rationalized in terms of the current theory.

In Chapter 4, a numerical solution to thin film polymer free energy equations in Chapter 2 will be presented, including the effect of conformational symmetry. The numerical solution will be compared to the results of the Flebbe and Binder analytical approach. It will be shown that in ultra-thin films ($h < 5R_g$),

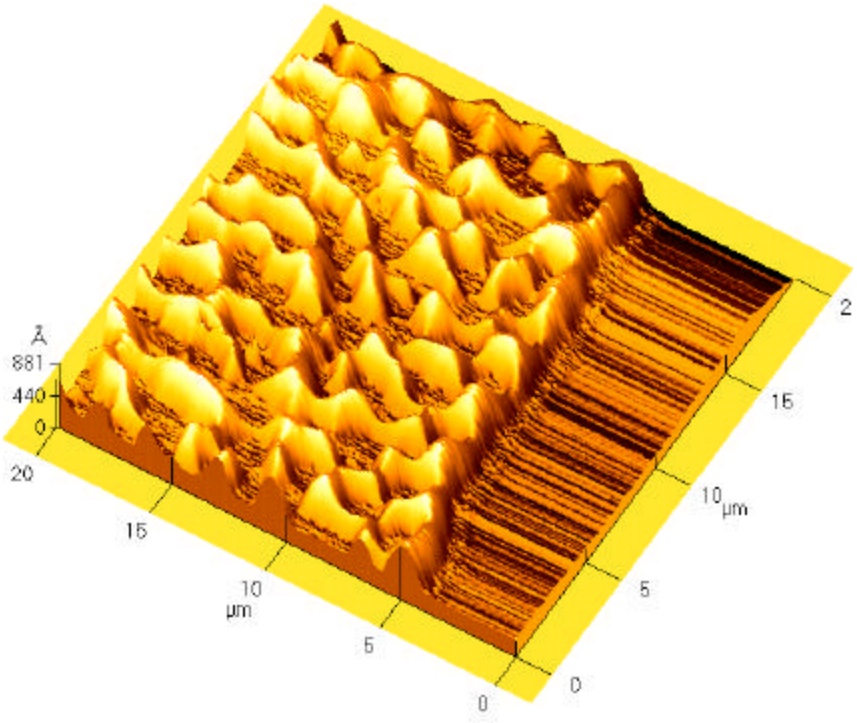

Figure 3.8: AFM scan of SAN-10/PMMA blend annealed at 210 ^{o}C. The polymer has been removed from the right portion of the scan to reveal the location of the substrate. There is obviously a wetting layer on the substrate, with dewet polymer layer. The pattern of droplets on the wetting layer seem to be consistent with spinodal dewetting.

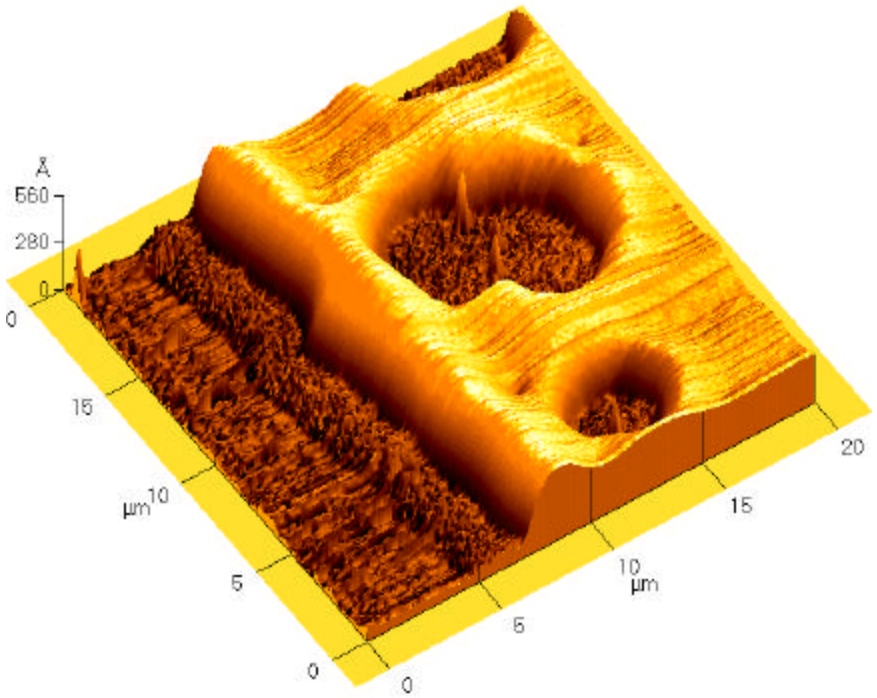

Figure 3.9: AFM scan of SAN-25/PMMA blend annealed at 210 ^{o}C. The polymer has been removed from the left portion of the scan to reveal the location of the substrate. There is obviously a wetting layer on the substrate, with dewet polymer layer. This blend seems to be dewetting via nucleation and growth of holes.

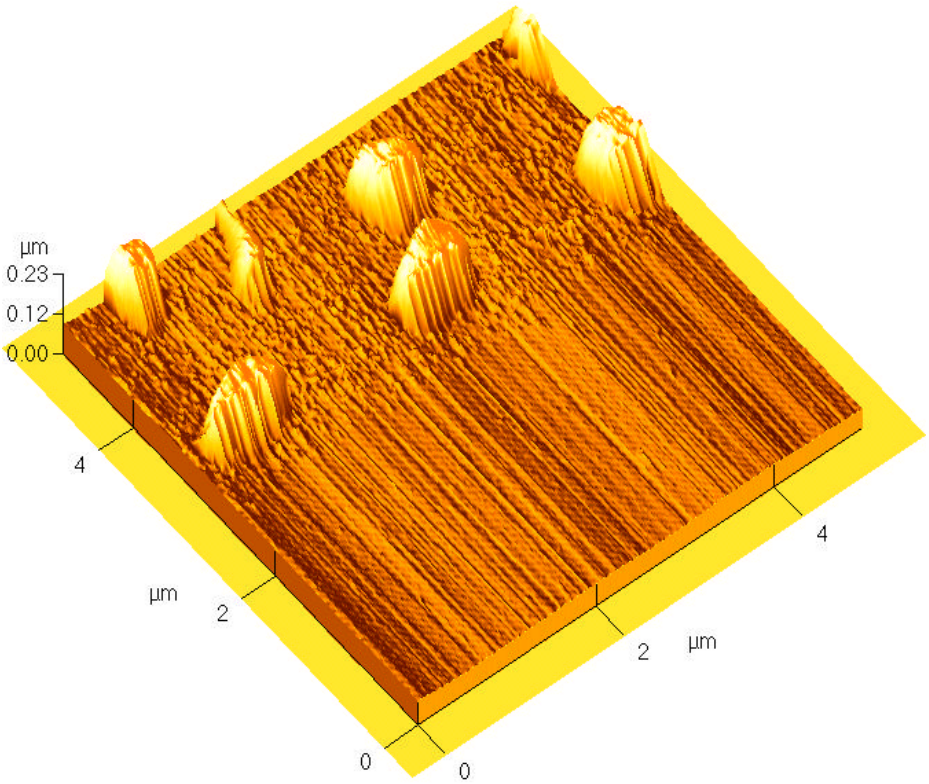

Figure 3.10: AFM scan of SAN-10/PMMA blend annealed at 210 ^{o}C. The polymer has been removed from the right portion of the scan to reveal the location of the substrate. The film has been washed with a solvent to selectively remove the PMMA. This reveals that the core of the droplets contains SAN-10 with an outer layer of PMMA. Obviously, segregation of the polymers has occurred in conjunction with the dewetting.

segmental asymmetry effects (entropic), not accounted for by Binder and coworkers, have a strong influence on the phase behavior of these systems.

These numerical calculations further enable a calculation of the interfacial free energy of the system as a function of film thickness. In Chapter 5, experimental AFM profiles acquired for a variety of ultra thin films of varying SAN copolymer composition, film thickness, and anneal temperature are explained based on these results. This is significant since the topographical instabilities that I observe in these films could not previously be explained.

3.6 REFERENCES

3.1 Hunter, R.J., *Foundations of Colloid Science*. Second ed. 2001: Oxford University Press. 806.

3.2 Cahn, J.W., "Critical point wetting," *J. Chem. Phys.*, 66(8) 1977 p. 3667-72.

3.3 De Gennes, P.G., "Wetting: statics and dynamics," *Rev. Mod. Phys.*, 57(3, Pt. 1) 1985 p. 827-63.

3.4 Reiter, G., *et al.*, "Destabilizing effect of long-range forces in thin liquid films on wettable substrates," *Europhysics Letters*, 46(4) 1999 p. 512-518.

3.5 Israelachvili, J.N., *Intermolecular and surface forces*. 2nd ed. 1991: London: Academic Press. 450.

3.6 Vrij, A. and J.T.G. Overbeek, "Rupture of thin liquid films due to spontaneous fluctuations in thickness," *J. Amer. Chem. Soc.*, 90(12) 1968 p. 3074-8.

3.7 Wyart, B.F. and J. Daillant, "Drying of solids wetted by thin liquid films," *CAN. J. PHYS.*, 68 1990 p. 1084-1088.

3.8 Seemann, R., S. Herminghaus, and K. Jacobs, "Dewetting Patterns and Molecular Forces: A Reconciliation," *Physical Review Letters*, 86(24) 2001 p. 5534-5537.

3.9 Seemann, R., S. Herminghaus, and K. Jacobs, "Gaining control of pattern formation of dewetting liquid films," *Journal of Physics: Condensed Matter*, 13(21) 2001 p. 4925-4938.

Chapter 4: Determination of Wetting and Phase Separation in Ultra-Thin Polymer Films Using Free Energy Optimization

4.1 INTRODUCTION

Segregation in semi-infinite, thin, and ultra thin polymer films was initially presented in Chapter 2 with the Flory-Huggins-DeGennes description of free energy of a polymer mixture at an interface, Equation 2.4 [4.1]. Equation 2.4 can be analytically minimized to develop a series of equations that describe segregation in semi-infinite films (Equations 2.11, 2.12 and 2.14) [4.2, 4.3]. The same approach can be extended to thin films bound by symmetric surfaces, with the addition of an another boundary condition (Equation 2.19) [4.4]. The resulting partial differential equation can also be solved analytically, resulting in two equations that must be solved simultaneously (Equations 2.26 and 2.28) [4.4]. These equations where incorporated into a FORTRAN program (Appendix A) that was used to determine concentration profiles at an interface and the phase diagram for a model system (Figures 2.13 and 2.14).

The approach presented by Flebbe and Binder works well for thin films ($h > 5R_g$), but does not take into consideration segmental symmetry effects. It is generally understood that these effects must be accounted for in order to accurately model segregation in ultra-thin films with thickness $h < 5R_g$ [4.4-4.9]. In this chapter, a novel approach to modeling the segregation in ultra-thin

polymer films, including the effect of segmental symmetry on the concentration profiles, is developed.

The inclusion of the segmental symmetry effects in the free energy function will be discussed. Then the development of a new approach to minimize the free energy function will be presented, along with a Visual Basic program based on this approach. Finally, modeling results will be presented that discuss the effect of segmental symmetry in ultra-thin films.

4.2 POLYMER ASYMMETRY EFFECTS ON SEGREGATION AT AN INTERFACE

The presence of a surface perturbs the conformation of a polymer in proximity to it, leading to an entropic surface potential that can influence the segregation of polymers at an interface. If two polymers have the same effective chain length, the polymer with a smaller statistical segment length will be more flexible [4.8]. The increased flexibility will have a tendency to increase the concentration of the more flexible component at an interface. The second conformational effect is related to two polymers with the same statistical segment length, but different chain lengths. The polymer with the larger chain length will have a larger radius of gyration and consequently the entropic surface potential will be greater near an interface.

The following surface potential was proposed by Fredrickson and Donley [4.8]:

$$w(z) = \frac{4Rg_x}{3\sqrt{\pi N_x}} U\left(\frac{z}{2Rg_x}\right) \tag{4.1}$$

where

$$U(x) \equiv \left(1+x^2\right)\exp\left(-x^2\right) - \sqrt{\pi}\, x\left(x^2+\frac{3}{2}\right) erfc(x), \tag{4.2}$$

N_x is the effective chain length of polymer x, z is the distance from the interface, and Rg_x is the radius of gyration of polymer x given by

$$Rg_x = a_x\left(\frac{N_x}{6}\right)^{\frac{1}{2}}, \tag{4.3}$$

where a_x is the statistical segment length of polymer x. Equations 4.1 to 4.3 are used to develop an expression for the free energy of a polymer blend at a surface related to polymer asymmetry,

$$F_{s(Conf)}(\phi) = \int_0^{D/2} dz[w_A(z) - w_B(z)]\frac{d\phi}{dz}. \tag{4.4}$$

In Equation 4.4, w_A and w_B are related to the surface potentials of polymers A and B, respectively. Equation 4.4 can be combined with Equation 2.19 to provide an expression for the free energy of a polymer mixture confined by two interfaces taking into account polymer asymmetry,

$$\frac{\Delta F}{k_B T} = \int_0^D dz\left\{ f_{FH}[\phi(z)] - \Delta\mu\phi(z) + \kappa\left[\frac{d\phi(z)}{dz}\right]^2 + 2[w_A(z) - w_B(z)]\frac{d\phi(z)}{dz}\right\}$$
$$+ f_s(\phi_0)^{(b)} + f_s(\phi_D)^{(b)}, \tag{4.5}$$

where

$$f_s(\phi_0)^{(b)} = f_s(\phi_D)^{(b)} = -\mu_s\phi_s - \frac{1}{2}g\phi_s^2. \tag{4.6}$$

Despite the fact that Equation 4.5 is similar to Equation 2.19, it does not lend itself to an analytical solution due to the inclusion of the conformational entropy with the concentration gradient term. For this reason a numerical technique was developed to minimize the free energy in Equation 4.5.

4.3 NUMERICAL SOLUTION TO FREE ENERGY EQUATION

Minimization of Equation 4.5 requires that we find a concentration profile $\phi(z)$ that minimizes the free energy ΔF for a specified average polymer concentration, ϕ_{Avg}. The average composition of the profile is related to $\Delta\mu$ and is given by the following equation:

$$\Delta m = \frac{1}{N}\ln\frac{f_{Avg}}{1-f_{Avg}} + c(1-2f_{Avg}). \tag{4.7}$$

The minimization of ΔF would be difficult unless a functional form is assumed for the shape of the profile $\phi(z)$. Choosing a functional form for $\phi(z)$ reduces the number of parameters in the function to be optimized. The hyperbolic tangent function, which is commonly used to describe concentration at polymer interfaces, was used as a model to describe the concentration profile:

$$f(z) = .5\left((f_1 + f_2) + (f_1 - f_2)\tanh\left(\frac{z - z_o}{w}\right)\right). \tag{4.8}$$

Equation 4.8 consists of four adjustable parameters, ϕ_1, ϕ_2, z_o, and w, which allow a variety of concentration profiles to be created. An overview of the effect of each of these parameters on the concentration profile is given in Figure 4.1. This figure shows, for example, how changes in *w* affect the breadth of the profile.

The system to be minimized is a thin polymer film in contact with symmetric surface potentials. Since the system is symmetric about the center of the polymer film, the center of the film will be defined as z=0 and the outer

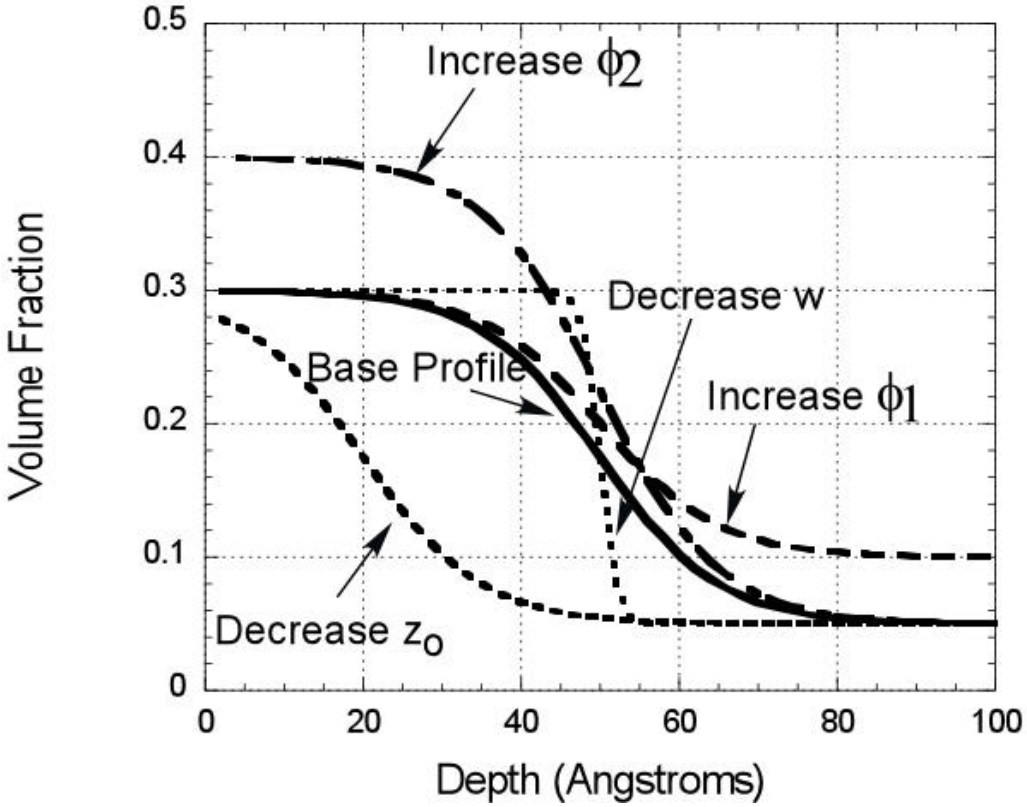

Figure 4.1: Concentration profile in a model polymer film using a hyperbolic tanget function. The base profile is adjusted by modifying each of the parameters in Equation 4.8. Changing ϕ_2 has the effect of modifying the concentration at small values of z. Changing ϕ_1 has the effect of modifying the concentration at large values of z. The parameter z_o controls the position of inflection and w controls the width of the inflection.

surfaces will be located at $z = -\frac{D}{2}$ and $z = \frac{D}{2}$. With this in mind, Equation 4.5 now becomes:

$$\frac{\Delta F}{k_B T} = \int_0^{D/2} dz \left\{ f_{FH}[\phi(z)] - \Delta\mu\phi(z) + \kappa\left[\frac{d\phi(z)}{dz}\right]^2 + [w_A(z) - w_B(z)]\frac{d\phi(z)}{dz} \right\}$$

$$+ f_s(\phi_{D/2})^{(b)}. \qquad (4.9)$$

The process of changing the parameters of Equation 4.8 in order to achieve optimization of Equation 4.9 where the average polymer concentration is $\phi_{A(Avg)} = 0.5$ can be visualized with the aid of Figure 4.2. In this example, the values at the center and the interface are constrained to $\phi_{(z=0)} = 0.6$ and $\phi_{(z=10)} = 0.3$. The value of *w* is fixed and the values of ϕ_1, ϕ_2, z_o are adjusted to create the profile that satisfies the constraints. As Figure 4.2 shows, there exists a limited number of solutions that meet all of the constraints.

If the free energy (ΔF) of the system is plotted as a function of the profile $\phi_{A(Avg)} = 0.85$ and the system is constrained at the center of the film by ϕ^* and at the surface by ϕ_s, Figure 4.3 results. In this plot, each free energy value resulted from a profile that is similar in construction to Figure 4.2, except ϕ_1, ϕ_2, z_o, and *w* were all varied simultaneously to minimize ΔF. As Figure 4.3 shows, there is a clear global minimum in ϕ^* and ϕ_s, so allowing these values to vary as $\phi(z, \phi_1, \phi_2, z_o, w)$ is optimized subject to a constrained $\phi_{A(Avg)}$, $\phi_{A(Max)}$, and $\phi_{A(Min)}$ should result in a global minimum.

The optimization of this function proceeds as follows. First, all of the input parameters (a_A, a_B, χ, N_A, N_B, g, μ_s, and $\frac{D}{2}$) are collected and passed to a

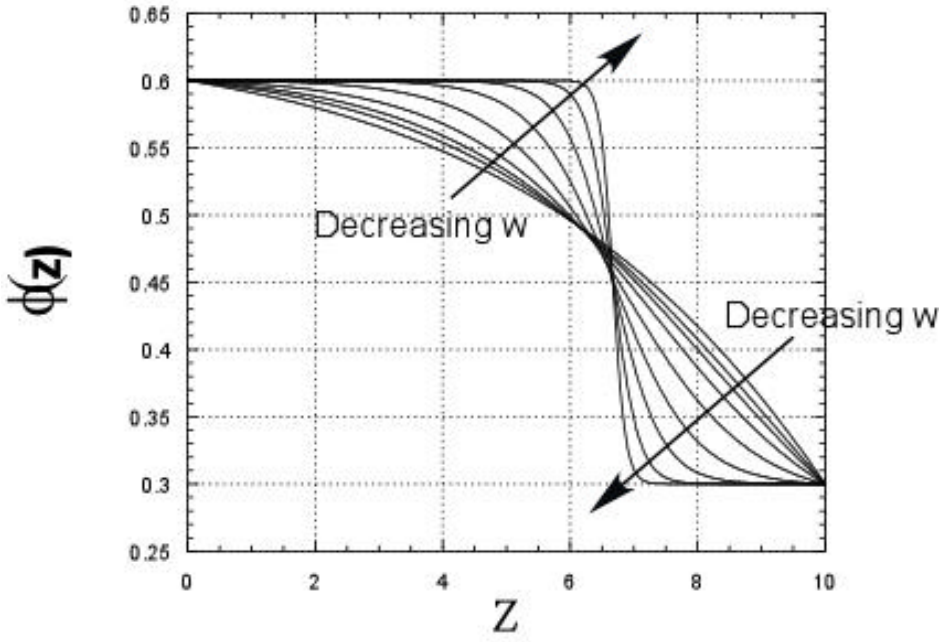

Figure 4.2: Visualization of possible minimized profiles using hyperbolic tangent function. The values at the center and the interface are constrained to $\phi_{(z=0)} = 0.6$ and $\phi_{(z=10)} = 0.3$. The average polymer concentration is $\phi_{A(Avg)} = 0.5$. The parameters ϕ_1, ϕ_2, z_o are adjusted to meet these constraints.

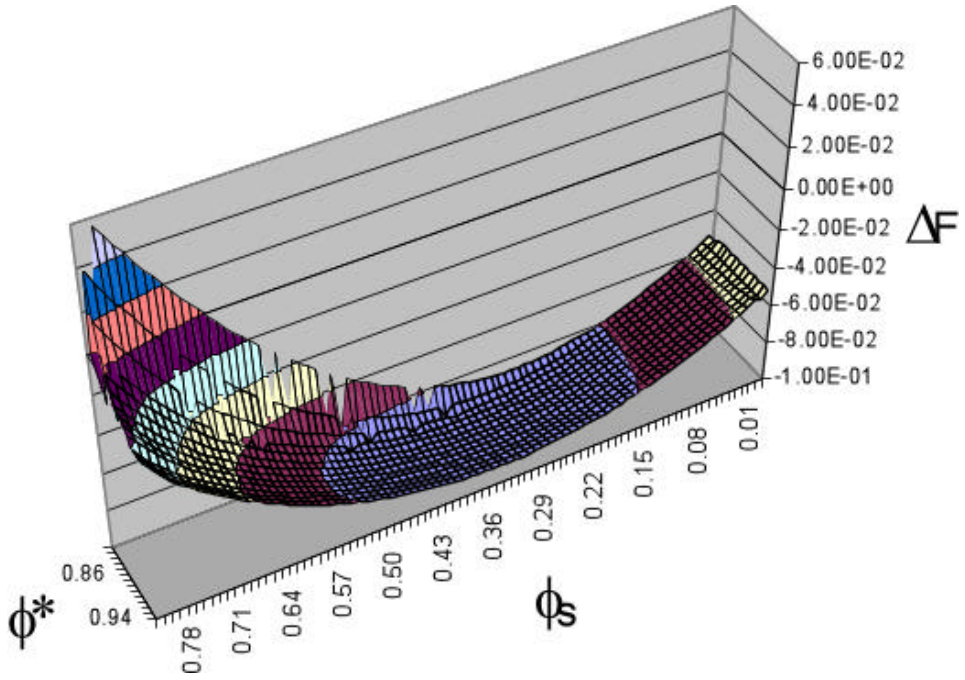

Figure 4.3: Free energy (ΔF) as function of the concentration at the center and the surface of the film, given by ϕ^* and ϕ_s respectively. The average concentration is constrained by $\phi_{A(Avg)} = 0.85$. There is a clear global minimum.

subroutine. An average value of the polymer composition $\phi_{A(Avg)}$ is fixed and initial parameters for the concentration fit function are chosen based on the $\phi_{A(Avg)}$ and $\frac{D}{2}$ values. These input functions are then used to determine the initial value of ΔF. The value of ΔF is then minimized by adjusting the parameters ϕ_1, ϕ_2, z_o, and w in Equation 4.8. The minimization procedure is subject to the constraints that the volume fraction at no point can exceed 1 ($\phi_{A(Max)} < 1$) or be less than 0 ($\phi_{A(Min)} > 0$), and that the average concentration for the total profile must be equal to $\phi_{A(Avg)}$. The last condition has the effect of making the $\Delta\mu$ term in Equation 4.9 redundant, thus leading to the following simplified equation:

$$\frac{\Delta F}{k_B T} = \int_0^{D/2} dz \left\{ f_{FH}[\phi(z)] + \kappa \left[\frac{d\phi(z)}{dz} \right]^2 - [w_A(z) - w_B(z)] \frac{d\phi(z)}{dz} \right\} + f_s(\phi_{D/2})^{(b)}. \quad (4.10)$$

Using the technique of minimizing ΔF by varying $\phi(z, \phi_1, \phi_2, z_o, w)$, subject to constraints on $\phi_{A(Avg)}$, $\phi_{A(Max)}$, and $\phi_{A(Min)}$, a Visual Basic program was constructed to produce free energy diagrams for ultra-thin polymer films. The primary parameter screen can be seen in Figure 4.4. The program takes the input parameters (a_A, a_B, N_A, N_B, g, μ_s, and $\frac{D}{2}$) and calculates the minimum free energy for a range of $\phi_{A(Avg)}$ and χ values that are defined by the user. The constrained nonlinear optimization is conducted using a Generalized Reduced Gradient (GRG) method, which is commercially sold by Frontline Systems, Inc., as Solver NLP/NSP DLL Platform v3.5.

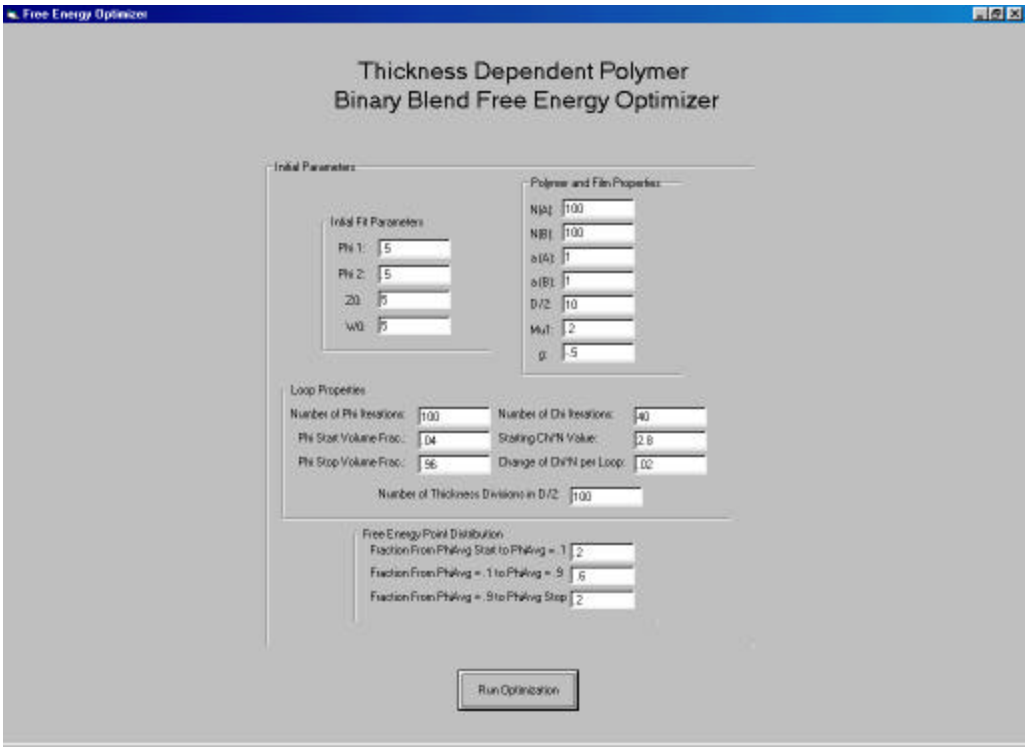

Figure 4.4: Primary parameter screen for Thickness Dependent Polymer Binary Blend Free Energy Optimization program.

For each value of χ, a free energy diagram is constructed, as seen in Figure 4.5. Each point on the free energy diagram corresponds to a specific composition profile. These profiles, seen in Figure 4.6, represent the profile $\phi(z)$ that minimizes the free energy (ΔF) for given values of (a_A, a_B, N_A, N_B, g, μ_s, χ, and D/2) constrained by $\phi_{A(Avg)}$.

The free energy diagram in Figure 4.5 is similar to the bulk free energy diagrams seen in Figure 1.1 and can be used to determine the location of the spinodal and the binodal in the same way. As the value of χ is changed, a series of free energy diagrams is constructed that allows the phase diagram of the thin film to be produced. The phase diagram for the thin film shown in Figure 4.5 is compared to the bulk phase diagram in Figure 4.7. Figure 4.7 clearly illustrates that phase diagram for the film D = 20 (units relative to $a_A = a_B \equiv 1$, in all future results where D/Rg is given, Rg is assumed to be 4.08 units, using a = 1 and N = 100) with the parameters $a_A = 1$, $a_B = 1$, $N_A = 100$, $N_B = 100$, g = -.5, μ_s =.2 is more stable than the corresponding bulk polymer mixture. It also appears that the critical point has shifted from the value $\phi = 0.5$ to a lower concentration of polymer A. These findings are similar to those using the technique developed by Flebbe and Binder described in Chapter 3. A direct comparison of the data calculated using the Flebbe-Binder technique and the Scheer et al. technique is presented in Figure 4.8. The results agree very well at D = 20 as seen in Figure 4.8(a). The data at D = 60 and D = 100 shows some minor discrepancies. These differences can be attributed to the difficulty in using the Flebbe and Binder technique at large values of D, as described in their paper [4.4].

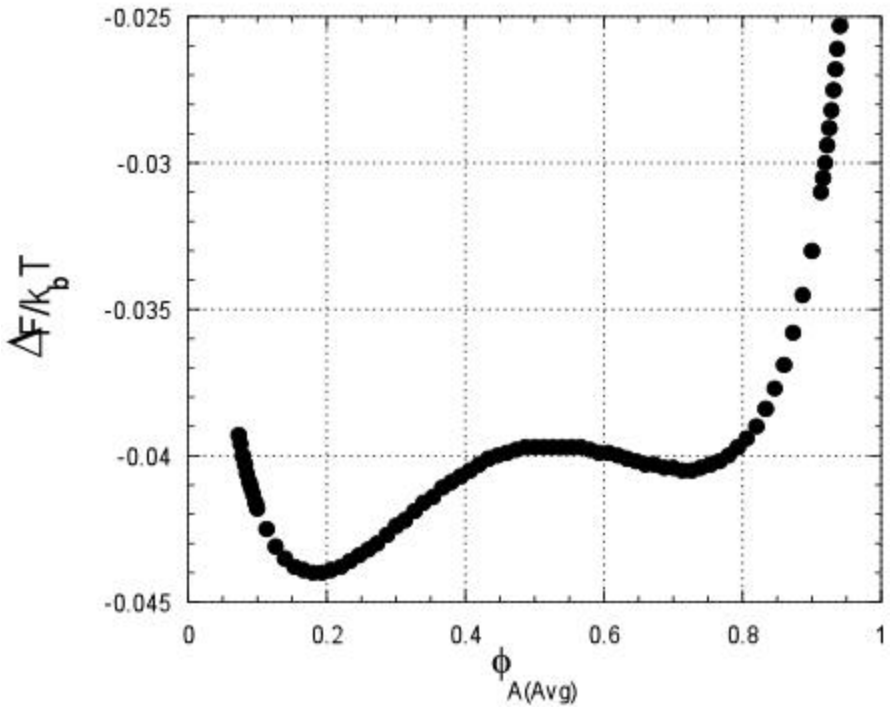

Figure 4.5: Free energy diagram for a polymer film bound by a symmetric interface. Simulation parameters are: χ = 0.0278, D/2 = 10, a_A = 1, a_B = 1, N_A = 100, N_B = 100, g = -.5, μ_s =.2

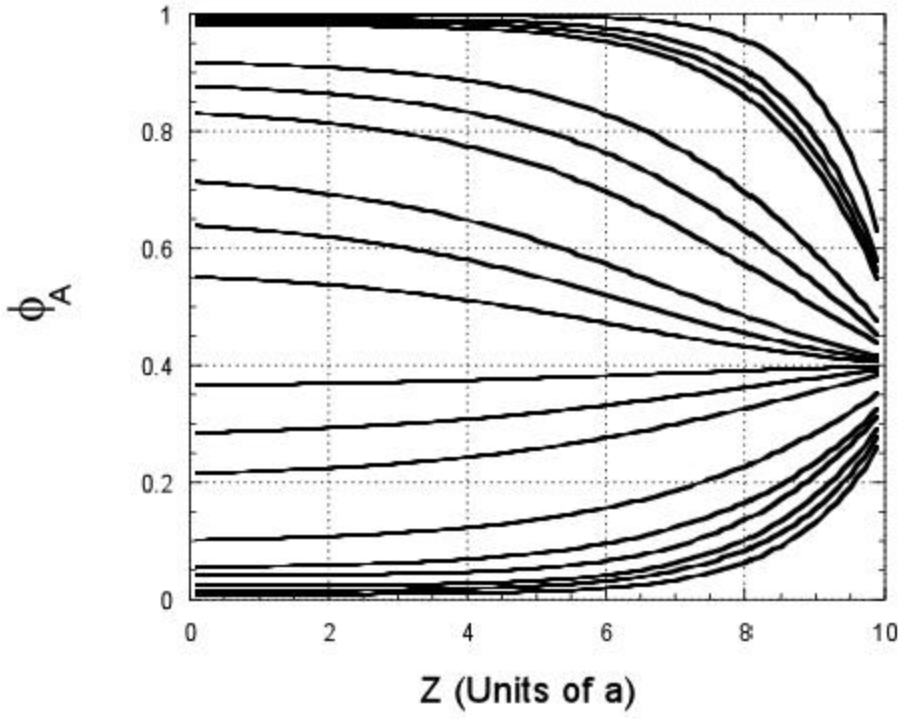

Figure 4.6: Profiles from free energy diagram in Figure 4.5. $\phi_{A(Avg)} = 0.04$ for the lowest curve and $\phi_{A(Avg)} = 0.96$ for the upper curve. The z axis is given in units relative to $a_A = a_B \equiv 1$.

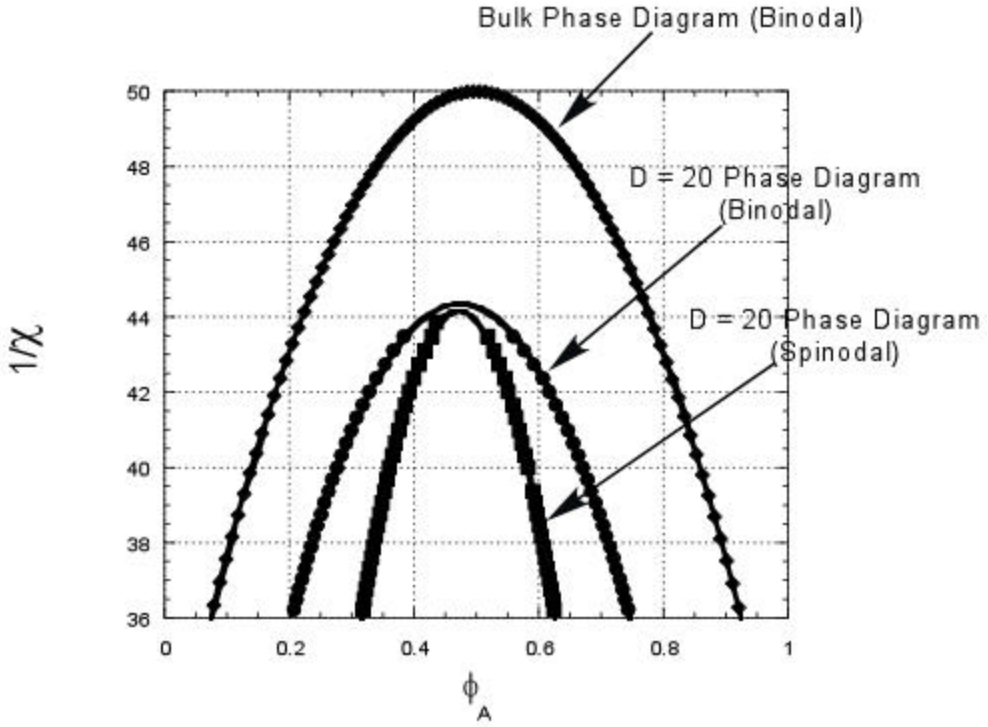

Figure 4.7: Phase diagram of film with thickness D = 20 (a_A = 1, a_B = 1, N_A = 100, N_B = 100, g = -.5, μ_s =.2).

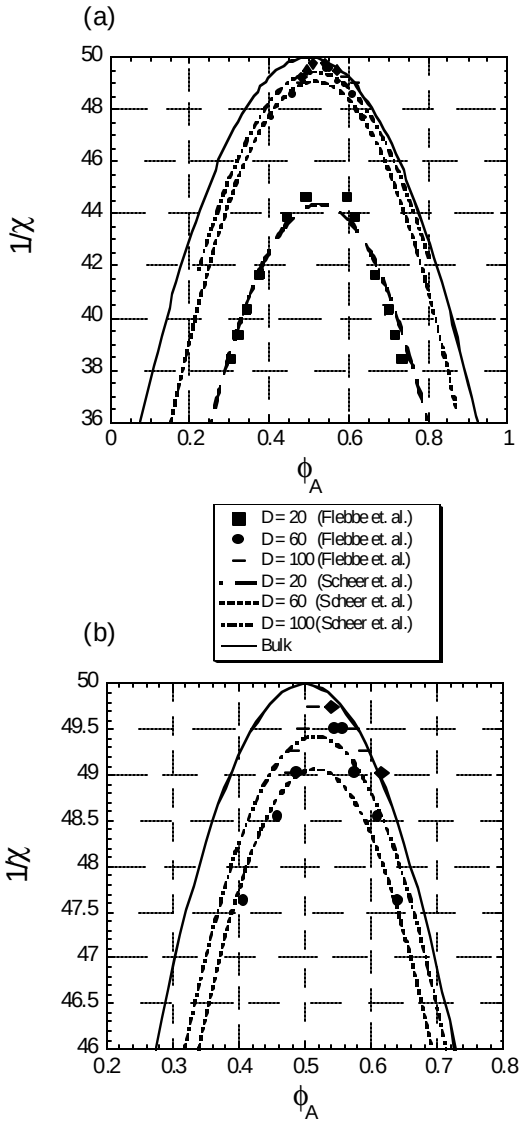

Figure 4.8: Comparison of free energy diagram produced by Flebbe and Binder with the diagram produced by Scheer et. al.

It is immediately apparent from Figure 4.8 that the phase diagram of a thin film rapidly approaches the bulk value as D is increased. Further discussions about the relationship between the parameters D, a_A, a_B, N_A, N_B, g, μ_s and the phase diagrams will be discussed later in section 4.4. It is important, at this point, to make a distinction between segregation perpendicular to the interface related to $\phi(z)$ and phase separation parallel to the interface as indicated by the phase diagram. Figure 4.9(a) contains the phase diagram of a bulk blend and a blend at thickness D = 20 nm. The diagram displays a tie line at $1/\chi$ = 40 at which the composition $\bar{f}$ will separate into two phases $\bar{f}_{(Coex1)}$ and $\bar{f}_{(Coex2)}$. These phases represent regions of the polymer surface in the x-y direction or regions of the surface as viewed from the top down position. Each of these two regions would have different z dependent composition profiles $\phi(z)$ as indicated by Figure 4.9(b), (c) and (d). As will be shown in section 4.4, it is possible to have very large z dependant polymer segregation without having any 2-D, x-y type, phase separation.

Before moving on, one final comparison between Flebbe and Binder's results and the new technique must be made. Figure 4.10 shows a comparison of the composition profiles from both techniques. Figure 4.10(a) compares the results of profiles in the A rich phase. The curves overlap to such an extent that it is difficult to tell the difference between them. Figure 4.10(b) compares the results of the B rich phase. The results in the B rich case tend to deviate as the surface of the film is reached with the maximum absolute (relative) deviation being about 1.8% (4.5%) at the surface. Given the A rich profile results, the fact

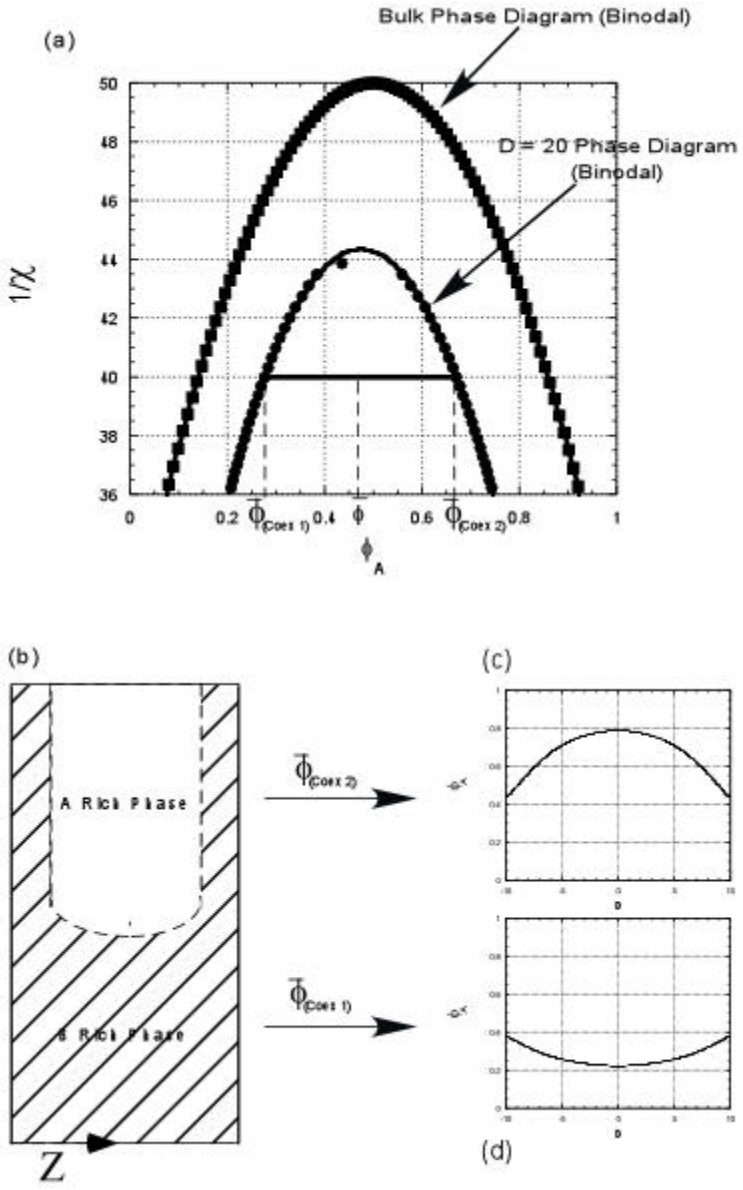

Figure 4.9: (a) Phase diagram from Figure 4.7, with tie line between A rich and B rich phases. (b) This diagram shows how the two phases would appear relative to each other in a cross section of the polymer film. (c) Examples of calculated concentration profiles for A rich $\bar{f}_{(Coex2)}$ and B rich $\bar{f}_{(Coex1)}$.

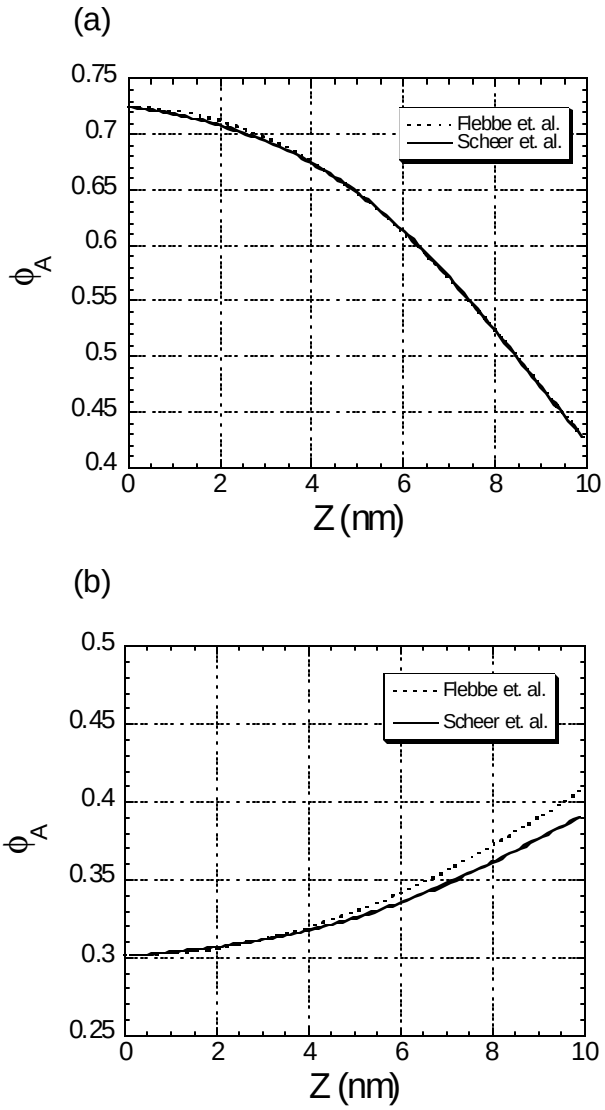

Figure 4.10: (a) Comparison of concentration profile calculated using analytical Flebbe *et al.* technique and for the A rich phase. (b) Comparison of concentration profile calculated using analytical Flebbe *et al.* technique and for the B rich phase.

that the phase diagram gives comparable results, and the fact that the error is relatively small, it is safely concluded that the optimization technique using the hyperbolic tangent function provides sufficiently accurate results.

4.4 Effect of Surface Free Energy on Segregation

The surface free energy term is divided into two parts, μ_s, or the chemical potential difference favoring one species at a surface, and g, which is due to the change of interactions near a surface ("missing neighbor" effect). Equation 4.6 illustrates the relative magnitudes of these contributions to the surface free energy term. The contribution due to μ_s, scales with the surface concentration ($\mu_s\phi_s$), and $\frac{g}{2}$ scales with the square of the surface concentration ($\frac{g}{2}\phi_s^2$).

The effect of independently modifying the terms of the surface free energy equation on the phase diagram of a film of thickness D = 20 (D/Rg ≈ 5, N_A = 100, N_B = 100, aA = 1, aB = 1) is shown in Figure 4.11. In Figure 4.11(a), the value of μ_s has been held constant at μ_s = 0.2, and the value of g has been varied between g = 0 and g = -0.8. Using the value g = -0.5 as a reference point, it is clear that increasing g has resulted in a shift of the phase diagram to preferentially larger values of ϕ_A. This shift is due to the increasing concentration of polymer A at the interface as g is increased. This effect can be seen on the A rich phase in Figure 4.12(a), and on the B rich phase in Figure 4.13(a). As g is increased, the A rich phase transitions from enriching in B to enriching in A at the interface. It is also interesting to note that as g is increased, the concentration of the A rich phase reaches a limiting value relative to the bulk phase diagram. Further decrease of g

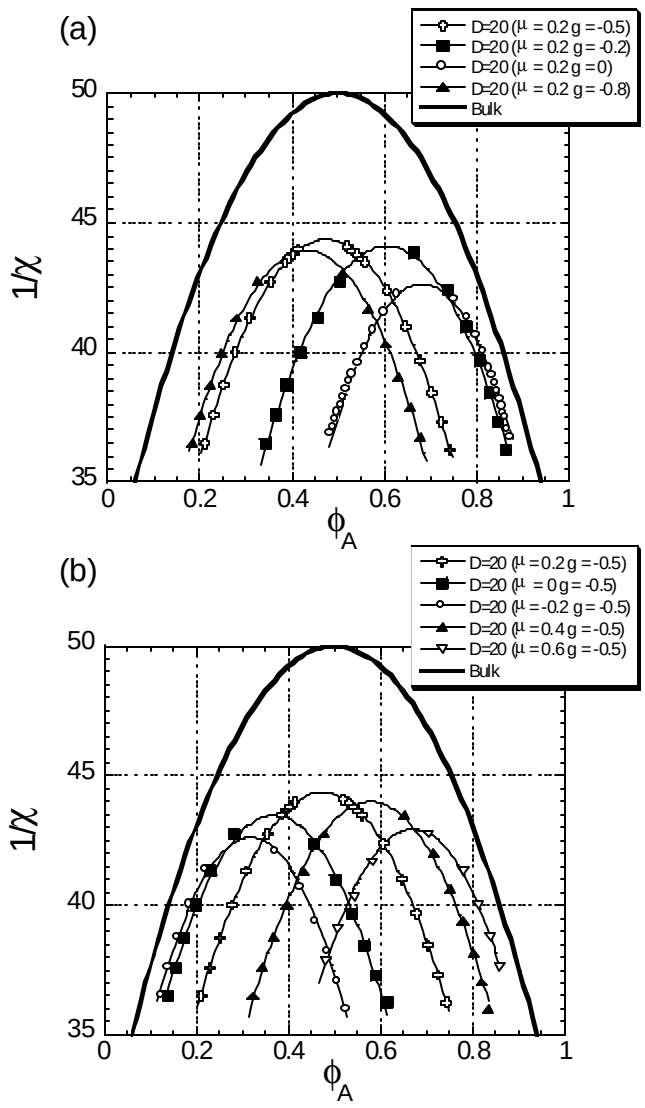

Figure 4.11: Phase diagram D = 20 as a function of surface potential (D/Rg ≈ 5, N_A = 100, N_B = 100, aA = 1, aB = 1). (a) μ_s constant while the term g is varied. (b) g constant while μ_s varied.

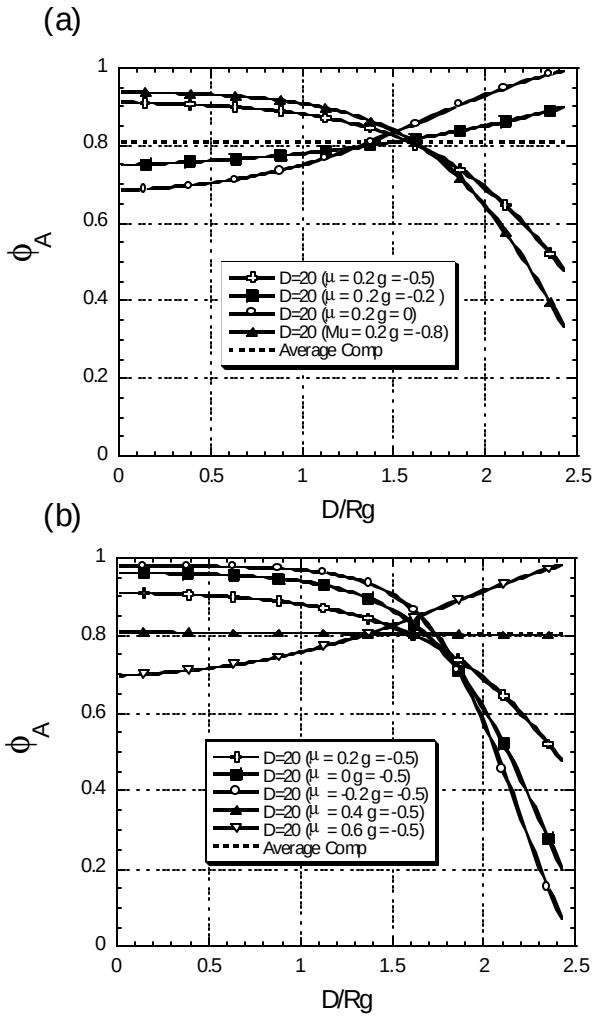

Figure 4.12: Concentration profile A rich phase as a function of surface potential D = 20 (D/Rg ≈ 5, N_A = 100, N_B = 100, aA = 1, aB = 1). (a) μ_s constant while the term g is varied. (b) g constant while μ_s varied.

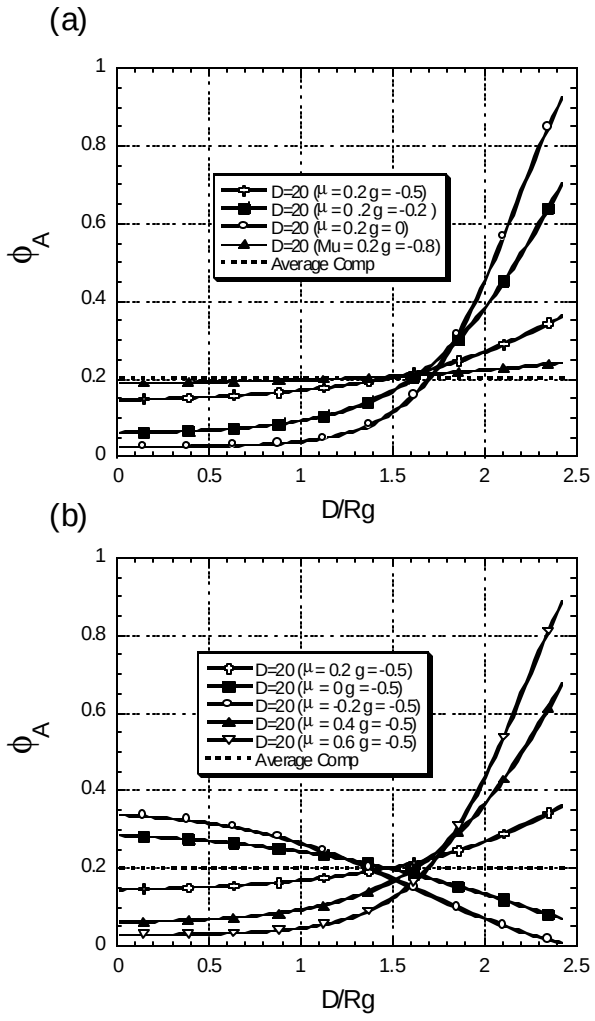

Figure 4.13: Concentration profile B rich phase as a function of surface potential D = 20 (D/Rg ≈ 5, N_A = 100, N_B = 100, aA = 1, aB = 1). (a) μ_s constant while the term g is varied. (b) g constant while μ_s varied.

only increases the A concentration of the B rich phase and lowers the critical point. As g is decreased, the phase diagram shifts to the lower values of ϕ_A. This is due to the increase of B at the interface as g is reduced, as seen in Figures 4.12(a) and 4.13(a). Limiting behavior similar to the decrease of g is observed on the phase diagram.

Modifying μ_s appears to have a similar result to modifying g. Figure 4.11 (b) clearly shows that increasing μ_s from a reference value of $\mu_s = 0.2$ results in a shift in the phase diagram to higher A concentrations. The effect of increasing μ_s on the concentration profile of the A rich phase is shown in Figure 4.12(b). It is clear that as μ_s is increased there is a switch from B enriching at the interface to A enriching at the interface. The B rich phase continues to increase the magnitude of the A enrichment at the interface as μ_s is increased, as shown in Figure 4.13(b). The decrease of μ_s shifts the phase diagram to lower concentrations of A, as seen in Figure 4.11(b). This shift also seems to exhibit a limiting behavior similar to that of decreases in g. The concentration profiles in the A rich phase will tend not to enrich in B as μ_s is decreased as seen in Figure 4.12(b). The B rich phase shows a transition from enriching in A to enriching in B as μ_s is decreased.

4.5 Effect of Segmental Asymmetry on Segregation

The inclusion of the conformational entropy term to the free energy equation allows the study of segmental asymmetry effects on the phase diagram and concentration profiles. The effect of independently changing the segmental length terms on the phase diagram of a film of thickness D = 20 ($D/Rg \approx 5$, N_A =

100, N_B = 100, μ_s = 0.2, g = -0.5) is shown in Figure 4.14. Figure 4.14(a) illustrates that reducing the segment length of the polymer has the effect of increasing the critical point of the mixture. This increase can most clearly be ascribed to the increase in configurational entropy, as represented by the κ term in Equation 4.10. If the effect where to be due to the conformational entropy terms, w_A and w_B, then the switch from aA = 1 with aB = 0.5 to aA = 0.5 should result in change in the sign of the value in Equation 4.4, resulting in one scenario having a critical point at a $1/\chi$ value larger than the aA = 1 aB = 1 scenario and the other scenario shifting to a lower $1/\chi$ value. Figure 4.14(a) indicates that both diagrams have seen an increase in the critical point. The κ term would account for the change due to both scenarios with an effect of the same magnitude and direction as seen in the results. The concentration profiles for the A rich and B rich phase diagrams are shown in Figures 4.15(a) and 4.16(a), respectively. It is clear that the segment length has a small effect on the concentration profiles in this example, but has a more noticeable effect in the enrichment of A at the interface of the B rich phase in Figure 4.16(a). As the segment length of A is reduced, the magnitude of A enrichment at the interface increases. It is interesting to note, that while the location of the critical point on the Y axis shifts appreciably, there is relatively little shifting of the critical point relative to the polymer concentrations.

An increase in the segment length is illustrated in Figure 4.14(b). The critical point shifts to lower values of $1/\chi$ as the segment length is increased, but there is little change in the polymer composition at the critical point. The concentration profiles for the A rich and B rich phase diagrams are shown in

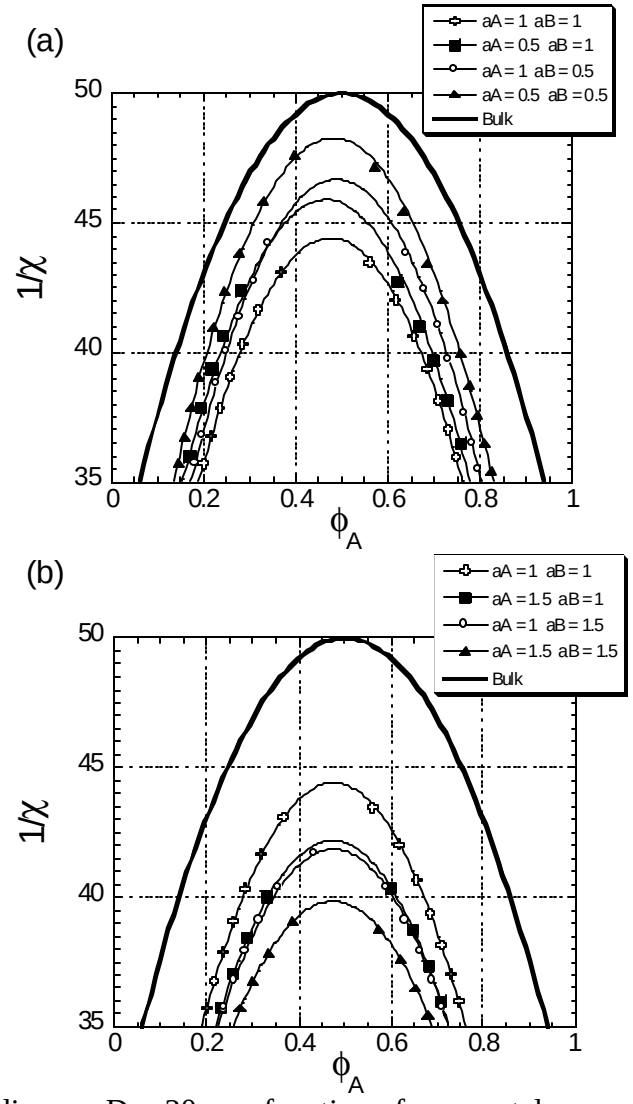

Figure 4.14: Phase diagram D = 20 as a function of segmental asymmetry (D/Rg ≈ 5, N_A = 100, N_B = 100, μ_s = 0.2, g = -0.5). (a) Segment length reduced. (b) Segment length increased.

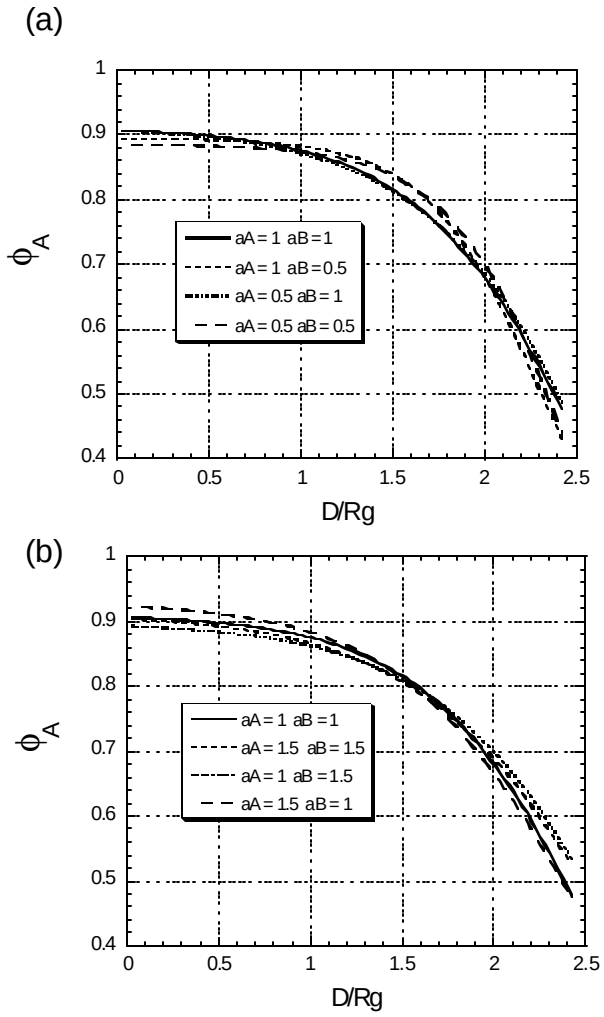

Figure 4.15: Concentration profiles A rich phase D = 20 as a function of segmental asymmetry (D/Rg ≈ 5, N_A = 100, N_B = 100, μ_s = 0.2, g = -0.5). (a) Segment length reduced. (b) Segment length increased.

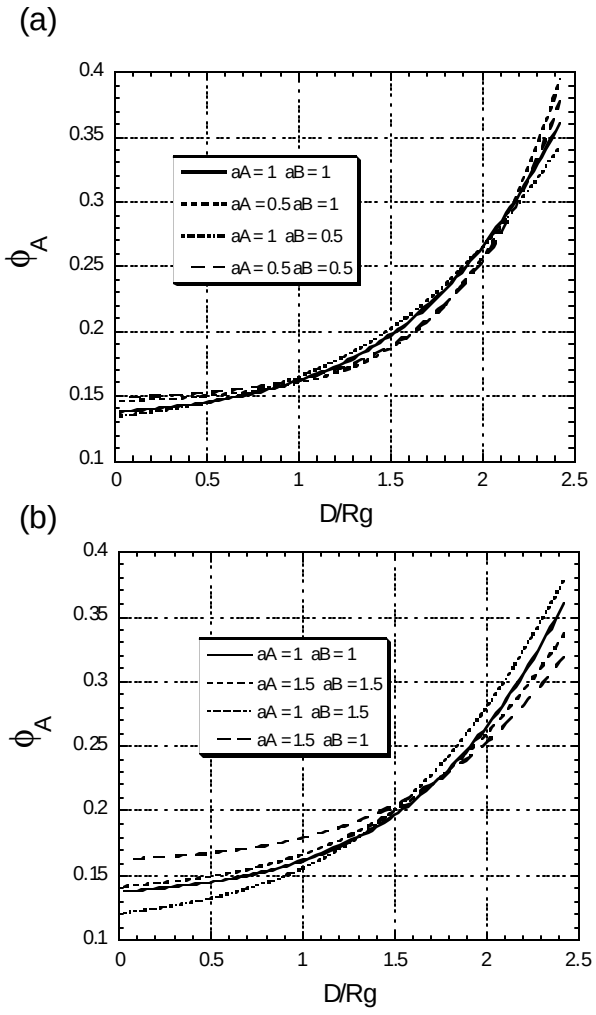

Figure 4.16: Concentration profiles B rich phase D = 20 as a function of segmental asymmetry (D/Rg ≈ 5, N_A = 100, N_B = 100, μ_s = 0.2, g = -0.5). (a) Segment length reduced. (b) Segment length increased.

Figures 4.15(b) and 4.16(b) respectively. Once again, there is a minor effect on the profile for the A rich phase, but the B rich phase shows more of an effect on enrichment of polymer A at the interface. It is clear that as the segment length of polymer A is increased, the magnitude of its enrichment at the interface is decreased. Conversely, as the segment length of B is increased the amount of A enrichment is increased. The same segmental length effects where modeled in a film of thickness D = 10 ($D/Rg \approx 2.5$, $N_A = 100$, $N_B = 100$, $\mu_s = 0.2$, $g = -0.5$), shown in Figure 4.17. Figure 4.17(a) shows, once again, that decreasing the segment length shifts the critical point to a larger $1/\chi$ value. The magnitude of the effect is much greater for this film thickness. For the film D = 20 the increase of $1/\chi$ is 2 to 4 units, while for D = 10 the increase is 4 to 10 units. Correspondingly, Figure 4.17(b) shows that increasing the segment length shifts the critical point to smaller $1/\chi$ values. The magnitude of the change is also much larger for the thinner films, with the $1/\chi$ shift being about 2 to 5 units for D = 20 and about 4 to 8 units for D = 10. The thinner films still do not exhibit significant shifting of the composition of the critical point.

Figures 4.18 and 4.19 show the composition profiles of the A rich and B rich phases, respectively. When these diagrams are compared to Figures 4.15 and 4.16 it is clear that the decrease in film thickness has increased the effect of segment length on the concentration at the interface. It is once again, most clear in the enrichment of A in the B rich phase, as seen in Figure 4.19. When Figure 4.19(a), aA = 0.5 and aB = 1, is compared with Figure 4.19(b), aA=1.5 and aB=1,

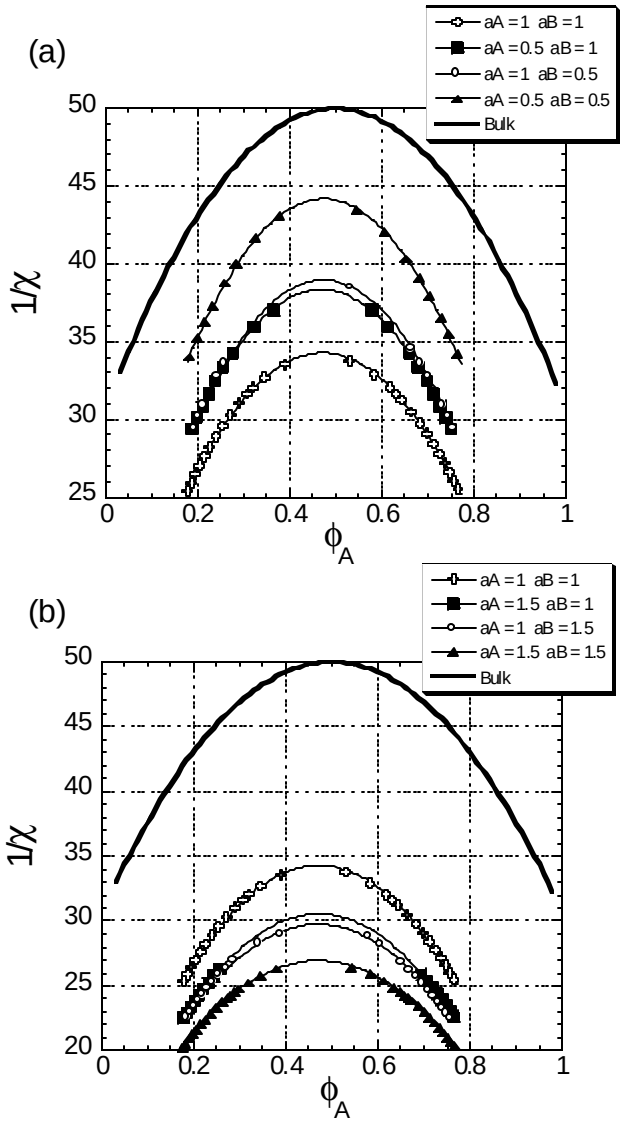

Figure 4.17: Phase diagram D = 10 as a function of segmental asymmetry (D/Rg ≈ 2.5, N_A = 100, N_B = 100, μ_s = 0.2, g = -0.5). (a) Segment length reduced. (b) Segment length increased.

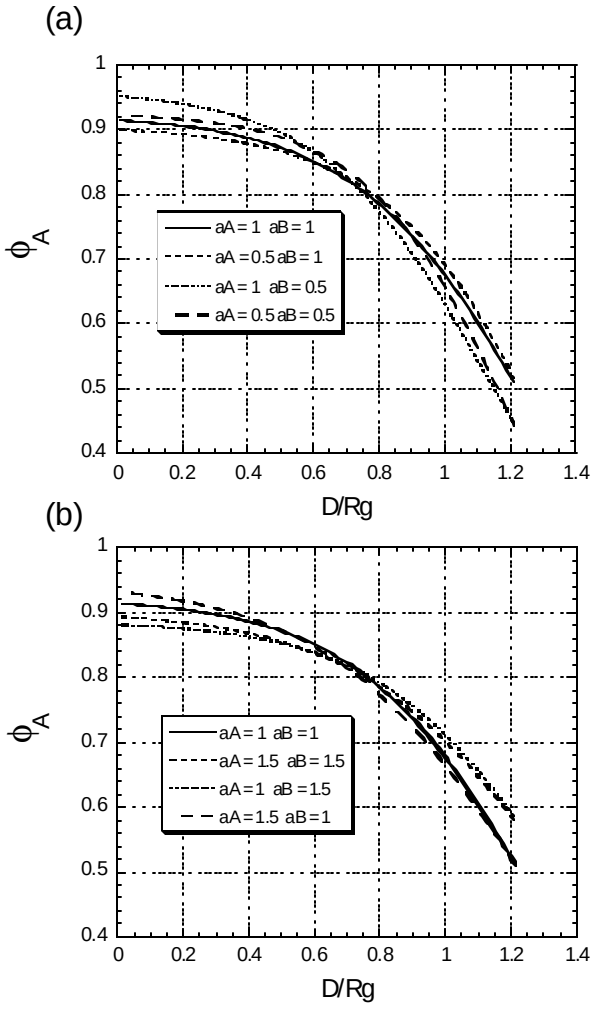

Figure 4.18: Concentration profiles A rich phase D = 10 as a function of segmental asymmetry ($D/Rg \approx 2.5$, $N_A = 100$, $N_B = 100$, $\mu_s = 0.2$, $g = -0.5$). (a) Segment length reduced. (b) Segment length increased.

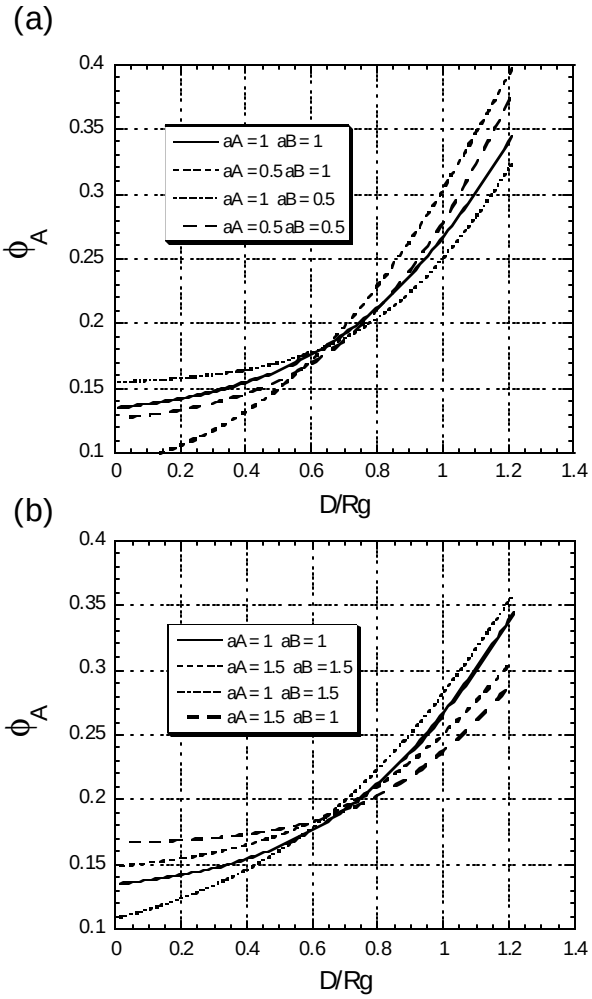

Figure 4.19: Concentration profiles B rich phase D = 10 as a function of segmental asymmetry (D/Rg ≈ 2.5, N_A = 100, N_B = 100, μ_s = 0.2, g = -0.5). (a) Segment length reduced. (b) Segment length increased.

a difference of greater than 10% in the concentration of polymer A at the interface is found. The difference in the film D = 20 is about 7.5%.

Since, the above results indicate that there is a connection between the thickness and segmental length effect on composition profiles, a new set of modeling results was produced to test this interaction. A series of films of thickness D = 5, 10, 20, 40, 80 corresponding to D/Rg = 1.2, 2.5, 5, 10, 20 were modeled. The surface potentials were set to encourage strong segregation of polymer A to the interface (μ_s = 0.2, g = 0). The polymers both had the same number of effective segments, $N=N_A=N_B=100$, and the segment length of polymer B was aB = 1. For each thickness, the segment length of polymer A was varied such that aA = 1, 1.25, 1.5, 2, 2.5. The solutions are presented in the series of Figures 4.20, 4.21, 4.22, 4.23, and 4.24, with (a) being the results for $\bar{f}_A$ = 0.2 and (b) the results for $\bar{f}_A$ = 0.4.

Figures 4.20(a,b), both show a strong segment length dependence. As the segment length of A is increased the profile of the film is forced to lower the concentration of polymer A enriching the interface, resulting in the concentration of polymer A at the interface being ϕ_A = 0.695 for aA = 1 and ϕ_A = 0.277 for aA = 2.5 when $\bar{f}_A$ = 0.2. The difference is ϕ_A = 0.854 for aA = 1 and ϕ_A = 0.534 for aA = 2.5 when $\bar{f}_A$ = 0.4. The results for D = 5, 10, 20, 40, 80 are summarized in the Table 4.1.

The results from Figures 4.20, 4.21, 4.22, 4.23, and 4.24 and Table 4.1 can be summarized as follows. First, there is a very strong segmental length effect on the composition profile for thin films. As the segment length is increased, the

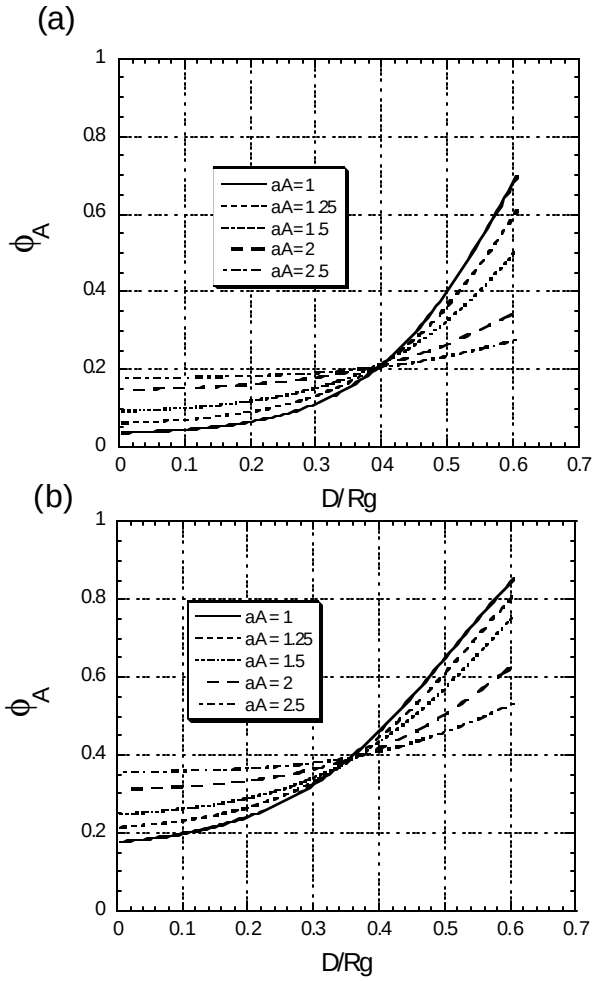

Figure 4.20: Concentration profiles D = 5 as a function of segmental asymmetry (D/Rg ≈ 1.2, N_A = 100, N_B = 100, aB = 1, μ_s = 0.2, g = 0). (a) $\bar{f}_A$ = 0.2 (b) $\bar{f}_A$ = 0.4

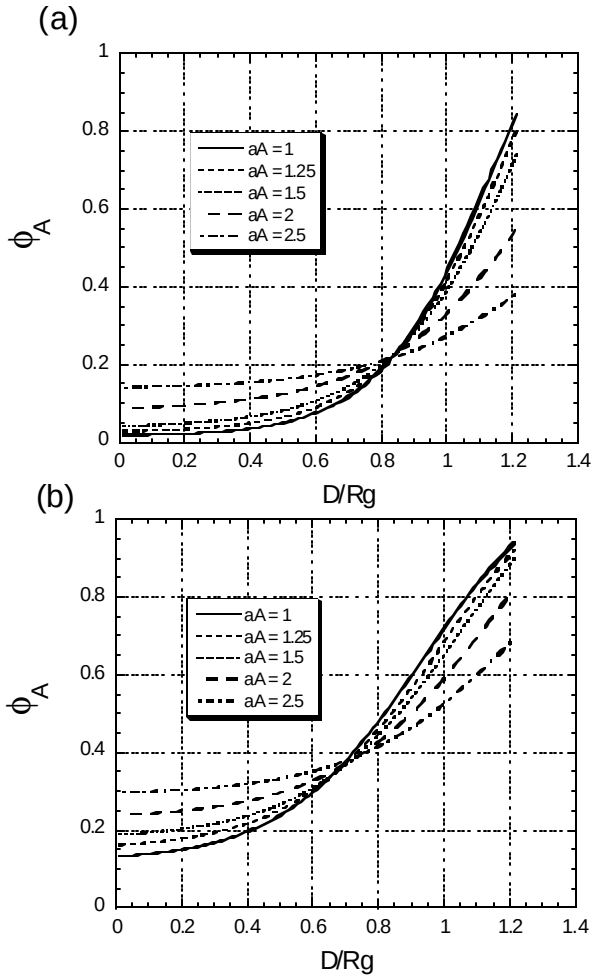

Figure 4.21: Concentration profiles D = 10 as a function of segmental asymmetry (D/Rg ≈ 2.4, N_A = 100, N_B = 100, aB = 1, μ_s = 0.2, g = 0). (a) $\bar{f}_A$ = 0.2 (b) $\bar{f}_A$ = 0.4

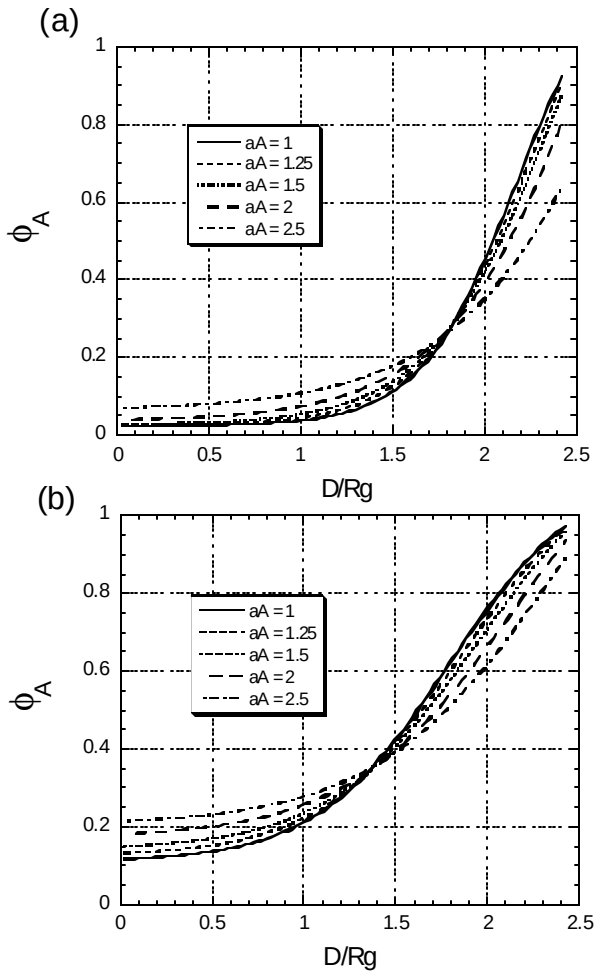

Figure 4.22: Concentration profiles D = 20 as a function of segmental asymmetry (D/Rg ≈ 5, N_A = 100, N_B = 100, aB = 1, μ_s = 0.2, g = 0). (a) $\bar{f}_A$ = 0.2 (b) $\bar{f}_A$ = 0.4

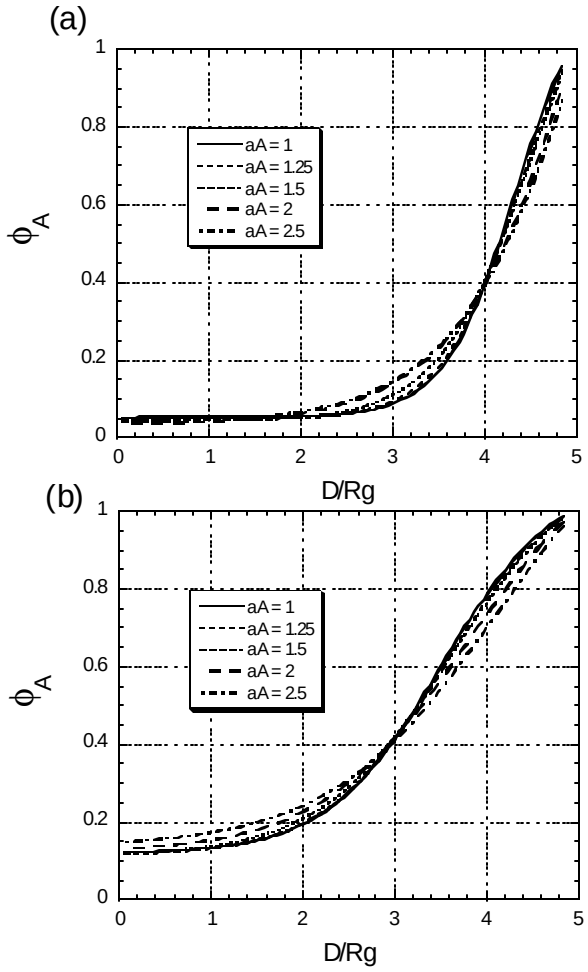

Figure 4.23: Concentration profiles D = 40 as a function of segmental asymmetry (D/Rg ≈ 10, N_A = 100, N_B = 100, aB = 1, μ_s = 0.2, g = 0). (a) $\bar{f}_A$ = 0.2 (b) $\bar{f}_A$ = 0.4

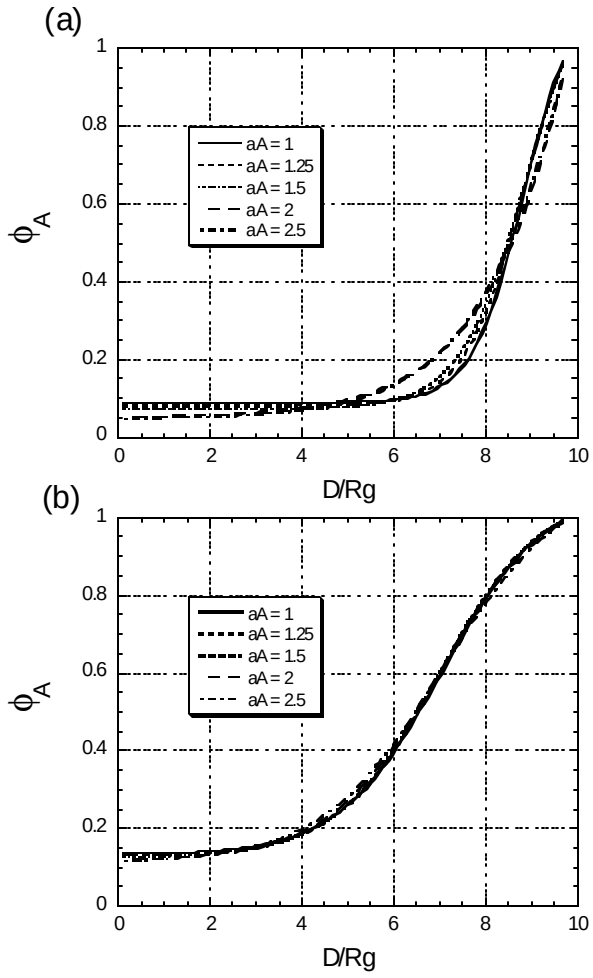

Figure 4.24: Concentration profiles D = 80 as a function of segmental asymmetry (D/Rg ≈ 20, N_A = 100, N_B = 100, aB = 1, μ_s = 0.2, g = 0). (a) $\bar{f}_A$ = 0.2 (b) $\bar{f}_A$ = 0.4

D	$\bar{f}_A$ = 0.2 (aA = 1)	$\bar{f}_A$ = 0.2 (aA = 2.5)	$\bar{f}_A$ = 0.4 (aA = 1)	$\bar{f}_A$ = 0.4 (aA = 2.5)
5	0.695	0.277	0.854	0.534
10	0.845	0.382	0.938	0.692
20	0.924	0.641	0.974	0.892
40	0.957	0.870	0.987	0.966
80	0.969	0.930	0.992	0.988

Table 4.1: The surface concentration ϕ_s of a polymer film attempting to enrich in polymer A. The experimental parameters are (N_A = 100, N_B = 100, aB = 1, μ_s = 0.2, g = 0). All thickness can be normalized to D/Rg by dividing by 4.08.

composition of A at the interface must decrease to compensate. Second, as the thickness of the film is increased, the magnitude of the segment length effect on the interface concentration is reduced. Finally, as the average polymer A composition in the film is increased, the magnitude of the segmental length effect is reduced. The final results seem to indicate that the normalizing effect is significant up to about D/Rg = 20 for films where $\bar{f}_A$ = 0.2 and D/Rg = 10 for films where $\bar{f}_A$ = 0.4. These results strongly support the conclusion that polymer asymmetry cannot be ignored in ultra-thin polymer films.

4.4 CONCLUSION

The inclusion of the segmental symmetry effects in the free energy function was discussed. The Fredrickson and Donley surface potential approach was used to model the polymer asymmetry. The inclusion of this term necessitated the use of a numerical solution to the free energy equation. The numerical solution was reached by approximating the concentration profile with a hyperbolic tanget function and performing a constrained optimization of this function. This approach was coded into a Visual Basic program using a Generalized Reduced Gradient approach for the optimization. The program was used to model a series of polymer films, focusing on the following effects:

1. Surface potential on phase diagrams and concentration profiles with symmetric polymers.
2. Segmental asymmetry on phase diagrams and concentration profiles with a balanced surface potential.

3. Segmental asymmetry as a function of film thickness for a polymer film exhibiting strong enrichment of one of the components to an interface.

From these results several conclusions can be drawn. First, the magnitude and sign of the surface potential has a direct effect on both the phase diagram and the composition profiles. Second, polymer segmental asymmetries have an effect on the phase diagram, but primarily on the magnitude of the $1/\chi$ not on the concentration of the critical point. Finally, the results of these simulations support the hypothesis that the determination of concentration profiles in ultra- thin films with $h < 5Rg$ requires that polymer asymmetries be taken into account.

The polymer modeling technique described in this chapter will be used the next chapter, to estimate the interfacial tension in polymer films. These results will be tied to the experimental observations to show how thickness, asymmetry, the bulk polymer free energy, and surface effects determine the segregation and ultimately the stability in an experimental polymer system.

4.5 REFERENCES

4.1 Cahn, J.W., "Critical point wetting," J. Chem. Phys., 66(8) 1977 p. 3667-72.

4.2 Schmidt, I. and K. Binder, "Model calculations for wetting transitions in polymer mixtures," J. Phys. (Les Ulis, Fr.), 46(10) 1985 p. 1631-44.

4.3 Binder, K., "Surface effects on polymer blends and block copolymer melts: theoretical concepts of surface enrichment, surface induced phase separation and ordering," Acta Polym., 46(3) 1995 p. 204-25.

4.4 Flebbe, T., B. Duenweg, and K. Binder, "Phase separation versus wetting: a mean field theory for symmetrical polymer mixtures confined between selectively attractive walls," J. Phys. II (France), 6(5) 1996 p. 667-695.

4.5 Binder, K., "Phase Transitions of Polymer Blends and Block Copolymer Melts in Thin Films," Avances in Polymer Science, 138 1999 p. 1-89.

4.6 Cohen, S.M. and M. Muthukumar, "Critical wetting in two-component polymer blends," J. Chem. Phys., 90(10) 1989 p. 5749-55.

4.7 Donley, J.P. and G.H. Fredrickson, "Influence of conformational asymmetry on the surface enrichment of polymer blends. II," J. Polym. Sci., Part B: Polym. Phys., 33(9) 1995 p. 1343-51.

4.8 Fredrickson, G.H. and J.P. Donley, "Influence of broken conformational symmetry on the surface enrichment of polymer blends," J. Chem. Phys., 97(12) 1992 p. 8941-6.

4.9 Rouault, Y., J. Baschnagel, and K. Binder, "Phase Separation of Symmetrical Polymer Mixtures in Thin-Film Geometry," Journal of Statistical Physics, 80(5/6) 1995 p. 1995.

Chapter 5: Study of Segregation and Stability in poly(styrene-co-acrylonitrile)/poly(methylmethacrylate) Blends

5.1 INTRODUCTION

The effect of interfacial segregation on thermodynamic phase stability on thin and ultra-thin films was discussed in great detail in Chapters 2 and 4. This chapter attempts to shed more light on these topics, through examinaton of mixtures of poly(styrene-co-acrylonitrile) (SAN-X), with X as the mass fraction of acrylonitrile (AN) in the random copolymer, and poly(methylmethacrylate) (PMMA). Segregation in PMMA/SAN-33 systems has been studied earlier by Wang et al. in thicker films (h > 100 nm) in the immiscible region of the phase diagram [5.1-5.3]. They determined that PMMA segregates symmetrically, [5.1-5.4], producing a trilayer structure where PMMA wets both the free interface and the silicon substrate, with SAN-X sandwiched between the PMMA. This tri-layer structure can then become unstable and dewet forming encapsulated droplets of SAN-X in a PMMA matrix. The structural stability of this system was examined as a function of film thickness, SAN-X copolymer composition, and temperature. The simulations described in Chapters 3 and 4 provide insight in many of the findings discussed later in this chapter.

5.2 STABILITY IN SEGREGATING BLENDS

To understand the stability of thin tri-layer polymer films, it is useful to begin by constructing a model bi-layer film, shown schematically in Figure 5.1 and Figure 5.2. It has been shown elsewhere [5.5] that films that are highly immiscibile will not mix at the interface of a bilayer, as seen in Figure 5.1. A sharp interface means that the interfacial width is small, consequently the interfacial tension between polymer A and polymer B (γ_{AB}) is large. Experiments have shown that even if the thickness of the polymer layers are several hundred nanometers, much greater than the distances that long range van der Waals forces act, the top layer of a bi-layer film will still dewet the lower film[5.5], as seen in Figure 5.1. A second scenario can be envisioned where the two polymer films interact more favorably, creating more mixing at the interface between polymer A and polymer B, as illustrated in Figure 5.2. This increased mixing indicates that the interfacial tension (width) between polymer A and B is reduced (increased) when compared to a strongly segregating polymer bi-layer. Experimental evidence indicates that as the interfacial tension between the polymer bi-layer is reduced, the top polymer layer will transition from an unstable to stable state [5.5]. The use of this energetic argument enables the stability study of the experimental SAN-X/PMMA system in terms of interfacial tension without immediate concern for the effect of van der Waals forces.

5.3 EXPERIMENTAL

The experimental system discussed in this chapter consists of mixtures of

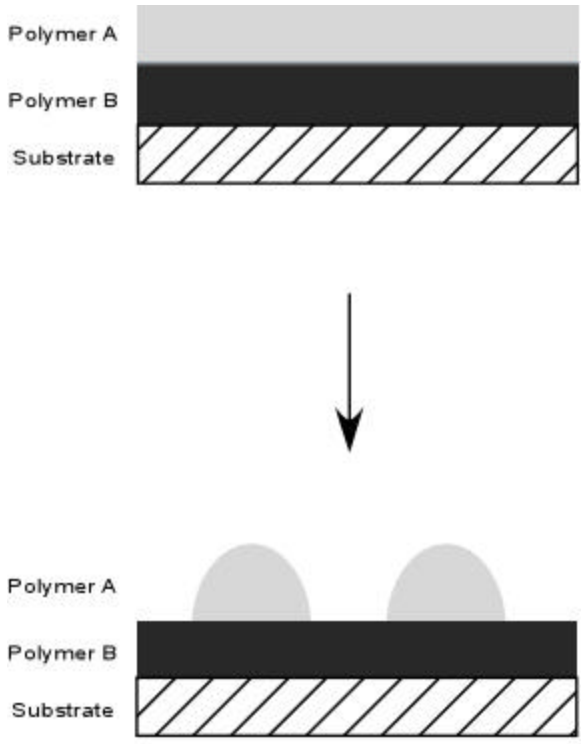

Figure 5.1: Highly immiscibile polymer bi-layer. The sharp interface indicates a large interfacial tension, consequently polymer A will dewet polymer B[5.5].

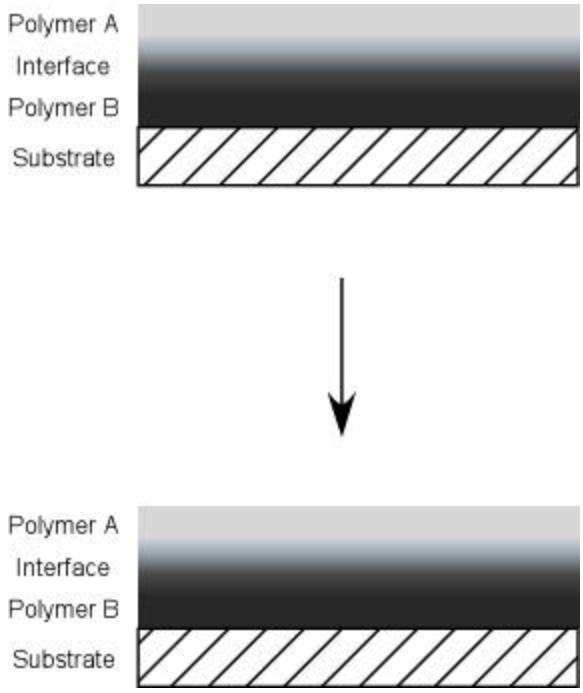

Figure 5.2: A more miscibile polymer bi-layer will exhibit a broader interface, indicating indicates a smaller interfacial tension. This decrease in interfacial tension can lead to stabilization of the bi-layer[5.5].

SAN-X and PMMA. The properties of the polymers used are summarized in Table 5.1. Solutions of PMMA mixed with SAN-X were made in 4-methyl-pentanone. All of the solutions consisted of 50/50 wt.% PMMA/SAN-X. These solutions were coated on silicon substrates, with a roughly 2 nm native oxide (SiO_x) using a commercial spin-coater. The resulting films ranged in thickness between 100 and 400 Å. The thickness of the films was verified using a VASE ellipsometer. Samples were then annealed for 12 hours in a vacuum oven at 170, 210, and 230 ^{o}C. After being removed from the oven, the samples were rapidly quenched to room temperature, ensuring that the structural morphology did not change. The samples were then scanned with an Autoprobe CP atomic force microscope (AFM) from Thermal Microscopes. The AFM allows the morphology of the film to be probed nondestructively and provides the ability to measure thickness variation on the order of Å over an 80 micron^2 area.

The thermal stability of PMMA at these temperatures was determined by coating a 400 angstrom film of PMMA on several silicon substrates. These samples were placed in vacuum overnight, at room temperature, to remove any residual solvent. The initial thickness was measured with the ellipsometer and then the samples were vacuum annealed at 170, 210, and 230 ^{o}C. The samples were periodically removed from the oven and scanned with the ellipsometer. The results are presented in Figure 5.3 and indicate that within the time range used for the experiments, the PMMA should see less than 12% decomposition at the highest temperature.

Polymer	M_w	N	a (nm)	Rg (nm)
PMMA	100,000	1000	.852	11.0
SAN-5.5	270,000	2643	1.012	21.2
SAN-9.5	196,000	1994	1.040	18.6
SAN-25	152,000	1773	1.130	19.4
SAN-30	168,000	2040	1.155	21.3
SAN-34	145,000	1816	1.174	20.4

Table 5.1: Properties of polymers used in thin film experiments[5.6].

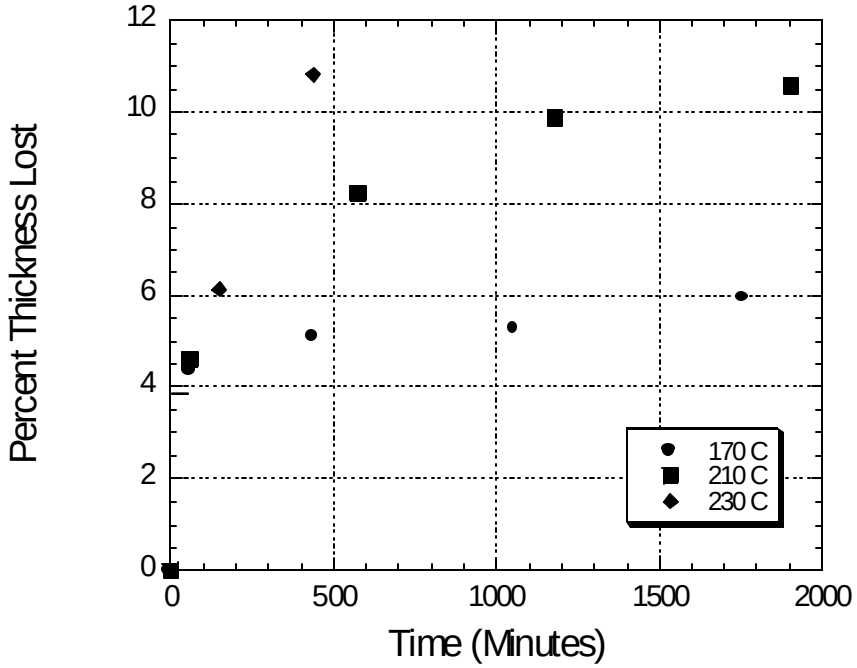

Figure 5.3: Results from experiment testing degradation in 400 angstrom PMMA film.

Angle resolved XPS was used to determine the surface concentration in some of the polymer films. XPS scans were first taken in survey mode scanning the 1-1400 eV (0.4 eV/step 200 ms/step) range using an Al source. High resolution scans were then taken in ranges of particular interest at 0.1 eV/step 1s/step.

5.3 RESULTS AND DISCUSSION

Blends of SAN-9.5, SAN-25, SAN-30, and SAN-34 with PMMA all exhibit LCST behavior with a critical point at approximately 280, 250, 175, and 165 ^{o}C respectively[5.7, 5.8]. SAN-5 exhibits UCST behavior when mixed with PMMA and has a critical point at approximately 250 ^{o}C[5.9]. The value of χ for SAN-X mixed with PMMA in the temperature range between 107 and 177 ^{o}C was calculated using the technique of Higashida[5.10] and is presented in Figure 5.4. The calculated values of χ are consistent with the LCST behavior in the mixtures containing SAN-9.5, SAN-25, SAN-30, and SAN-34. SAN-5 exhibits a UCST, therefore χ decreases with increasing temperature.

Figure 5.5 shows the AFM scans of samples of SAN-5, SAN-10, SAN-25, SAN-30, and SAN-34 mixed with PMMA (50/50 wt.%), with thicknesses between h = 100 and h = 400 Å (~ 1 to 4 times the Rg of the PMMA), that were annealed at 170 ^{o}C. The SAN-5 and SAN-34 systems, both in the two phase region of the bulk phase diagram, are unstable throughout the entire thickness range. It is reasonable to assume that these samples phase separated due to this thermodynamic instability. One should be cautioned, nevertheless, that as it was

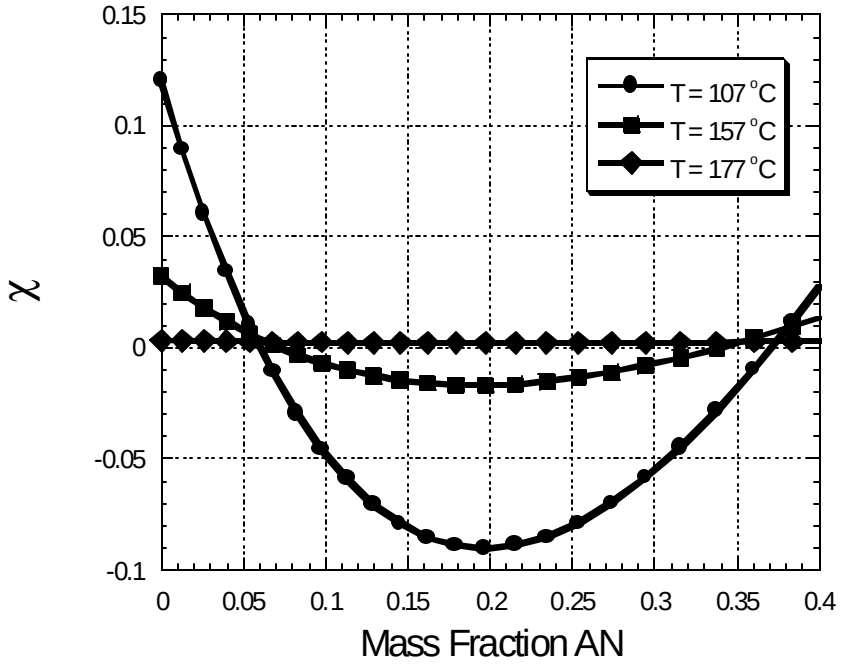

Figure 5.4: χ as a function of mass fraction AN in the SAN-X copolymer, for a SAN-X/PMMA mixture. Results calculated from [5.10].

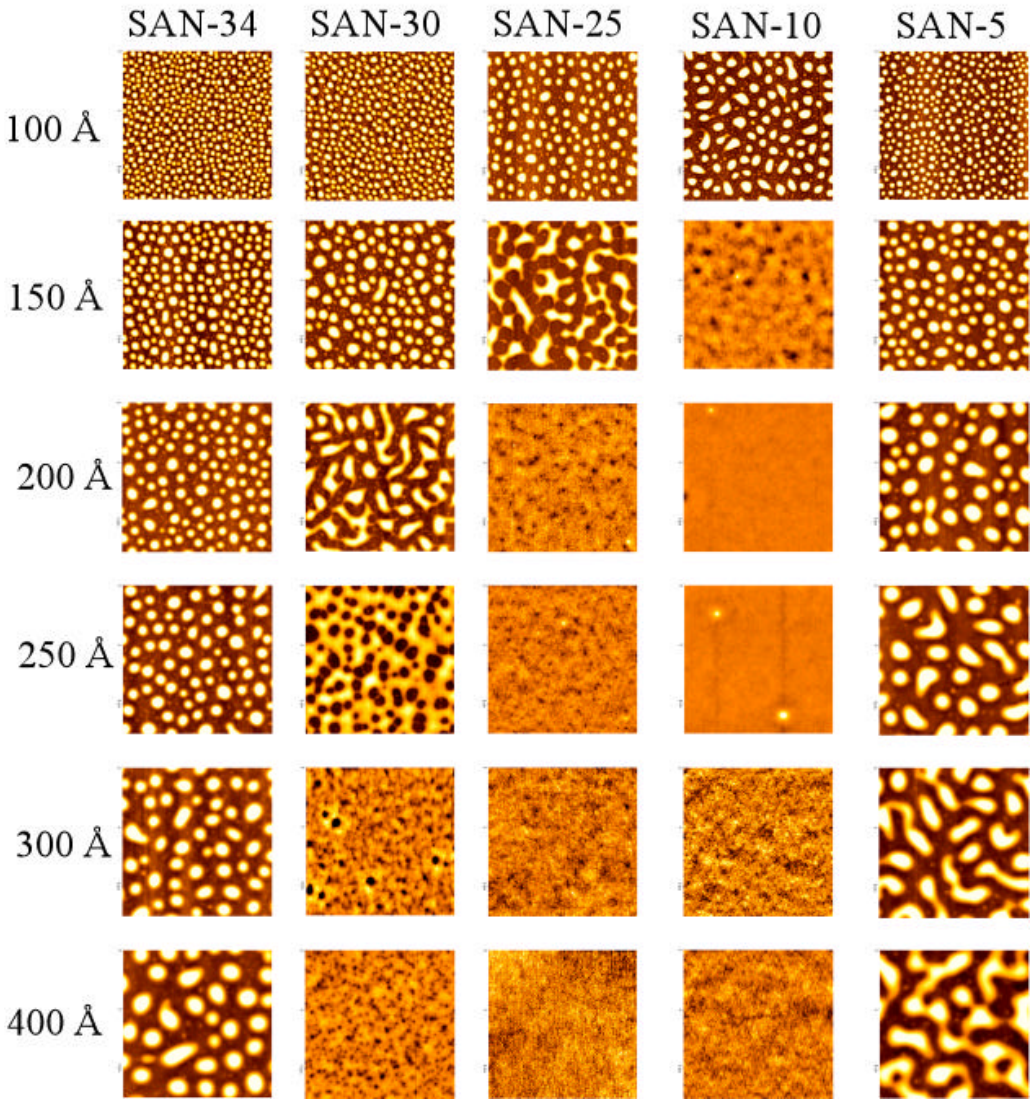

Figure 5.5: AFM scans of SAN-X/PMMA samples annealed at 170 ^{o}C. The initial thickness of the polymer films is listed to the left, and the SAN-X copolymer blend is listed across the top. All blends where 50/50 wt.% SAN-X/PMMA. All scans are 10 X 10 microns.

shown in Chapter 4, films in this thickness range exhibit a significant shift in the critical point, resulting in an enhancement of the thermodynamic phase stability.

The situation involving the other mixtures is quite different. These mixtures reside in the single-phase region of the phase diagram, below the LCST. These films become structurally unstable as the thickness decreases from h= 40 nm. The SAN-30 mixture becomes unstable at h=25 nm and the SAN-10 and SAN-25 mixtures become stable at smaller h. In light of the simulations, which suggest that mixture become more stable with decreasing h, we see the opposite trend. In Chapter 4, evidence was presented proving that even if a film does not phase separate laterally, it can still segregate perpendicular to the substrate, due possibly to interfacial interactions. The images in Figures 5.6 and 5.7 reveal very similar trends in the behavior of the mixtures at higher temperatures. The only qualitative difference is that the SAN-30, SAN-25 and SAN-10 mixtures become unstable at slightly larger film thicknesses.

In the h=100 and h=400 Å thick films, the interfacial interactions are such that a tri-layer structure is produced as illistrated schematically in Figure 5.8. Figure 5.9 presents XPS data obtained for a 200 Å 50/50 wt% mixture of SAN-25/PMMA vacuum annealed for 15 minutes at 210 ^{o}C. The results clearly show enrichment of PMMA at the free interface. This is consistent with independent experiments conducted by others [5.1, 5.3]. In Figure 5.8, it is assumed that χ is positive, resulting in a situation where the polymer does not want to mix, so sharp A/B interfaces are created. A sharp interface is indicative of a small interfacial width or large interfacial tension, and creates a situation where the middle film in

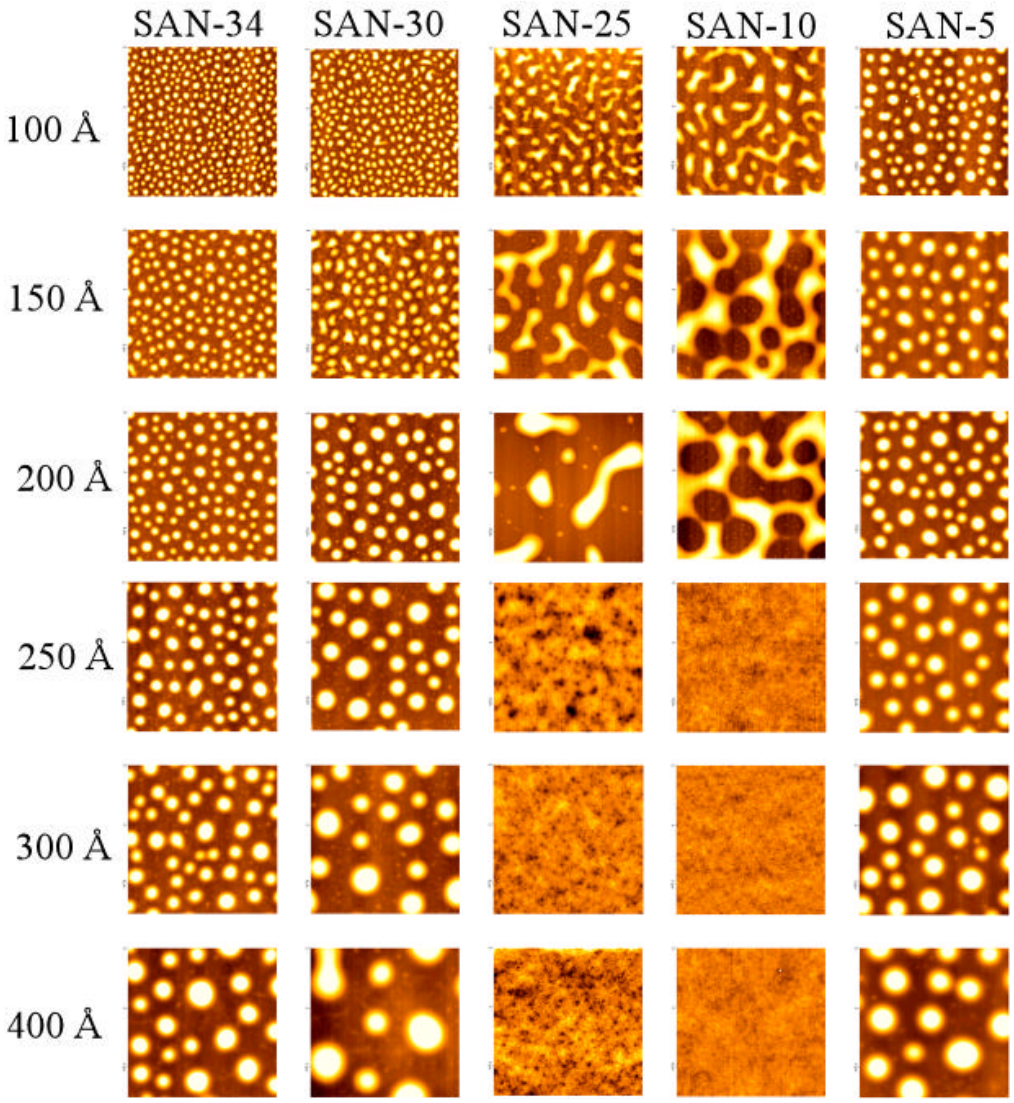

Figure 5.6: AFM scans of SAN-X/PMMA samples annealed at 210 ^{o}C. The initial thickness of the polymer films is listed to the left, and the SAN-X copolymer blend is listed across the top. All blends where 50/50 wt.% SAN-X/PMMA. All scans are 10 X 10 microns.

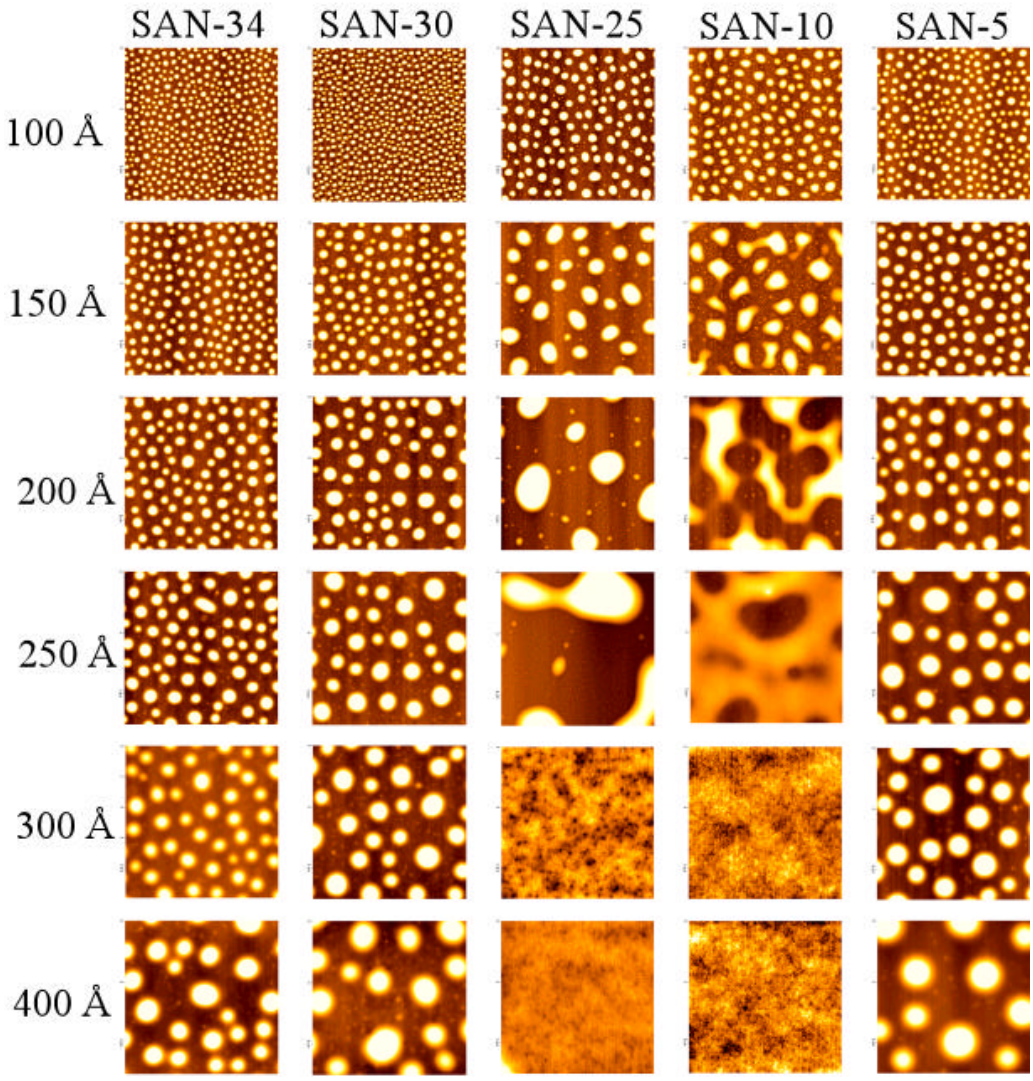

Figure 5.7: AFM scans of SAN-X/PMMA samples annealed at 230 ^{o}C. The initial thickness of the polymer films is listed to the left, and the SAN-X copolymer blend is listed across the top. All blends where 50/50 wt.% SAN-X/PMMA. All scans are 10 X 10 microns.

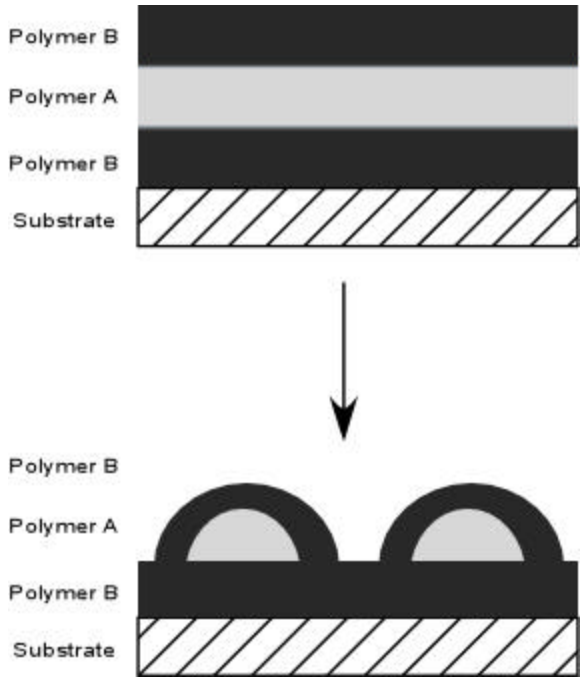

Figure 5.8: Tri-layer structure in a strongly segregating film. The interfaces are sharp indicating a large interfacial tension. This results in an instability as the film is annealed.

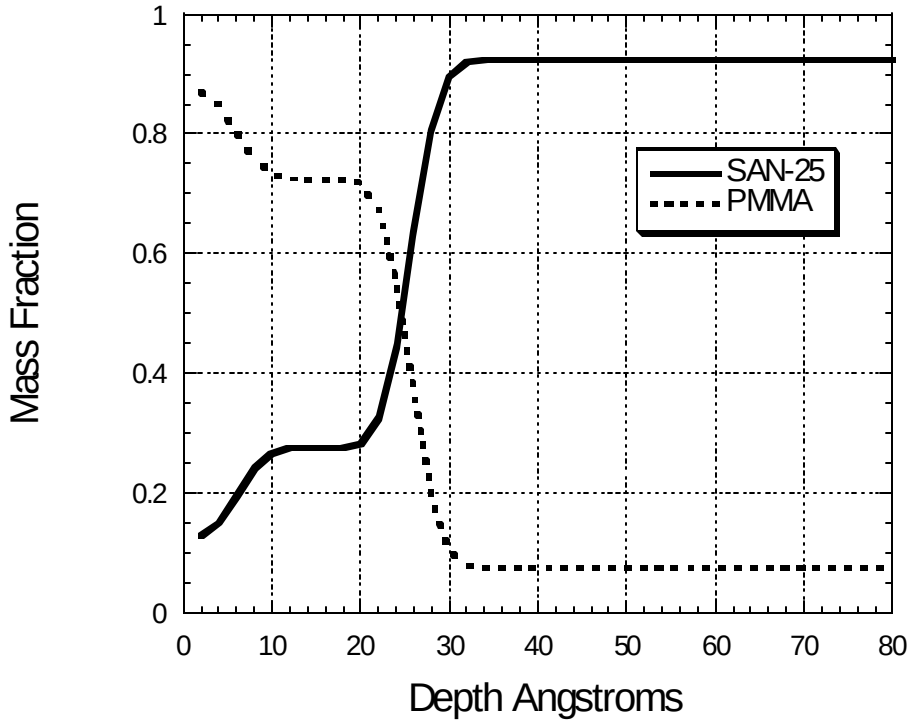

Figure 5.9: Angle resolved XPS depth profile of a 200 Å 50/50 wt. % SAN-25/PMMA film, annealed in a vacuum oven for 15 minutes at 210 ^{o}C. The profile clearly shows that the PMMA is segregating to the free interface.

the tri-layer structure will become unstable and dewet. χ is positive for both the SAN-34 and SAN-5 blends at this temperature, and as expected they both show structural instabilities. On the other hand, the h= 100 Å samples of the SAN-10, SAN-25, and SAN-30 mixtures, despite being in the bulk single phase region of the phase diagram, dewet, leaving a layer of PMMA on the substrate. As the film thickness of these blends is increased, the films become stable. The stability of the thicker films can be though to be due to a larger interfacial width for the thicker films, as illustrated in Figure 5.10. It will be shown that as the film thickness is decreased, the interfacial width decreases even if the polymer-polymer interactions have not changed. It will also be shown that in thin films the polymer-polymer interactions have less of an effect on the interfacial width. This decrease in interfacial width leads to the instability of all films at small thickness. Evidence to support this hypothesis will be given using polymer modeling later in the chapter.

A second set of AFM stability results for films annealed at 210 ^{o}C is given in Figure 5.6. As with the previous set of results, the SAN-34 and SAN-5 blends are unstable in the thickness regime ranging from 100 to 400 Å. The SAN-30 system is now also unstable at all film thicknesses studied. The SAN-10 and SAN-25 blends show instabilities up to 200 Å. The final set of films was annealed at 230 ^{o}C, Figure 5.7. These films look similar in character to the films annealed at 210 ^{o}C, with the exception of the SAN-10 and SAN-25 blends becoming unstable at 250 Å.

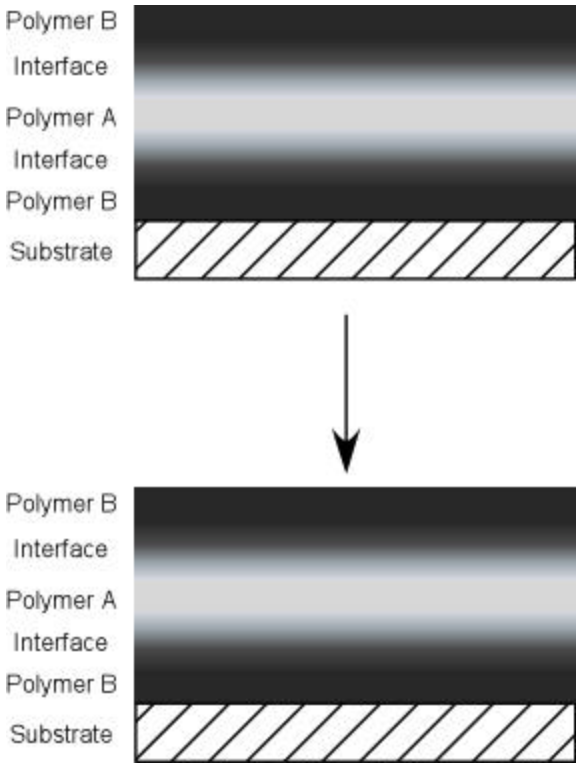

Figure 5.10: Tri-layer structure in a weakly segregating film. The interfaces are diffuse indicating a smaller interfacial tension. This results in a stable film.

Some of the films shown in Figures 5.5, 5.8 and 5.6 were subjected to selective removal of PMMA, which was accomplished by immersing the sample into an acetic acid bath for 2 minutes. Acetic acid acts as a selective solvent for PMMA, leaving behind only the SAN-X rich regions. The results for selectively dissolved 400 angstrom SAN-34/PMMA films are shown in Figure 5.11. It is clear that the core of the dewet drops is SAN-34 and that PMMA is encapsulating the SAN-34 drops and covering the substrate. This result agrees with the model proposed in Figure 5.6. The next set of samples selectively dissolved were 400 angstrom SAN-30/PMMA films, as seen in Figure 5.12. The films annealed at 230 and 210 ^{o}C look very similar to the SAN-34/PMMA blends, but the film annealed at 170 ^{o}C goes from being featurless to showing some underlying structure. All of the results from the SAN-25/PMMA system are initially featureless and show underlying structure after washing as shown in Figure 5.13. The SAN-10/PMMA system shows the same behavior that the SAN-30/PMMA system shows at 170 ^{o}C at all of the anneal temperatures, as seen in Figure 5.14. These films are initially featureless and remain that way after the selective dissolution occurs, as seen in Figure 5.14. The thickness of the films has been reduced from 400 to about 265 Å for all three samples. This result again agrees with the model of a film that exhibits symmetric segregation with a diffuse interface, as shown in Figure 5.7. Finally, Figure 5.15 shows selectively dissolved 400 angstrom SAN-5/PMMA films. It is clear from Figure 5.15 that the droplets on the surface of the substrate

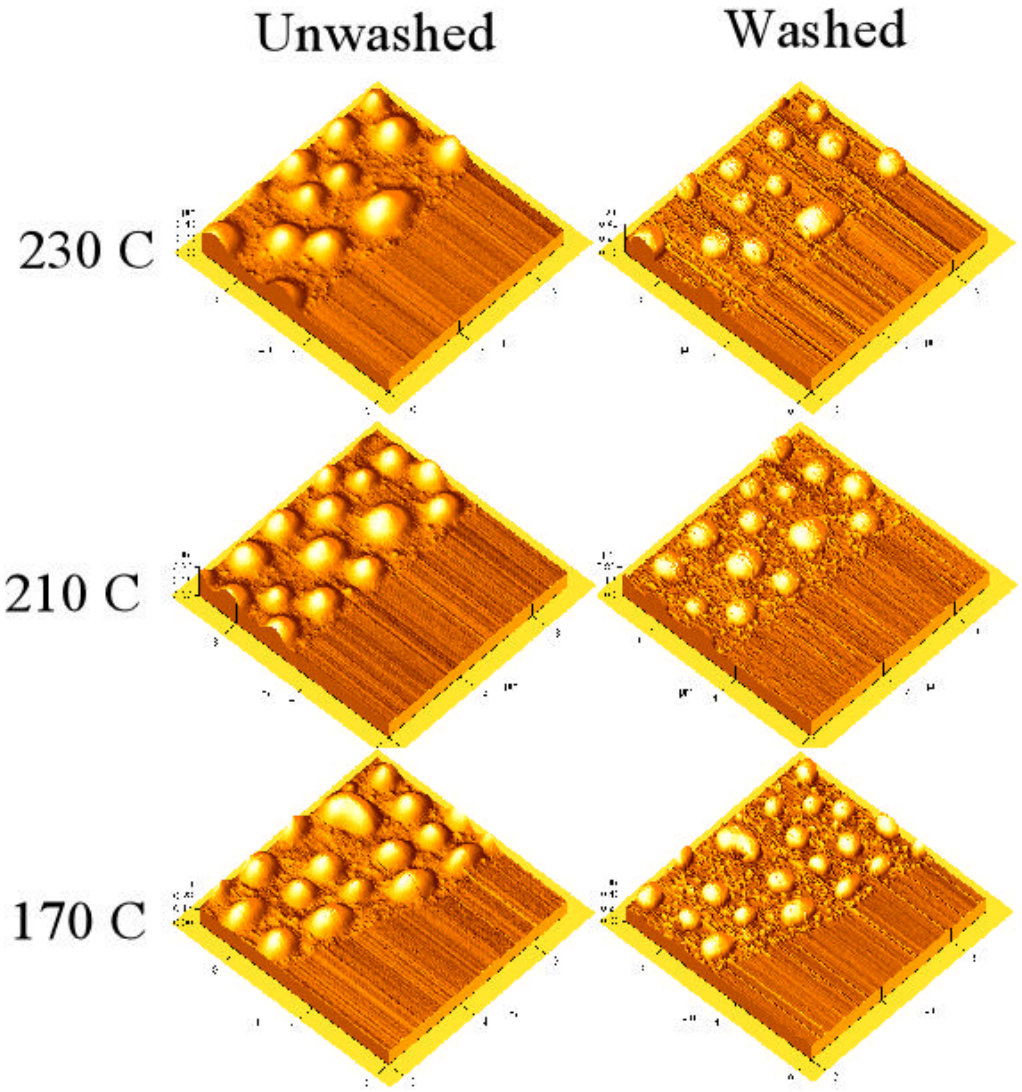

Figure 5.11: AFM scans of 400 angstrom films of a SAN-34/PMMA blend. The films have been washed with acetic acid, which is a selective solvent for PMMA. The scans on the left are prior to the wash, and the scans on the right are after the wash has occurred. The polymer in the right side of the scan has been scraped away, so that the substrate can be used as a reference for the polymer topography.

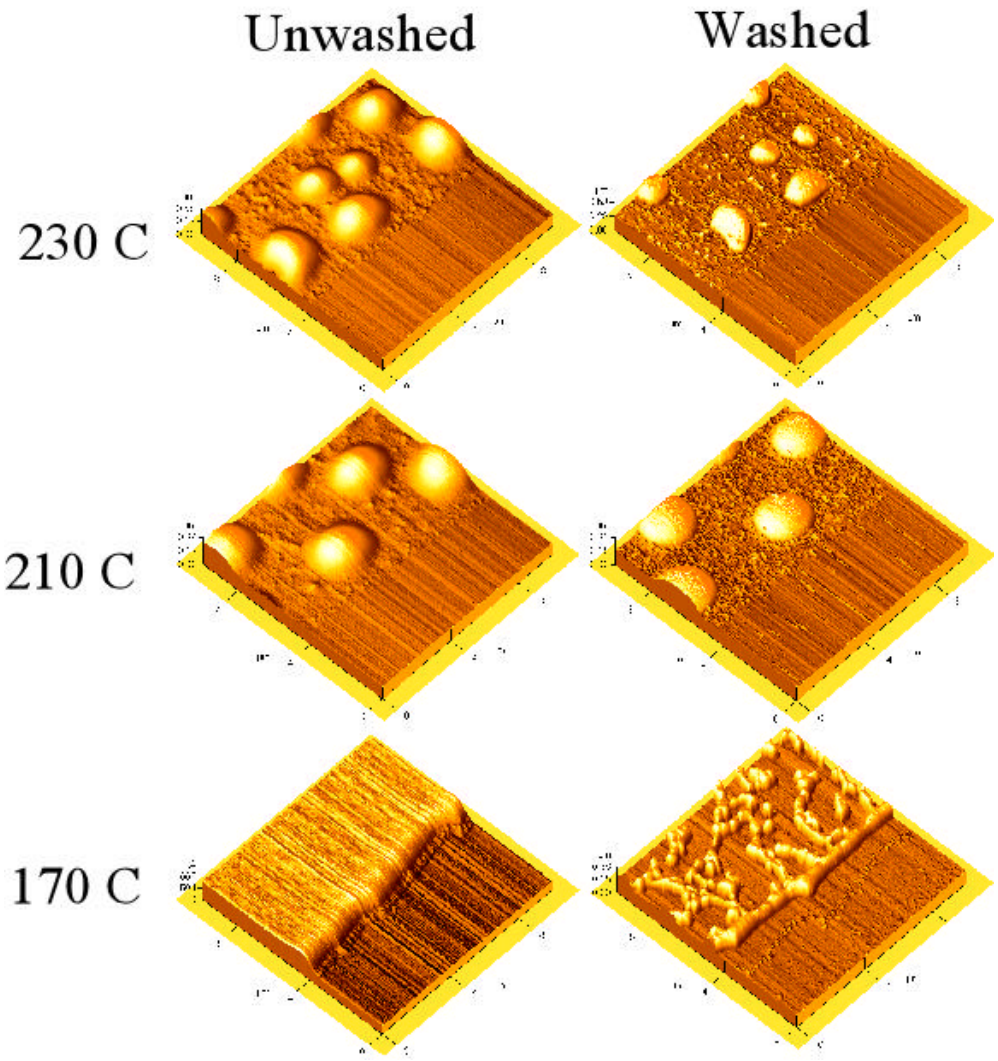

Figure 5.12: AFM scans of 400 angstrom films of a SAN-30/PMMA blend. The films have been washed with acetic acid, which is a selective solvent for PMMA. The scans on the left are prior to the wash, and the scans on the right are after the wash has occurred. The polymer in the right side of the scan has been scraped away, so that the substrate can be used as a reference for the polymer topography.

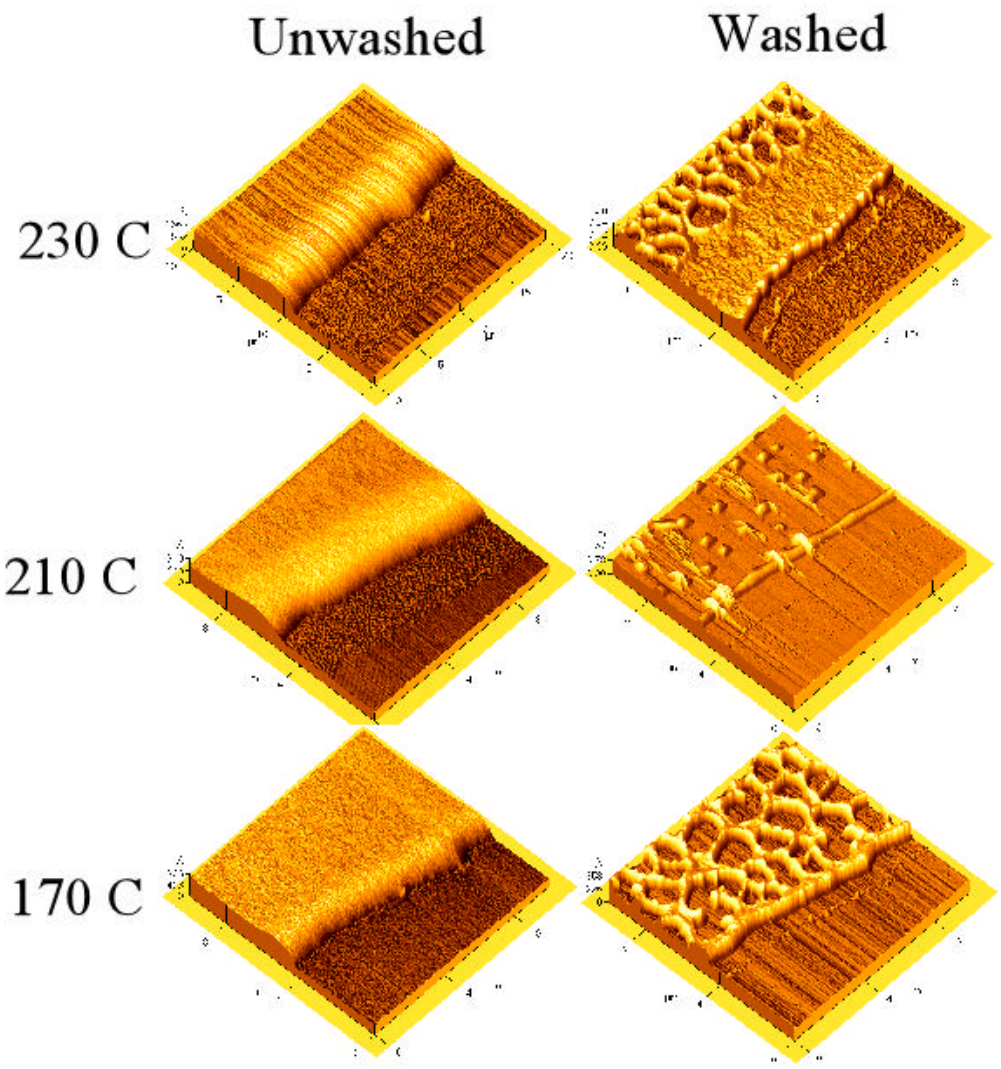

Figure 5.13: AFM scans of 400 angstrom films of a SAN-25/PMMA blend. The films have been washed with acetic acid, which is a selective solvent for PMMA. The scans on the left are prior to the wash, and the scans on the right are after the wash has occurred. The polymer in the right side of the scan has been scraped away, so that the substrate can be used as a reference for the polymer topography.

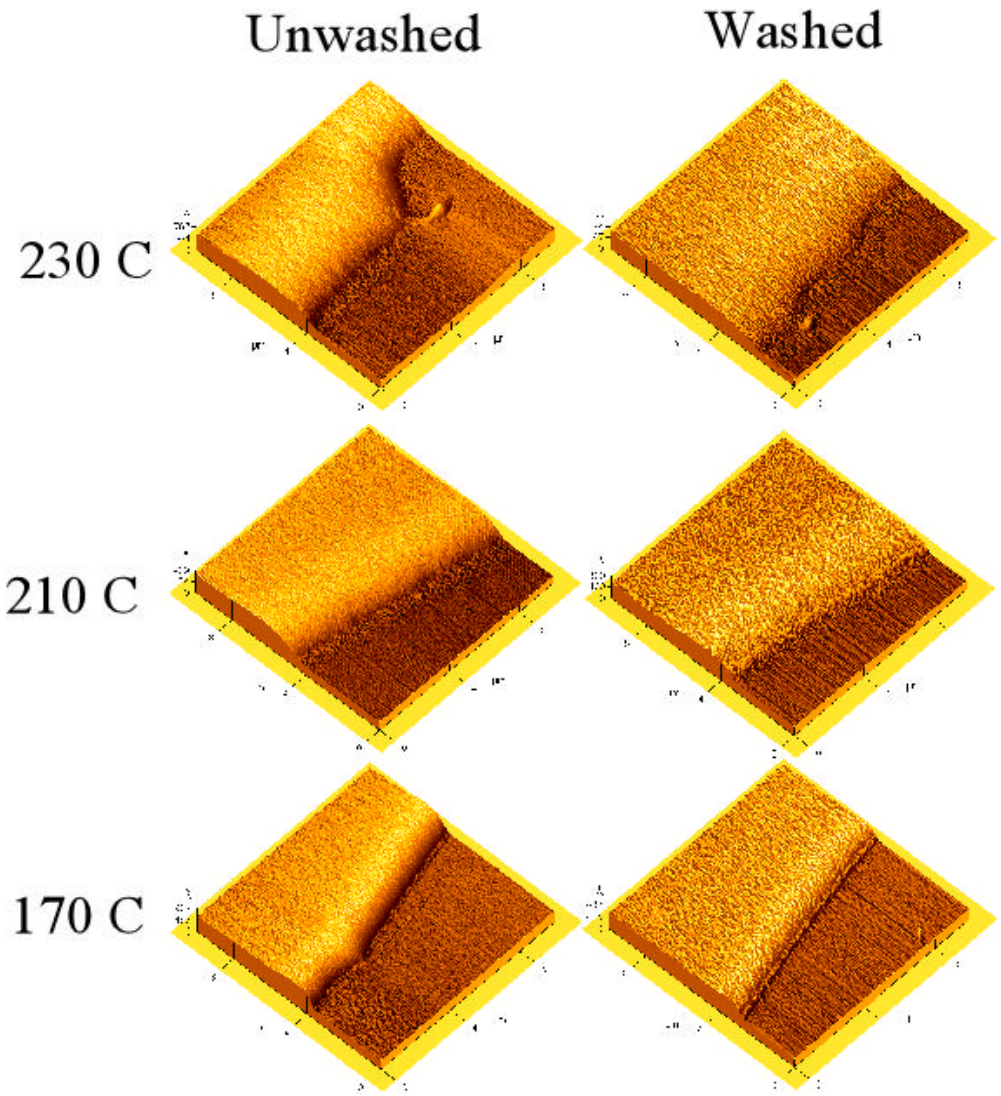

Figure 5.14: AFM scans of 400 angstrom films of a SAN-10/PMMA blend. The films have been washed with acetic acid, which is a selective solvent for PMMA. The scans on the left are prior to the wash, and the scans on the right are after the wash has occurred. The polymer in the right side of the scan has been scraped away, so that the substrate can be used as a reference for the polymer topography. The thickness of the films has been reduced from 400 to about 265 Å for all three samples.

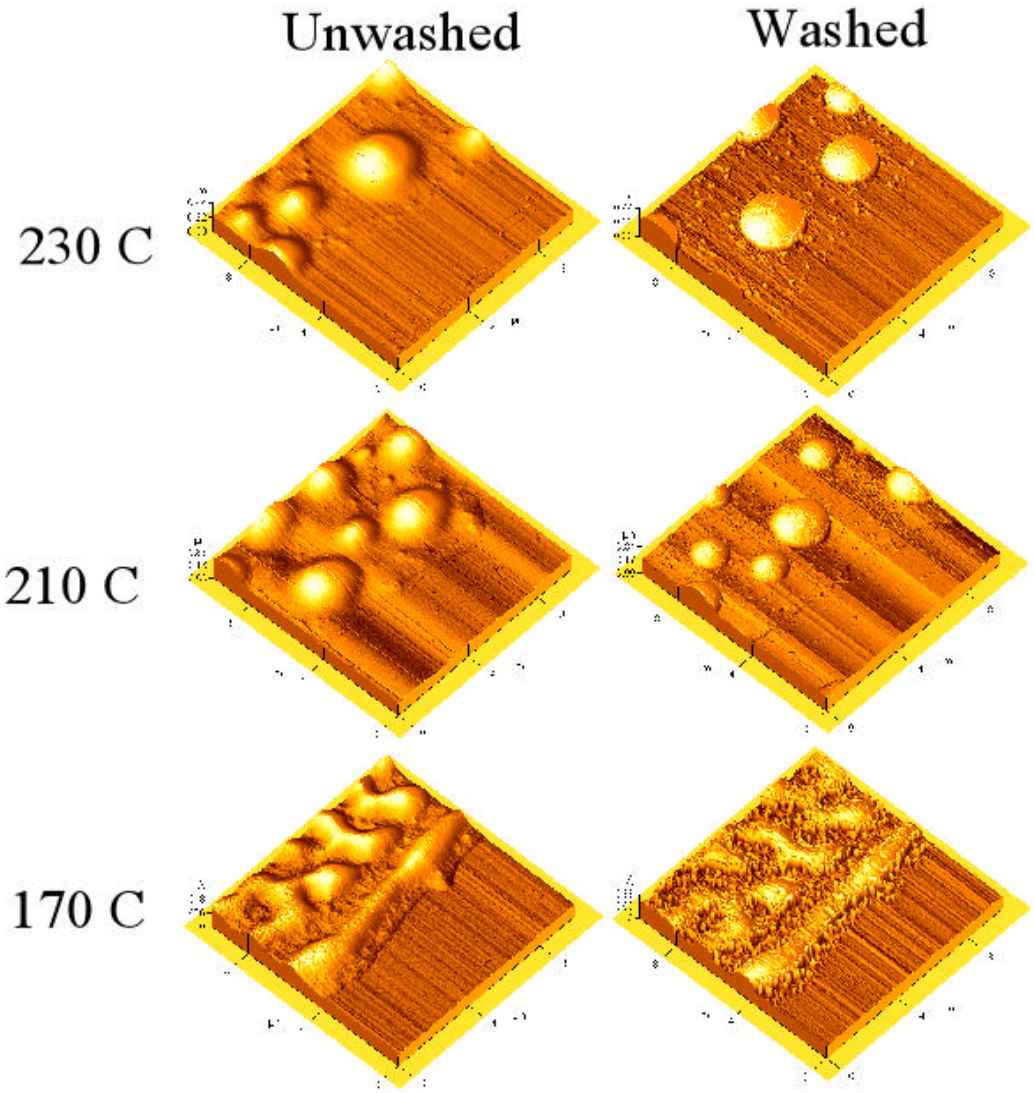

Figure 5.15: AFM scans of 400 angstrom films of a SAN-5/PMMA blend. The films have been washed with acetic acid, which is a selective solvent for PMMA. The scans on the left are prior to the wash, and the scans on the right are after the wash has occurred. The polymer in the right side of the scan has been scraped away, so that the substrate can be used as a reference for the polymer topography.

consist of SAN-5 encapsulated by PMMA, with a layer of PMMA on the surface of the substrate.

Taken together the results from the SAN-30, SAN-25, and SAN-10 blends tell an interesting story. It seems that when χ is positive and large enough the system will be unstable and for droplets, as seen at 230 and 210 ^{o}C for the SAN-30 blend. When χ is positive and small, the films appear to be featureless from the initial AFM scans, but have some structure only indicated after selective dissolution. This unusual structure is seen in all of SAN-25 blends and SAN-30 annealed at 170 ^{o}C. As χ approaches zero, or becomes negative, the films form a true tri-layer structure. The structure remains apparent even after the film has been selectively dissolved, as seen in the SAN-10 blend system.

One final test of the consistency of the model in Figure 5.6 with the experimental system is provided by plotting the thickness of the PMMA wetting layer on the substrate after dewetting versus the original film thickness, as seen in Figure 5.16. The average of all dewet blends results in a wetting layer thickness that is consistently about ¼ the overall film thickness, agreeing well with the concept of tri-layer formation and subsequent instability.

To better understand the deweting mechanism, the early stages of deweting were also studied in 100 Å films of the SAN-5, 9.5, 25, 30, and 34 blends annealed at 210 ^{o}C. Each blend system was annealed for 5 – 10 minute intervals, then quenched to room temperature to lock in the morphology and scanned with the AFM. This technique allows the change in morphology with time to be studied for each of these blend systems. The results are presented in

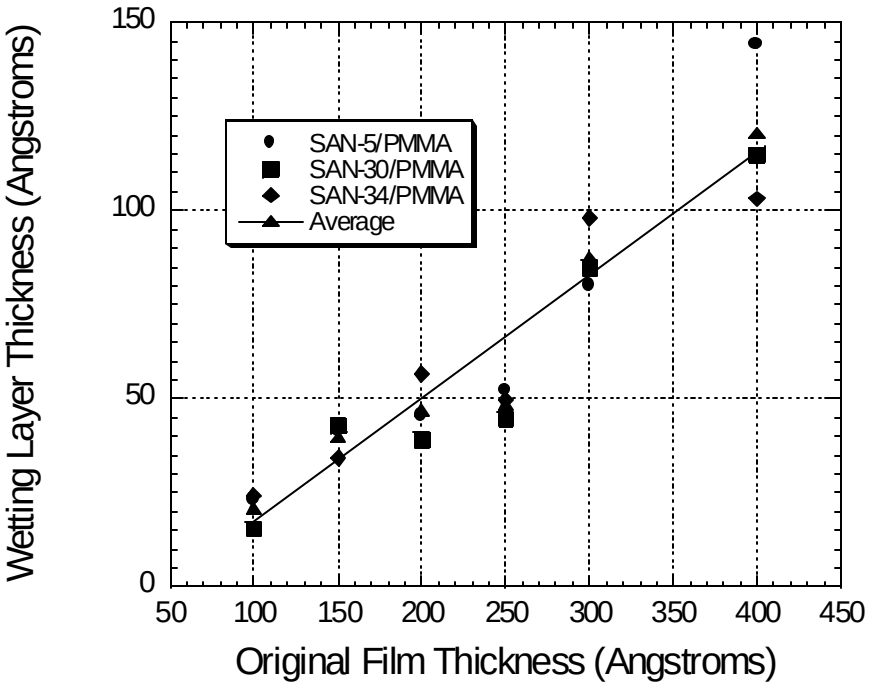

Figure 5.16: Comparison of wetting layer thickness on the silicon substrate, as a function of original film thickness.

Figures 5.17, 5.18, 5.19, 5.20, and 5.21, which represent the results for 50/50 wt. % PMMA blends with SAN-34, SAN-30, SAN-25, SAN-9.5, and SAN-5. The results for blends of SAN-34 and SAN-30 both seem to indicate that the deweting mechanism is spinodal. At this temperature both of these films should be above the bulk critical point, consequently they should have small interfacial widths and would be expected to readily become unstable at any thickness between 100 and 400 Å. Blends of SAN-25 are deweting via a nucleation and growth mechanism. At this temperature the SAN-25 blend is below its critical point, and would be expected to be stable at this temperature in the bulk. Based on the results from Figure 5.6, it is clear that small value of χ would indicate a stable film when the thickness is greater than 250 Å. This film becomes unstable though due to confinement effects on the interfacial width, as opposed to the polymer-polymer interaction controlled interfacial width in the SAN-34 and SAN-30 blends. These results indicate that a difference in the polymer-polymer interaction manifest itself in the mechanism via which a polymer dewets. The SAN-9.5 blend system, as seen in Figure 5.20, does not show any signs of deweting in the time scale that was studied. This blend has the highest critical point, so it would be expected that it would be the most stable system. Finally, the SAN-5 blend dewets in an unusual way. It appears as though this blend has characteristics of both spinodal deweting and nucleation and growth. It is difficult to explain exactly why the SAN-5 blends behave in this way. One possible cause is due to the fact that SAN-5 is the only blend studied to exhibit a UCST. At this temperature it is still below the critical point, indicating that it should be unstable in the bulk as are the

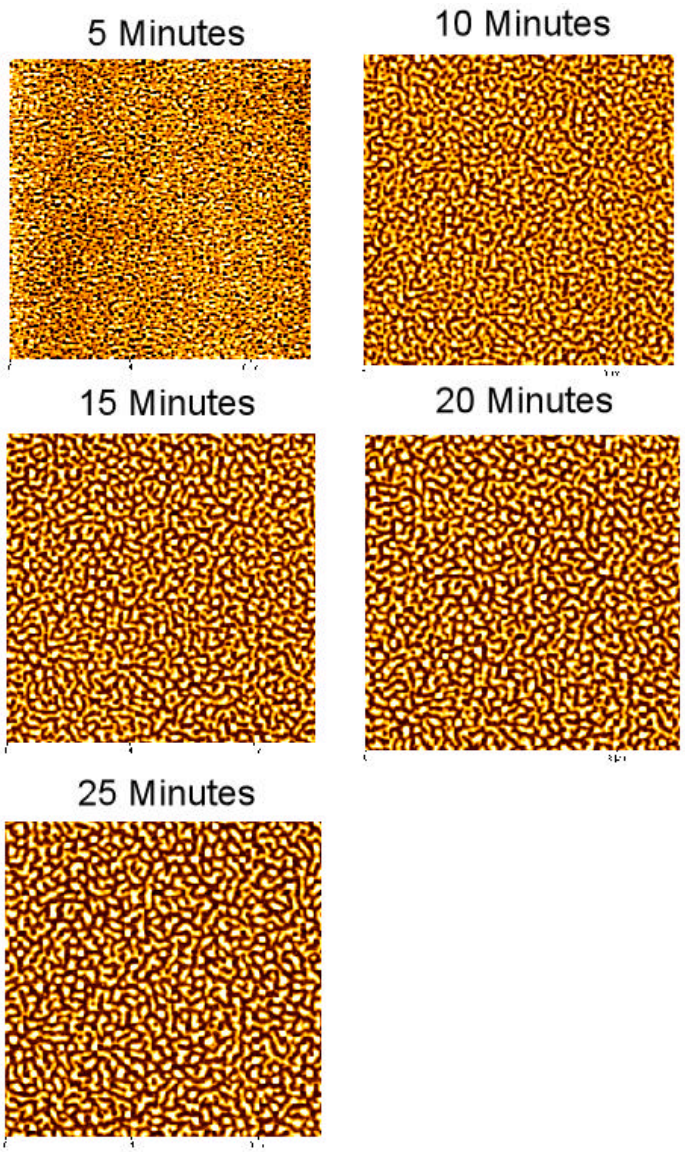

Figure 5.17: 100 Å film of SAN-34/PMMA 50/ 50 wt. % annealed at 210 ^{o}C from 5 to 25 minutes. This film exhibits a spinodal type instability.

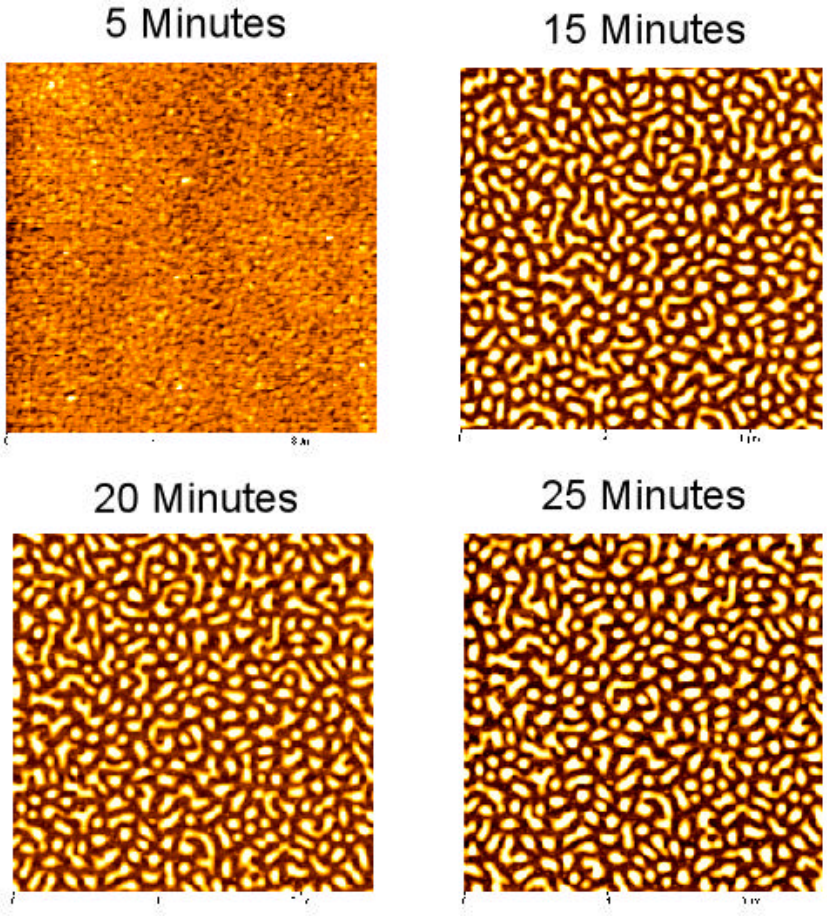

Figure 5.18: 100 Å film of SAN-30/PMMA 50/ 50 wt. % annealed at 210 ^{o}C from 5 to 25 minutes. This film seems to exhibit a spinodal type instability.

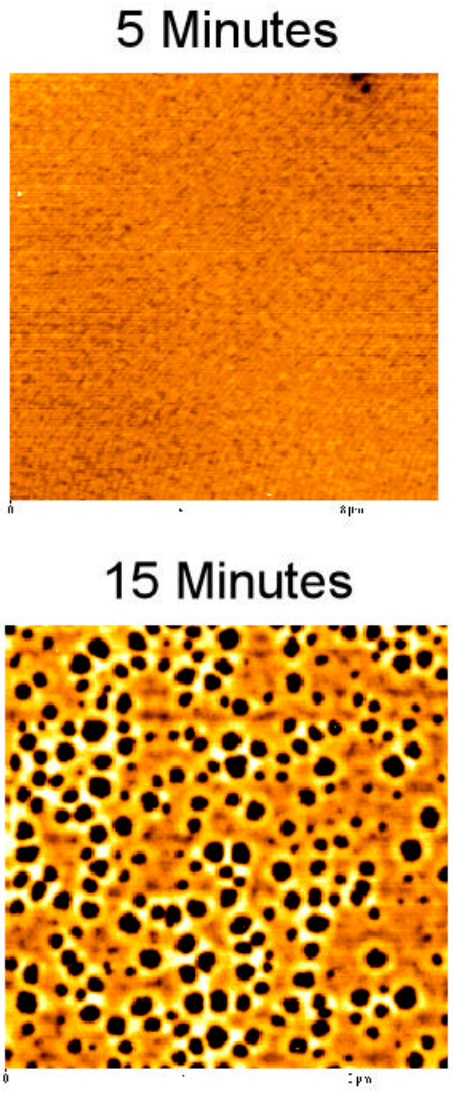

Figure 5.19: 100 Å film of SAN-25/PMMA 50/ 50 wt. % annealed at 210 ^{o}C from 5 to 15 minutes. This film seems to exhibit a nucleation and growth type instability.

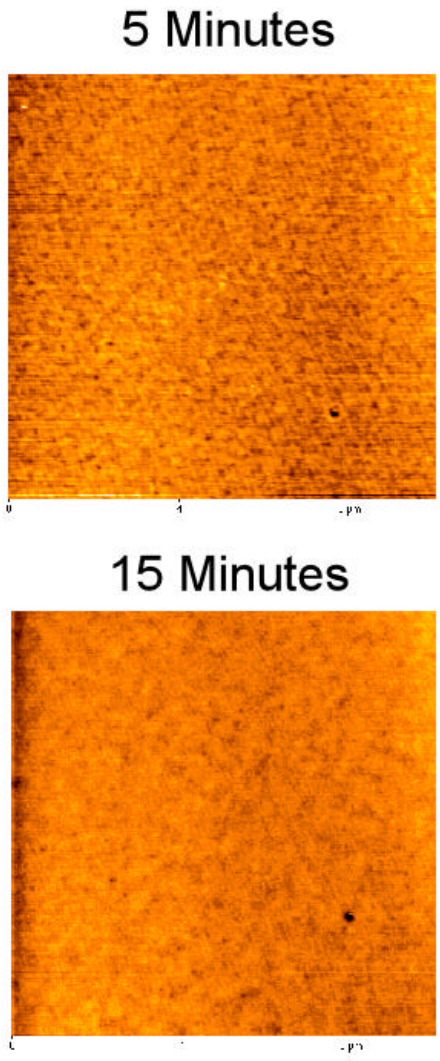

Figure 5.20: 100 Å film of SAN-10/PMMA 50/ 50 wt. % annealed at 210 ^{o}C from 5 to 15 minutes. This film seems to exhibit no instabilities during this time period.

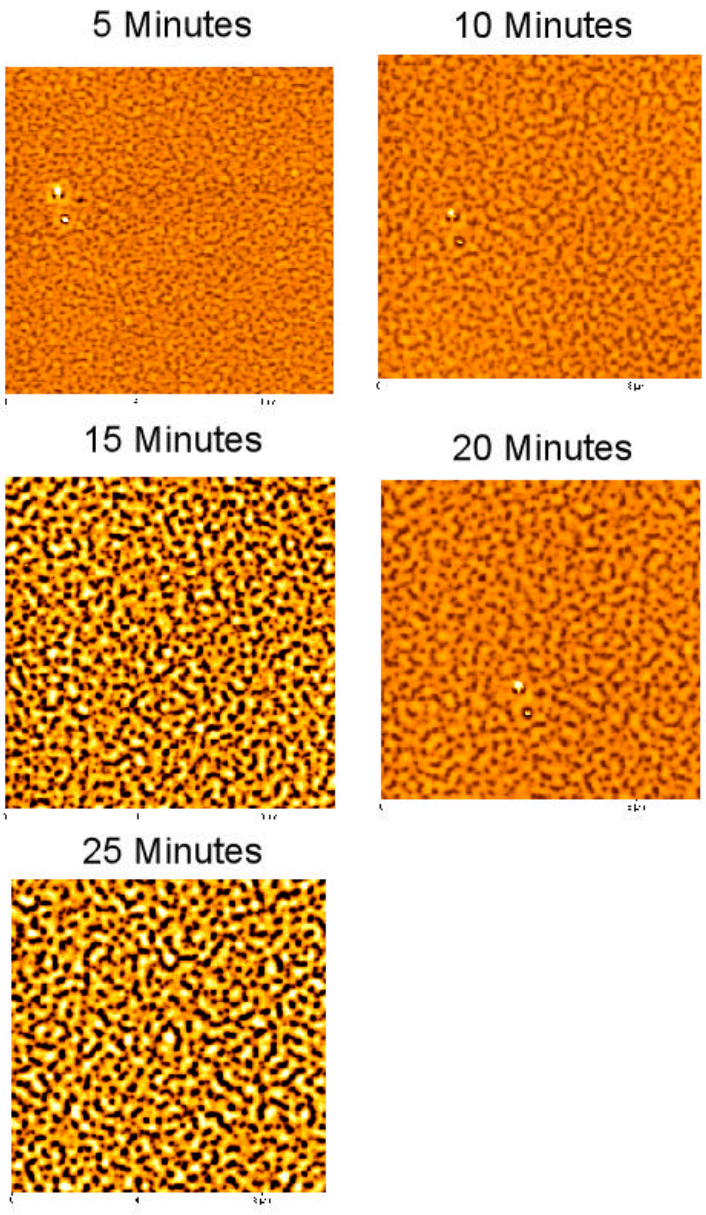

Figure 5.21: 100 Å film of SAN-5/PMMA 50/ 50 wt. % annealed at 210 ^{o}C from 5 to 15 minutes. This film seems to exhibit a combination nucleation and growth and spinodal type instability.

SAN-34 and SAN-30 systems. Perhaps the polymer-polymer interactions of UCST system relative to a LCST system create the difference in the deweting behavior between the SAN-5 and the SAN-34/30 systems.

5.4 Simulation Results and Discussion

The Visual Basic program from Chapter 4 was used to model segregation in the experimental polymer system. The model system consisted of polymer A, which is equivalent to PMMA, and polymer B which symbolizes SAN-X. It was assumed that polymer A preferentially segregated to the interfaces, so the surface potential was studied at two values of surface energy difference. A small surface energy difference was studied, $\Delta\gamma$ = .01 mJ/m^2 (μ_s = 0.02, g = 0), and a large surface energy difference was studied, $\Delta\gamma$ = .1 mJ/m^2 (μ_s = 0.2, g = 0). Based on the properties of the polymers used in the experiments N_A = 1000, N_B = 2000, a_A = 0.852, and a_B = 1.155. Composition profiles for a range of χ Chi values between .002 and 0 where calculated for films with thicknesses of 40, 25, 20, 15, and 10 nm.

The concentration profile of the films as a function of film thickness (D) is presented in Figure 5.22. Figure 5.22 (a) shows the results of the small surface energy difference ($\Delta\gamma$ = .01 mJ/m^2). There is obviously segregation of polymer A to the interface, but the concentration at the interface is largely dependant on the thickness of the film. As the film thickness is reduced, the concentration of A at the interface is reduced. This indicates that the surface energy of the two polymers is not great enough to completely overcome the square gradient effect,

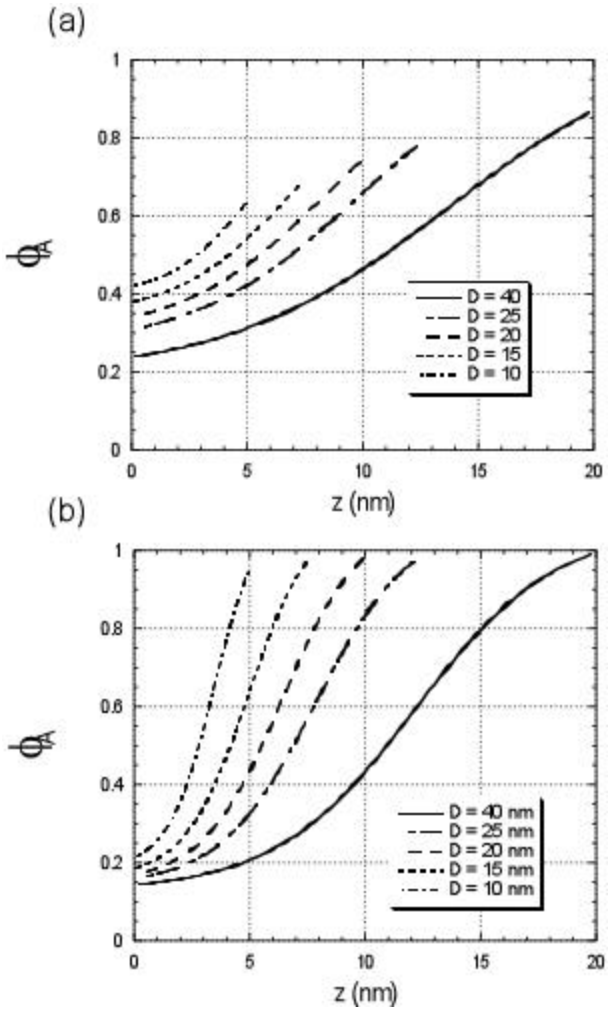

Figure 5.22: Concentration profiles as a function of D. (g = 0, N_A = 1000, N_B = 2000, aA = 0.852, aB = 1.155) (a) Profiles for a system with a 0.01 mJ/m^2 difference between the surface energy of the two polymers (μ_s = 0.02) (b) Profiles for a system with a 0.1 mJ/m^2 difference between the surface energy of the two polymers (μ_s = 0.2)

which tries to prevent concentration gradients perpendicular to the interface. Figure 5.22 (b) clearly shows however that when the surface energy difference is increased to $\Delta\gamma$ = .1 mJ/m^2, the concentration of polymer A at the interface does not vary to any significant extent. This is indicative of the surface energy difference overcoming the gradient reducing effects of the square gradient term in the free energy expression.

Figure 5.23 demonstrates the effect of modifying the value of χ on the profile the films with thicknesses D = 10 and D = 40 nm, for a polymer system with a surface energy difference of $\Delta\gamma$ = .01 mJ/m^2. It is clear that as the film thickness is increased from 10 to 40 nm, the effect of χ on the interfacial width becomes more significant. Figure 5.24 shows the same effect for a polymer system with a surface energy difference of $\Delta\gamma$ = .1 mJ/m^2. This system also shows an increase in the effect of χ on the interfacial width of as the film thickness is increased, but to a much lesser extent than at small values of $\Delta\gamma$. It seems that for these larger values of $\Delta\gamma$, the surface energy difference dominates the effect of changing χ on the interfacial width.

In order to better understand the interaction between the values of $\Delta\gamma$, χ, and thickness variation on the interfacial width, an analytical description of the interfacial width is necessary. A crude quantitative approach is to define the intrinsic width (L) by:

$$L = \frac{\frac{1}{2}\left(f_{z=h} - f_{z=0}\right)}{\left.\frac{df}{dz}\right|_{\frac{1}{2}\left(f_{z=h} - f_{z=0}\right)}} \tag{5.1}$$

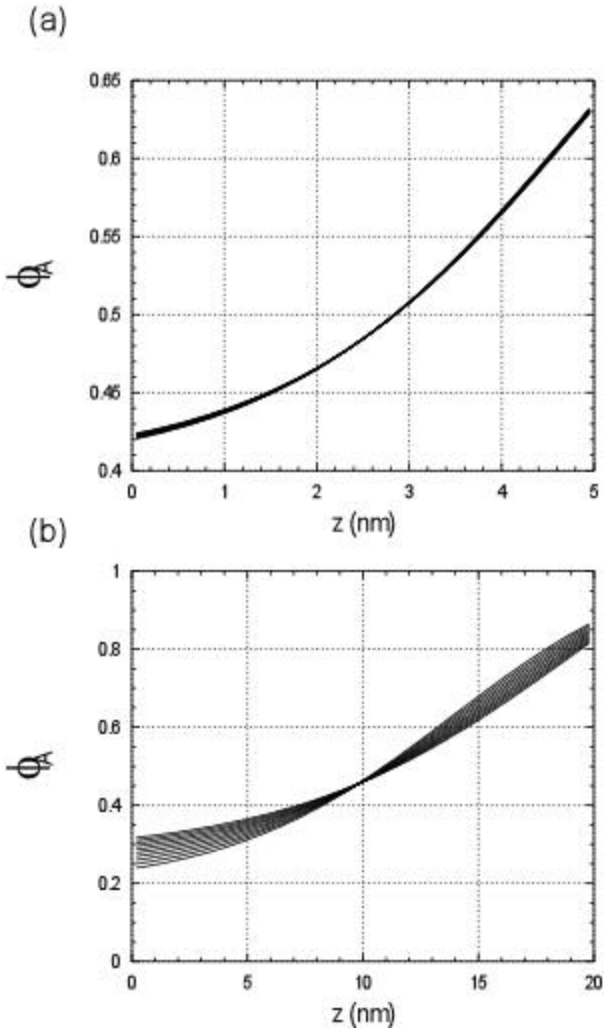

Figure 5.23: Concentration profiles as a function of χ (0.002 thru 0) for a system with a 0.01 mJ/m^2 difference between the surface energy of the two polymers (μ_s = 0.02, g = 0, N_A = 1000, N_B = 2000, aA = 0.852, aB = 1.155) (a) D = 10 nm (b) D = 40 nm

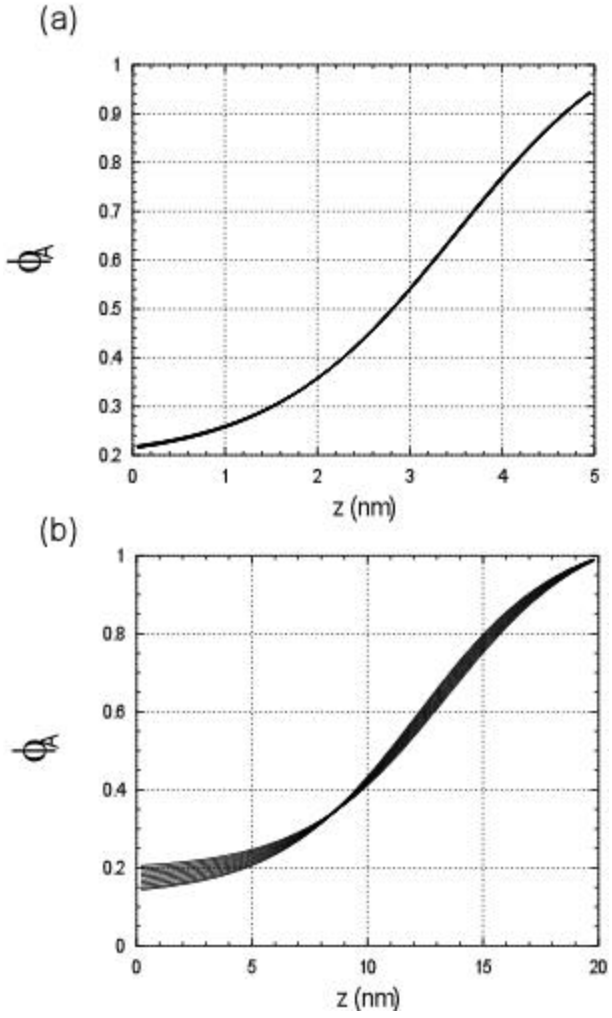

Figure 5.24: Concentration profiles as a function of χ (0.002 thru 0) for a system with a 0.1 mJ/m^2 difference between the surface energy of the two polymers (μ_s = 0.2, g = 0, N_A = 1000, N_B = 2000, aA = 0.852, aB = 1.155) (a) D = 10 nm (b) D = 40 nm

where $\phi_{z=h}$ is the composition at the interface, and $\phi_{z=0}$ is the composition at the center of the film. The results of this calculation of L as a function of $\Delta\gamma$, χ, and thickness variation are presented in Figure 5.25. Figure 5.25 (a) presents the effect of changing χ and thickness on the interfacial width for a system with $\Delta\gamma$ = .01 mJ/m^2. As expected increasing the value of χ decreases the intrinsic width. The value of L also decreases as the thickness of the film is decreased. The magnitude of the decrease in intrinsic width relative to a change in χ gets smaller as the thickness of a film is decreased. The decrease in this slope means that for a film with a thickness of 10 nm the intrinsic width is relatively insensitive to changes in changes in thickness. Figure 5.25 (b) presents the effect of changing χ and thickness on the interfacial width for a system with $\Delta\gamma$ = .1 mJ/m^2. It is clear that the general effects of changing χ and film thickness are similar to those for $\Delta\gamma$ = .01 mJ/m^2. There are several changes that result from the increase of $\Delta\gamma$. First, the overall value of L has shifted to lower values for an equivalent thickness. This is not surprising since as discussed previously the increase in $\Delta\gamma$ will tend to increase the segregation of polymer A to the interface, as seen in Figure 5.22. This concentration is relatively independent of the overall film thickness in the range from 100 to 400 Å. It is also clear from Figure 5.25 (b) that the magnitude of the decrease in L relative to a change in χ gets smaller as the thickness of a film is decreased, as seen in Figure 5.25 (a). There are several differences in the behavior of the intrinsic width relative to χ and thickness as $\Delta\gamma$ is increased. First, the intrinsic width becomes invariant with χ at 20 nm rather than 10 nm, as seen in the example where $\Delta\gamma$ = .01 mJ/m^2. Second, the magnitude

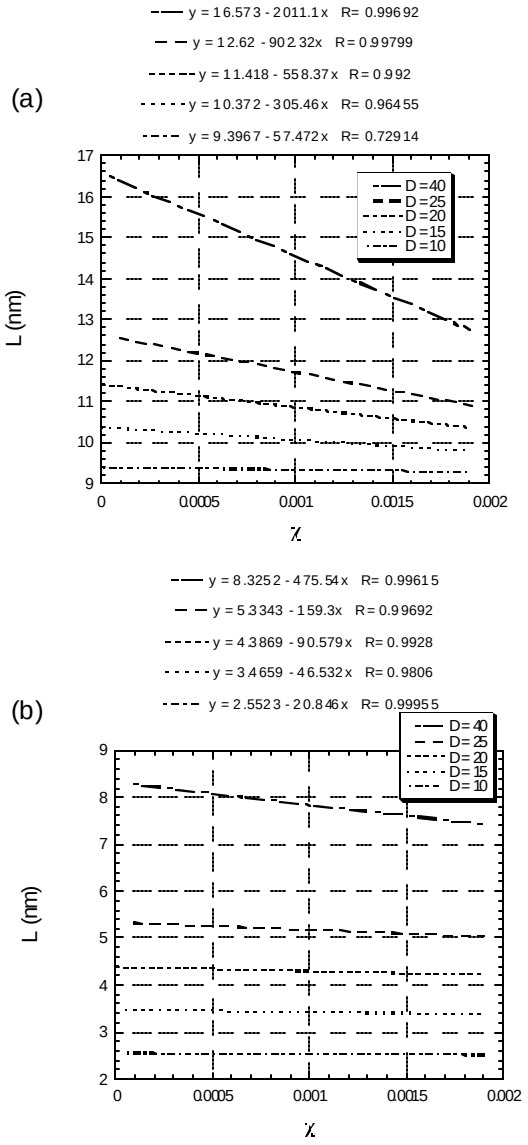

Figure 5.25: Intrinsic width as a function of χ for polymer films with D = 40, 25, 20, 15, and 10 nm. (g = 0, N_A = 1000, N_B = 2000, aA = 0.852, aB = 1.155) (a) Profiles for a system with a 0.01 mJ/m^2 difference between the surface energy of the two polymers (μ_s = 0.02) (b) Profiles for a system with a 0.1 mJ/m^2 difference between the surface energy of the two polymers (μ_s = 0.2)

of the decrease in L relative to a change in χ is much smaller for the system with a larger $\Delta\gamma$. This change can be seen by comparing the difference of the slope for D = 40 nm, between the two systems. The $\Delta\gamma$ = .01 mJ/m^2 system has a slope of -2011, while the $\Delta\gamma$ = .1 mJ/m^2 system only has a slope of -475. This represents about a fourfold decrease in the magnitude of the χ effect on intrinsic width as $\Delta\gamma$ is increased by an order of magnitude. The decrease in the χ effect on intrinsic width is not surprising in light of the fact that the concentration of A at the interface is largely independent of the film thickness, as seen in Figure 5.22.

If reexamine at the experimental results in light of these modeling results, the driving force behind the change in stability with thickness, AN content in the copolymer, and temperature become clear. The results from Figures 5.5, 5.6 and 5.7 indicate that all films that are 100 Å thick dewet, regardless of temperature or copolymer composition. This makes sense, since by changing temperature or copolymer composition results in the modification of χ. As Figure 5.25 indicates, all films in this thickness range will have a much smaller interfacial width, relative to similar thicker films. The results also indicate that the interfacial width of films in this thickness range will be insensitive to changes in χ. Consequently, little effect will be seen in the stability of films as the temperature or copolymer composition are modified for films that are 100 Å thick. On the other hand, it appears as though changing temperature and copolymer composition has the largest effect in the 400 angstrom film, exactly were the simulations show that these variables will have the most effect on the interfacial width. The exact relationship between the structural stability of these films and the interfacial width

is still unclear at this point. It is clear that there is a relationship between intrinsic width, related to $\Delta\gamma$, χ, and film thickness variation, and structural stability in these films. Further characterization of the relationship will require additional work.

5.5 CONCLUSIONS

Segregation and stability in ultra-thin polymer blends of SAN-X/PMMA were studied as a function of polymer thickness, anneal temperature and SAN-X copolymer composition using an AFM. These results where compared to calculations using the mean field approach described in Chapter 4.

First, the experimental angle resolved XPS results indicate that PMMA is enriching at the free interface. These results in conjunction with using the AFM to study the selective dissolution of the PMMA, clearly indicate that the system does segregate symmetrically with PMMA enriching at both interfaces.

The AFM results show that all polymer blends where unstable at a thickness of 100 Å. The polymer modeling showed that films in this thickness range have a small interfacial width, regardless of temperature or copolymer composition. Experimental results showed that as the thickness of the films was increased, the stability of the film depended more strongly on the polymer-polymer interactions. This dependence was confirmed with the modeling results to be due to an increase in broadening the interface as χ is decreased in thicker films. As the interface broadens, the interfacial tension is reduced, increasing the stability of the tri-layer. The overall effect creates a mechanism for stabilizing the 400 Å films that does

not exist in 100 Å films. Finally, the modeling results show a clear effect between $\Delta\gamma$ and the interfacial width. As $\Delta\gamma$ is increased, the interfacial width is decreased, and the sensitivity of interfacial width to changes in χ is decreased.

5.6 REFERENCES

5.8 Wang, H. and R.J. Composto, "Thin film polymer blends undergoing phase separation and wetting: Identification of early, intermediate, and late stages," *J. Chem. Phys.*, 113 (22) 2000.: p. 10386-10397.

5.2 Wang, H. and R.J. Composto, "Hydrodynamic-flow-driven wetting in thin film polymer blends: Growth kinetics and morphology," *Phys. Rev. E: Stat. Phys., Plasmas, Fluids, Relat. Interdiscip. Top.*, 61 (2) 2000.: p. 1659-1663.

5.3 Wang, H., *et al.*, "Multiple Lateral Length Scales in Phase-Separating Thin-Film Polymer Blends," *Langmuir*, 17 (9) 2001.: p. 2857-2860.

5.4 Newby, B.-m.Z. and R.J. Composto, "Influence of Lateral Confinement on Phase Separation in Thin Film Polymer Blends," *Macromolecules*, 33 (9) 2000.: p. 3274-3282.

5.5 Lee, W.-K., *et al., Surface mixing morphology in bilayer-polymer films,* in *Polymer Testing*. 1998. p. 167-177.

5.6 Glockner, G., "On the Behaviour of Styrene-Acrylonitrile Copolymer in Solution - VI," *European Polymer Journal*, 15 1979.: p. 727-732.

5.7 Fowler, M.E., J.W. Barlow, and D.R. Paul, "Effect of copolymer composition on the miscibility of blends of styrene-acrylonitrile copolymers with poly(methyl methacrylate)," *Polymer*, 28 (7) 1987.: p. 1177-84.

5.8 Suess, M., J. Kressler, and H.W. Kammer, "The miscibility window of poly(methyl methacrylate)/poly(styrene-co-acrylonitrile) blends," *Polymer*, 28 (6) 1987.: p. 957-60.

5.9 Ruzette, A.-V.G. and A.M. Mayes, *A Simple Free Energy Model for Weakly Interacting Polymer Blends*, in *Macromolecules*. 2001. p. 1894-1907.

5.10 Higashida, N., J. Kressler, and T. Inoue, "Lower critical solution temperature and upper critical solution temperature phase behavior in random copolymer blends: poly(styrene-co-acrylonitrile)/poly(methyl methacrylate) and poly(styrene-co-acrylonitrile)/poly(.epsilon.-caprolactone)," *Polymer*, 36 (14) 1995.: p. 2761-4.

Chapter 6: Recommendations for Future Work

6.1 POLYMER MODELING

The current mean field model accounts for bulk polymer interactions, the effect of a symmetric surface, and polymer asymmetry. The effect of long range van der Walls forces have not yet been introduced into the model. This is a straight forward modification to the current Visual Basic code using the approach of Jones [6.1]. Including asymmetric surface potentials would also expand the capabilities to include polymer systems that attract different polymers to each interface, or improve modeling of symmetric systems by not requiring the magnitude of the potential be the same at both interfaces.

It would also be interesting to better calculate the interfacial tension between the polymers. An approach is discussed in Binder's work [6.2], but the fact that the interface truncates the transition between phases must be though about carefully to insure accurate results.

It is possible to determine the hamaker constant of the segregated film. Using this information in conjunction with the interfacial tension, could allow the mechanism of the instability (spinodal or nucleation and growth of holes) to be determined.

6.2 ADDITIONAL EXPERIMENTS

The current series of experiments could be modified in expanded in several directions. First of all, the molecular weight of the PMMA could be increased. This would have the effect of counteracting the surface potential, and reduce the magnitude of the segregation. This should cause some of the films that are currently unstable to stabilize. Secondly, the SAN-5 system exhibits a UCST, but these films always remained unstable for the experimental conditions. It should be possible, with a thicker film, to observe a transition from an unstable film to a stable film as thickness is increased. This would be the opposite of the behavior observed in the current set of experiments, and would provide further proof of the mechanism.

It could also be interesting to modify the surface potential at one of the interfaces, perhaps by coating the substrate with a self assembled mono-layer. This could possible have the effect of just changing the magnitude, or perhaps even the sign of the potential at the second interface. These experiments would of course require modifications to the modeling software to accurately predict their behavior.

6.3 REFERENCES

6.1 Jones, R.A.L., "Effect of long-range forces on surface enrichment i n polymer blends," *Physical Review E*, 47 (2) 1993.: p. 1437-1440.

6.2 Binder, K., "Surface effects on polymer blends and block copolymer melts: theoretical concepts of surface enrichment, surface induced phase separation and ordering," *Acta Polym.*, 46 (3) 1995.: p. 204-25.

Appendix

```
!This program is designed to calculate the concentration profile of a polymer
!confined between selectivly attractive walls.  It was written by Steven Scheer
!in July of 2002.  It is based on the work by
!Thomas Flebbe et. al., J. Phys. II France, 6 (1996) 667-695


Double Precision a, N, Chi, ChiN, ChemPot, g, Mu1, FPhi(100000), PhiCent,
PhiB, D
Double Precision ChiCoex1, ChiCoex2, MinCoex, LowLim, UpLim, Guess,
Brent, Brent2
Double Precision MinPhiB, FB, DeltaPhi, GPhi(100000), Kappa(100000)
Double Precision SumZ, SurfSumZ(1000), OutGCent(1000), PhiEst(100)
Double Precision NuCenter(1000), PNuCent, MinNu
Double Precision DeltaLim, ConPCent(100), MNuCent(100), TempConc(100),
TempMNu(100)
Double Precision Z(40,100000), SurfConc(40), Conc(40,100000), DeltaF(40),
FTemp
Double Precision KapTemp, DPhi, FDeltaF(40,40), FDPhi(40), FConCent(40,40),
FSurfCon(40,40)
Double Precision AvePhi(40), FAvePhi(40,40)
Integer Select, i, NumPts, NumConv, TempNum,Set
Integer PSurfI, Loop, NLoops, Coex, SurfI(400), PhiFnd, RootLoop, Count
Integer NZPts(40),j, OutLoop, DPhiLoop, FNumConv(40), MNumConv,
ChiLoop, OutLoop2
Character OutName*40, Numbers*100, OutValue*15


!1 - Means Brent solves for ChiCoex1 and 2 - Means Brent solves for MinPhiB

!For the variable Coex, 1 means approaching Coex1 from single phase region,
!2 means approaching Coex2 from the single phase region


OutLoop2=0

Do ChiLoop=0,10

OutLoop2=OutLoop2+1
OutLoop=0
MNumConv=0
```

```
Do DPhiLoop=0,24

Coex=2
Set=2

Chi = 2.2-ChiLoop*.02
D=60
N=100
LowLim = .00001
UpLim = .49999
Guess =.25
If (Set.Eq.1) Then
        ChemPot=.000679
        If (Coex.Eq.1) ChemPot=-ChemPot
Else
        DPhi=dble(.001+Dble(DPhiLoop*.002))
Endif
a=1
g=-.5
Mu1=.2
NumPts=100000
PhiFnd=0
DeltaPhi=1/dble(NumPts)

ChiN = Chi/N

OutLoop=OutLoop+1


Numbers='12345678910111213141516171819202122232425262728293O'

Write(*,*) 'Running Chi= ', ChiN
Write(*,*) 'Running DPhi= ', DPhi


Select = 1

MinCoex = Brent(LowLim,Guess,UpLim,ChiCoex1,N,ChiN,ChemPot,Select)

ChiCoex2 = 1-ChiCoex1
```

```
If (Set.Eq.1) Then
        Select = 2

        If (Coex.Eq.1) Then
                Guess = ChiCoex1-ChiCoex1/100
        Else
                LowLim = .5001
                UpLim = .9999
                Guess = ChiCoex2+ChiCoex1/100
        Endif


        MinPhiB = Brent(LowLim,Guess,UpLim,PhiB,N,ChiN,ChemPot,Select)

        If (Coex.Eq.1) Then
                DPhi=ChiCoex1-PhiB
        Else
                DPhi=ChiCoex2+PhiB
        Endif


Else
        If (Coex.Eq.1) Then
                PhiB=ChiCoex1-DPhi
        Else
                PhiB=ChiCoex2+DPhi
        Endif

        ChemPot=((1/N)*(dlog(PhiB/(1-PhiB))))+ChiN*(1-2*PhiB)

Endif

FB=((PhiB/N*dlog(PhiB)+(1-PhiB)/N*dlog(1-PhiB))+(ChiN*PhiB*(1-PhiB)))


Do i = 1,NumPts-1
        FPhi(i)=((dble(i*DeltaPhi)/N*dlog(dble(i*DeltaPhi))+(1-
dble(i*DeltaPhi))/N*dlog(1-dble(i*DeltaPhi)))+(ChiN*dble(i*DeltaPhi)*(1-
dble(i*DeltaPhi))))
        GPhi(i)=(FPhi(i)-FB+(ChemPot*(PhiB-dble(i*DeltaPhi))))
        Kappa(i)=(a**2)/(36*dble(i*DeltaPhi)*(1-dble(i*DeltaPhi)))
```

```
End do

NLoops=(Int((ChiCoex2-ChiCoex1)/.001))

PhiFnd=0

Do Loop=1,NLoops

        If (Coex.Eq.1) Then
                PhiCent = ChiCoex1+(Loop*((ChiCoex2-ChiCoex1)/NLoops))
        Else
                PhiCent = ChiCoex2-(Loop*((ChiCoex2-ChiCoex1)/NLoops))
        Endif

        SumZ = 0


        If ((PhiCent.gt.ChiCoex1).And.(PhiCent.lt.ChiCoex2)) Then
        Call
NuCalc(D,NumPts,DeltaPhi,N,ChiN,Coex,g,ChemPot,PhiB,PhiCent,FB,GPhi,Ka
ppa,SumZ,PSurfI,PNuCent)
        End If

        If (SumZ.gt.0) Then
                OutGCent(Loop)=PhiCent
                SurfI(Loop)=PSurfI
                SumZ=SumZ*DeltaPhi
                SurfSumZ(Loop)=SumZ
                NuCenter(Loop)=PNuCent
        Endif

        !If ((PhiFnd.Eq.0).And.(PNuCent.Gt.Mu1).And.(Coex.Eq.1)) Then
        !       PhiFnd=1
        !       PhiEst(PhiFnd)=PhiCent
        If ((PhiFnd.Eq.0).And.(PNuCent.Lt.Mu1)) Then
                PhiFnd=1
                PhiEst(PhiFnd)=PhiCent
        Endif

        !If ((Mod(PhiFnd,2).Eq.1).And.(PNuCent.Lt.Mu1)) Then
        !       PhiFnd=PhiFnd+1
        !       PhiEst(PhiFnd)=PhiCent
```

```
        !Elseif ((Mod(PhiFnd,2).Eq.0).And.(PNuCent.Gt.Mu1)) Then
        !       PhiFnd=PhiFnd+1
        !       PhiEst(PhiFnd)=PhiCent
        If ((Mod(PhiFnd,2).Eq.1).And.(PNuCent.Gt.Mu1)) Then
                PhiFnd=PhiFnd+1
                PhiEst(PhiFnd)=PhiCent
        Elseif ((Mod(PhiFnd,2).Eq.0).And.(PNuCent.Lt.Mu1)) Then
                PhiFnd=PhiFnd+1
                PhiEst(PhiFnd)=PhiCent
        Endif

End Do

If (OutLoop2.lt.10) Then
        If (OutLoop.Lt.10) Then
                OutName='EtaOut' // Numbers(OutLoop:OutLoop) // 'Chi' //
Numbers(OutLoop2:OutLoop2) // '.txt'
        Else
                OutName='EtaOut' // Numbers(OutLoop-(OutLoop-
10)+((OutLoop-10)*2):OutLoop-(OutLoop-10)+((OutLoop-10)*2)+1) // 'Chi' //
Numbers(OutLoop2:OutLoop2) // '.txt'
        Endif

Else

        If (OutLoop.Lt.10) Then
                OutName='EtaOut' // Numbers(OutLoop:OutLoop) // 'Chi' //
Numbers(OutLoop2-(OutLoop2-10)+((OutLoop2-10)*2):OutLoop2-(OutLoop2-
10)+((OutLoop2-10)*2)+1) // '.txt'
        Else
                        OutName='EtaOut' // Numbers(OutLoop-(OutLoop-
10)+((OutLoop-10)*2):OutLoop-(OutLoop-10)+((OutLoop-10)*2)+1) // 'Chi' //
Numbers(OutLoop2-(OutLoop2-10)+((OutLoop2-10)*2):OutLoop2-(OutLoop2-
10)+((OutLoop2-10)*2)+1) // '.txt'
        Endif
Endif

OPEN(2,FILE=OutName)

OutValue = 'Coex='
Write (2,30) OutValue, Coex
OutValue = 'Set='
```

```
Write (2,30) OutValue, Set
OutValue = 'Chi='
Write (2,50) OutValue, Chi
OutValue = 'ChiCoex1='
Write (2,50) OutValue, ChiCoex1
OutValue = 'ChiCoex2='
Write (2,50) OutValue, ChiCoex2
OutValue = 'D='
Write (2,50) OutValue, D
OutValue = 'N='
Write (2,50) OutValue, N
OutValue = 'Mu1='
Write (2,50) OutValue, Mu1
OutValue = 'g='
Write (2,50) OutValue, g
OutValue = 'a='
Write (2,50) OutValue, a
OutValue = 'DPhi='
Write (2,50) OutValue, DPhi
OutValue = 'ChemPot='
Write (2,50) OutValue, ChemPot
OutValue = 'NumPts='
Write (2,30) OutValue, NumPts



DO I=1,NLoops-1
        WRITE(2,10) OutGCent(i), SurfI(i)*DeltaPhi, NuCenter(i), SurfSumZ(i)
END DO

10      Format (1X, ES15.8, 1X, ES15.8, 1X, ES15.8, 1X, ES15.8)
30  Format (1X, A15, 1X, I10)
50  Format (1X, A15, 1X, ES15.8)

close(2)

NumConv=0

Do i=1,20
        MNuCent(i)=1000
End Do
```

```
Do RootLoop=1,PhiFnd

        DeltaLim = .0001
        TempNum=0
        NLoops=40
        Do Loop=1,NLoops


                If (((PhiEst(RootLoop)-.002)+Dble(DeltaLim*(Loop-1))-
.005).gt.ChiCoex1) then
                        LowLim=(PhiEst(RootLoop)-
.002)+Dble(DeltaLim*(Loop-1))-.005
                Else
                        LowLim = ChiCoex1
                Endif

                If (((PhiEst(RootLoop)-
.002)+Dble(DeltaLim*(Loop))+.005).lt.ChiCoex2) then
                        UpLim=(PhiEst(RootLoop)-
.002)+Dble(DeltaLim*(Loop))+.005
                Else
                        UpLim = ChiCoex2
                Endif

                Guess=LowLim+(UpLim-LowLim)/2



                MinNu =
Brent2(LowLim,Guess,UpLim,D,NumPts,DeltaPhi,N,ChiN,Coex,g,Mu1,ChemPo
t,PhiB,PhiCent,FB,GPhi,Kappa,SumZ,PSurfI,PNuCent)

                !If (MinNU.Lt.1) Then
                        TempNum=TempNum+1
                        TempConc(TempNum)=PhiCent
                        TempMNu(TempNum)=MinNu
                !End If

        End Do

        NumConv=NumConv+1
```

```
        Do i=1,TempNum
                If (TempMNu(i).Lt.MNuCent(NumConv)) Then
                        ConPCent(NumConv)=TempConc(i)
                        MNuCent(NumConv)=TempMNu(i)
                Endif
        End Do



End Do

Do Count=1,NumConv

        PhiCent = ConPCent(Count)

        Call
PhiZCalc(D,NumPts,DeltaPhi,N,ChiN,ChemPot,PhiB,PhiCent,FB,GPhi,Kappa,Z,
Conc,Count,NZPts,SurfConc)

End Do



Do j=1,NumConv

        If (OutLoop2.lt.10) Then
                If (OutLoop.Lt.10) Then
                        OutName='DCurEta' // Numbers(OutLoop:OutLoop) //
'Chi' // Numbers(OutLoop2:OutLoop2) // 'Conv' // Numbers(j:j) // '.txt'
                Else
                        OutName='DCurEta' // Numbers(OutLoop-(OutLoop-
10)+((OutLoop-10)*2):OutLoop-(OutLoop-10)+((OutLoop-10)*2)+1) // 'Chi' //
Numbers(OutLoop2:OutLoop2) // 'Conv' // Numbers(j:j) // '.txt'
                Endif
        Else
                If (OutLoop.Lt.10) Then
                        OutName='DCurEta' // Numbers(OutLoop:Out Loop) //
'Chi' // Numbers(OutLoop2-(OutLoop2-10)+((OutLoop2-10)*2):OutLoop2-
(OutLoop2-10)+((OutLoop2-10)*2)+1) // 'Conv' // Numbers(j:j) // '.txt'
                Else
```

```
                    OutName='DCurEta' // Numbers(OutLoop-(OutLoop-
10)+((OutLoop-10)*2):OutLoop-(OutLoop-10)+((OutLoop-10)*2)+1) // 'Chi' //
Numbers(OutLoop2-(OutLoop2-10)+((OutLoop2-10)*2):OutLoop2-(OutLoop2-
10)+((OutLoop2-10)*2)+1) // 'Conv' // Numbers(j:j) // '.txt'
                Endif
        Endif

        OPEN(2,FILE=OutName )

        OutValue = 'Coex='
        Write (2,30) OutValue, Coex
        OutValue = 'Set='
        Write (2,30) OutValue, Set
        OutValue = 'Chi='
        Write (2,50) OutValue, Chi
        OutValue = 'ChiCoex1='
        Write (2,50) OutValue, ChiCoex1
        OutValue = 'ChiCoex2='
        Write (2,50) OutValue, ChiCoex2
        OutValue = 'D='
        Write (2,50) OutValue, D
        OutValue = 'N='
        Write (2,50) OutValue, N
        OutValue = 'Mu1='
        Write (2,50) OutValue, Mu1
        OutValue = 'g='
        Write (2,50) OutValue, g
        OutValue = 'a='
        Write (2,50) OutValue, a
        OutValue = 'DPhi='
        Write (2,50) OutValue, DPhi
        OutValue = 'ChemPot='
        Write (2,50) OutValue, ChemPot
        OutValue = 'NumPts='
        Write (2,30) OutValue, NumPts



        DO I=1,NZPts(j),20
                WRITE(2,20) Z(j,i),Conc(j,i)
        END DO
```

```
        close(2)

End Do

20      Format (1X, ES15.8, 1X, ES15.8)

If (NumConv.Gt.MNumConv) Then
        MNumConv=NumConv
Endif

Do j=1,NumConv

DeltaF(j) = 0
AvePhi(j) = 0

        DO I=2,NZPts(j)

                If ((Z(j,i)-Z(j,i-1)).Ne.0) Then
                        FTemp=((Conc(j,i)/N*dlog(Conc(j,i))+(1-
Conc(j,i))/N*dlog(1-Conc(j,i)))+(ChiN*Conc(j,i)*(1-Conc(j,i))))-
ChemPot*Conc(j,i)
                        KapTemp=(a**2)/(36*dble(Conc(j,i))*(1-Conc(j,i)))

                        DeltaF(j)=DeltaF(j)+(1/a)*(FTemp+KapTemp*(((Conc(j,i)
                -Conc(j,i-1))/(Z(j,i)-Z(j,i-1)))**2))*(Z(j,i)-Z(j,i-1))
                        AvePhi(j)=AvePhi(j)+(2/D)*(Conc(j,i))*(Z(j,i)-Z(j,i-1))
                Endif

        END DO

        DeltaF(j)=2*DeltaF(j)-2*(SurfConc(j)*Mu1+.5*g*SurfConc(j)**2)
        FDeltaF(OutLoop,j)=DeltaF(j)
        FConCent(OutLoop,j)=ConPCent(j)
        FSurfCon(OutLoop,j)=SurfConc(j)
        FAvePhi(OutLoop,j)=AvePhi(j)



End Do


FNumConv(OutLoop)=NumConv
```

```
FDPhi(OutLoop)=DPhi

!If (OutLoop.Lt.10) Then
!       OutName='DeltaF' // Numbers(OutLoop:OutLoop)  // '.txt'
!Else
!       OutName='DeltaF' // Numbers(OutLoop-(OutLoop-10)+((OutLoop-
10)*2):OutLoop-(OutLoop-10)+((OutLoop-10)*2)+1)  // '.txt'
!Endif

Do i=1,MNumConv

        If (OutLoop2.Lt.10) Then
                If (i.lt.10.then)
                        OutName= 'DeltaF' // Numbers(i:i) // 'Chi' //
Numbers(OutLoop2:OutLoop2) // '.txt'
                Else
                        OutName= 'DeltaF' // Numbers(i-(i-10)+((i-10)*2):i-(i-
10)+((i-10)*2)+1) // 'Chi' // Numbers(OutLoop2:OutLoop2) // '.txt'
                Endif
        Else
                If (i.lt.10.then)
                        OutName= 'DeltaF' // Numbers(i:i) // 'Chi' //
Numbers(OutLoop2-(OutLoop2-10)+((OutLoop2-10)*2):OutLoop2-(OutLoop2-
10)+((OutLoop2-10)*2)+1) // '.txt'
                Else
                        OutName= 'DeltaF' // Numbers(i-(i-10)+((i-10)*2):i-(i-
10)+((i-10)*2)+1) // 'Chi' // Numbers(OutLoop2-(OutLoop2-10)+((OutLoop2-
10)*2):OutLoop2-(OutLoop2-10)+((OutLoop2-10)*2)+1) // '.txt'
                Endif
        Endif


        OPEN(2,FILE=OutName )

        OutValue = 'Coex='
        Write (2,30) OutValue, Coex
        OutValue = 'Set='
        Write (2,30) OutValue, Set
        OutValue = 'Chi='
        Write (2,50) OutValue, Chi
        OutValue = 'ChiCoex1='
        Write (2,50) OutValue, ChiCoex1
```

```
        OutValue = 'ChiCoex2='
        Write (2,50) OutValue, ChiCoex2
        OutValue = 'D='
        Write (2,50) OutValue, D
        OutValue = 'N='
        Write (2,50) OutValue, N
        OutValue = 'Mu1='
        Write (2,50) OutValue, Mu1
        OutValue = 'g='
        Write (2,50) OutValue, g
        OutValue = 'a='
        Write (2,50) OutValue, a
        !OutValue = 'DPhi='
        !Write (2,50) OutValue, DPhi
        OutValue = 'ChemPot='
        Write (2,50) OutValue, ChemPot
        OutValue = 'NumPts='
        Write (2,30) OutValue, NumPts



        DO j=1,OutLoop
                WRITE(2,40) FDPhi(j), FConCent(j,i), FSurfCon(j,i),
FAvePhi(j,i), FDeltaF(j,i)
        END DO

        close(2)

40      Format (1X, ES15.8, 1X , ES15.8, 1X , ES15.8, 1X , ES15.8, 1X ,
ES15.8)

End Do

End Do

End Do

End
```

```
Subroutine
PhiZCalc(D,NumPts,DeltaPhi,N,ChiN,ChemPot,PhiB,PhiCent,FB,GPhi,Kappa,Z,
Conc,Count,NZPts,SurfConc)

Double Precision N, ChiN, ChemPot, PhiB, PhiCent, GPhi(100000),
Kappa(100000)
Double Precision FCenter, GCenter, FB, DeltaPhi
Double Precision D, ZTemp(100000), Z(40,100000), SurfConc(40),
Conc(40,100000)
Integer Center, NumPts, Dir, StopVal, i, NumInt, j, t, Count
Integer NZPts(40)

Center=Int(NumPts*PhiCent)
FCenter=((PhiCent/N*dlog(PhiCent)+(1-PhiCent)/N*dlog(1-
PhiCent))+(ChiN*PhiCent*(1-PhiCent)))
GCenter=(FCenter-FB+(ChemPot*(PhiB-PhiCent)))

If ((GPhi(Center-500)-GCenter).gt.0) then
        Dir=-1
Else
        Dir=1
Endif

Do i = 1,100000
        ZTemp(i) = 0
End Do

SumZ=0
StopVal=0
i=Center

Do While (StopVal.eq.0)

        i=i+Dir

        If ((Kappa(i)/(GPhi(i)-GCenter)).gt.0) Then
                ZTemp(i)=ZTemp(i-Dir)+(dsqrt(Kappa(i)/(GPhi(i)-GCenter)))
        Endif
```

```
        If (ZTemp(i).gt.(D/2)/DeltaPhi) StopVal = 1
        If ((i.eq.1).or.(i.eq.(NumPts-1))) StopVal = 1
        If (GPhi(i+Dir)*10000-GCenter*10000.lt.1e-10) Then
                StopVal = 1
        Endif

End Do

SurfConc(Count)=i*DeltaPhi

If (ZTemp(i).lt.(D/2)/DeltaPhi) then
        NumInt=Int(D/2-((ZTemp(i)*DeltaPhi)))*10

        Do j = 0,NumInt
                Z(Count,j+1)=j*.1
                Conc(Count,j+1)=PhiCent
        End Do

        t=NumInt+1

        If (Dir.eq.1) then
                Do j = Center+1,i
                        t=t+1
                        Z(Count,t)=Ztemp(j)*DeltaPhi+((ZTemp(i)*DeltaPhi)-D/2)
                                Conc(Count,t)=j*DeltaPhi
                End Do
        Else
                Do j = Center-1,i,-1
                        t=t+1
                        Z(Count,t)=Ztemp(j)*DeltaPhi+((ZTemp(i)*DeltaPhi)-D/2)
                                Conc(Count,t)=j*DeltaPhi
                End Do
        Endif

Else
        t=1
        Z(Count,t)=0
        Conc(Count,t)=PhiCent
        NumInt=0
        If (Dir.eq.1) then
                Do j = Center+1,i
                        t=t+1
```

```
                    Z(Count,t)=Ztemp(j)*DeltaPhi
                    Conc(Count,t)=j*DeltaPhi
                End Do
        Else
                Do j = Center-1,i,-1
                    t=t+1
                    Z(Count,t)=Ztemp(j)*DeltaPhi
                    Conc(Count,t)=j*DeltaPhi
                End Do
        Endif
Endif

If (Dir.eq.1) then
        NZPts(Count)=NumInt+(i-Center)
Else
        NZPts(Count)=NumInt+(Center-i)
Endif

Return

End


Subroutine
NuCalc(D,NumPts,DeltaPhi,N,ChiN,Coex,g,ChemPot,PhiB,PhiCent,FB,GPhi,Ka
ppa,PSumZ,PSurfI,PNuCent)

Double Precision N, ChiN, ChemPot, PhiB, PhiCent, GPhi(100000),
Kappa(100000)
Double Precision PSumZ, PNuCent, FCenter, GCenter, FB, SumZ, DeltaPhi
Double Precision g, D
Integer Center, NumPts, Dir, StopVal, i, PSurfI, Coex

Center=Int(NumPts*PhiCent)

FCenter=((PhiCent/N*dlog(PhiCent)+(1-PhiCent)/N*dlog(1-
PhiCent))+(ChiN*PhiCent*(1-PhiCent)))
GCenter=(FCenter-FB+(ChemPot*(PhiB-PhiCent)))

If ((GPhi(Center-500)-GCenter).gt.0) then
        Dir=-1
Else
```

```
        Dir=1
Endif

SumZ=0
StopVal=0
i=Center

Do While (StopVal.eq.0)

        i=i+Dir

        If ((Kappa(i)/(GPhi(i)-GCenter)).gt.0) Then
                SumZ=SumZ+(dsqrt(Kappa(i)/(GPhi(i)-GCenter)))
        Endif

        If (SumZ.gt.(D/2)/DeltaPhi) StopVal = 1
        If ((i.eq.1).or.(i.eq.(NumPts-1))) StopVal = 1
        If (GPhi(i+Dir)*10000-GCenter*10000.lt.1e-10) Then
                StopVal = 1
        Endif

End Do


If (SumZ/DeltaPhi.gt.1) Then
        PSurfI=i
        PSumZ=SumZ
        FSurf=(((dble(PSurfI)*DeltaPhi)/N*dlog((dble(PSurfI)*DeltaPhi))+(1-
(dble(PSurfI)*DeltaPhi))/N*dlog(1-
(dble(PSurfI)*DeltaPhi)))+(ChiN*(dble(PSurfI)*DeltaPhi)*(1-
(dble(PSurfI)*DeltaPhi))))
        GSurf=(FSurf-FB+(ChemPot*(PhiB-(dble(PSurfI)*DeltaPhi))))

        !If ((Coex.Eq.1).And.(Kappa(i)*(GSurf-GCenter).gt.1e-9)) Then
        If ((Coex.Eq.1).And.(Kappa(i)*(GSurf-GCenter).gt.0)) Then
                PNuCent=-(g*dble(PSurfI)*DeltaPhi)-
2*(dsqrt((Kappa(PSurfI))*(GSurf-GCenter)))
        Elseif (Kappa(i)*(GSurf-GCenter).gt.0) then
                PNuCent=-(g*dble(PSurfI)*DeltaPhi)-
2*(dsqrt((Kappa(PSurfI))*(GSurf-GCenter)))
        EndIf
```

```
Endif

Return

End


Double Precision Function BulkF(Conc,ChiN,N)

Double Precision Conc,ChiN,N

BulkF=((Conc/N*dlog(Conc)+(1-Conc)/N*dlog(1-Conc))+(ChiN*Conc*(1-
Conc)))*100

Return

End Function

Double Precision Function MuValue(Conc,ChiN,N,ChemPot)

Double Precision Conc,ChiN,N,ChemPot

MuValue=(((((dlog(Conc))/N)-((dlog(1-Conc))/N)+ChiN*(1-Conc)-ChiN*Conc)-
ChemPot)**2)*1

Return

End Function


Double Precision Function
NuDelta(D,NumPts,DeltaPhi,N,ChiN,Coex,g,Mu1,ChemPot,PhiB,PhiCent,FB,G
Phi,Kappa,SumZ,PSurfI,PNuCent)

Double Precision N, ChiN, ChemPot, PhiB, PhiCent, GPhi(100000),
Kappa(100000)
Double Precision PNuCent, FB, SumZ, DeltaPhi
Double Precision g, D, Mu1
Integer Coex, PSurfI
```

```
Call
NuCalc(D,NumPts,DeltaPhi,N,ChiN,Coex,g,ChemPot,PhiB,PhiCent,FB,GPhi,Ka
ppa,SumZ,PSurfI,PNuCent)

NuDelta = ((Mu1-PNuCent)**2)*1000

Return

End Function


Double Precision Function Brent(ax,bx,cx,xmin,N,ChiN,ChemPot,Select)
!xmin is the x location of the min found
!This function is copied from the "Numeral Recipt Fortran", please read the book
for documantation

INTEGER ITMAX, iter, Select
Double Precision ax,bx,cx,tol,xmin,CGOLD,ZEPS, N, ChiN, BulkF
Double Precision MuValue, ChemPot
Double Precision a,b,d,e,etemp,fu,fv,fw,fx,p,q,r,tol1,tol2,u,v,w,x,xm
PARAMETER (CGOLD=.3819660,ZEPS=1.0e-10)


tol = .0001  ! tol is the accuracy range, this value should be large than
sqrt(min(Real(8)))
ITMAX = 10000
iter=0
a=min(ax,cx)
b=max(ax,cx)
v=bx
w=v
x=v
e=0
u=0

if (Select.eq.1) then
        fx=BulkF(x,ChiN,N)
else
        fx=MuValue(x,ChiN,N,ChemPot)
endif
```

```
fv=fx
fw=fx
do 11 iter=1,ITMAX
      xm=0.5*(a+b)
      tol1=tol*abs(x)+ZEPS
      tol2=2.*tol1
      if(abs(x-xm).le.(tol2-.5*(b-a))) goto 3

      if(abs(e).gt.tol1) then
         r=(x-w)*(fx-fv)
         q=(x-v)*(fx-fw)
         p=(x-v)*q-(x-w)*r
         q=2.*(q-r)
         if(q.gt.0.) p=-p
         q=abs(q)
         etemp=e
         e=d
      else
         if(abs(p).ge.abs(.5*q*etemp).or.p.le.q*(a-x).or.p.ge.q*(b-x)) goto 1
         d=p/q
         u=x+d
         if(u-a.lt.tol2 .or. b-u.lt.tol2) d=sign(tol1,xm-x)
         goto 2
      endif
1      if(x.ge.xm) then
         e=a-x
      else
         e=b-x
      endif
      d=CGOLD*e
2      if(abs(d).ge.tol1) then
        u=x+d
      else
        u=x+sign(tol1,d)
      endif

      if (Select.eq.1) then
         fu=BulkF(u,ChiN,N)
      else
         fu=MuValue(u,ChiN,N,ChemPot)
     endif
```

```
      if(fu.le.fx) then
        if(u.ge.x) then
          a=x
        else
          b=x
        endif
        v=w
        fv=fw
        w=x
        fw=fx
        x=u
        fx=fu
      else
        if(u.lt.x) then
          a=u
        else
          b=u
        endif
        if(fu.le.fw .or. w.eq.x) then
          v=w
          fv=fw
          w=u

          fw=fu
        else if(fu.le.fv .or. v.eq.x .or. v.eq.w) then
          v=u
          fv=fu
        endif
      endif
11    continue
      pause 'Brent exceed maximum iterations'
3     xmin=x
      Brent=fx

   Return


   End Function

Double Precision Function
Brent2(ax,bx,cx,Thick,NumPts,DeltaPhi,N,ChiN,Coex,g,Mu1,ChemPot,PhiB,Phi
Cent,FB,GPhi,Kappa,SumZ,PSurfI,PNuCent)
```

```
!xmin is the x location of the min found
!This function is copied from the "Numeral Recipt Fortran", please read the book
for documantation

INTEGER ITMAX, iter
Double Precision ax,bx,cx,tol,CGOLD,ZEPS
Double Precision a,b,d,e,etemp,fu,fv,fw,fx,p,q,r,tol1,tol2,u,v,w,x,xm
Double Precision N, ChiN, ChemPot, PhiB, PhiCent, GPhi(100000),
Kappa(100000)
Double Precision PNuCent, FB, SumZ, DeltaPhi
Double Precision g, Thick, Mu1, NuDelta
Integer NumPts, PSurfI,Coex
PARAMETER (CGOLD=.3819660,ZEPS=1.0e-13)


tol = 1e-14  ! tol is the accuracy range, this value should be large than
sqrt(min(Real(8)))
ITMAX = 100
iter=0
a=min(ax,cx)
b=max(ax,cx)
v=bx
w=v
x=v
e=0
u=0


fx=NuDelta(Thick,NumPts,DeltaPhi,N,ChiN,Coex,g,Mu1,ChemPot,PhiB,x,FB,G
Phi,Kappa,SumZ,PSurfI,PNuCent)


fv=fx
fw=fx
do 11 iter=1,ITMAX
      xm=0.5*(a+b)
      tol1=tol*abs(x)+ZEPS
      tol2=2.*tol1
      if(abs(x-xm).le.(tol2-.5*(b-a))) goto 3

      if(abs(e).gt.tol1) then
        r=(x-w)*(fx-fv)
```

```
        q=(x-v)*(fx-fw)
        p=(x-v)*q-(x-w)*r
        q=2.*(q-r)
        if(q.gt.0.) p=-p
        q=abs(q)
        etemp=e
        e=d
      else
         if(abs(p).ge.abs(.5*q*etemp).or.p.le.q*(a-x).or.p.ge.q*(b-x)) goto 1
        d=p/q
        u=x+d
        if(u-a.lt.tol2 .or. b-u.lt.tol2) d=sign(tol1,xm-x)
        goto 2
      endif
1     if(x.ge.xm) then
        e=a-x
      else
        e=b-x
      endif
      d=CGOLD*e
2     if(abs(d).ge.tol1) then

        u=x+d
      else
        u=x+sign(tol1,d)
      endif

          fu=NuDelta(Thick,NumPts,DeltaPhi,N,ChiN,Coex,g,Mu1,ChemPot,PhiB,
u,FB,GPhi,Kappa,SumZ,PSurfI,PNuCent)

      if(fu.le.fx) then
        if(u.ge.x) then
          a=x
        else
          b=x
        endif
        v=w
        fv=fw
        w=x
        fw=fx
        x=u
        fx=fu
```

```
      else
        if(u.lt.x) then
          a=u
        else
          b=u
        endif
        if(fu.le.fw .or. w.eq.x) then
          v=w
          fv=fw
          w=u

          fw=fu
        else if(fu.le.fv .or. v.eq.x .or. v.eq.w) then
          v=u
          fv=fu
        endif
      endif
11    continue
      !pause 'Brent exceed maximum iterations'
3     PhiCent=x
      Brent2=fx

    Return


    End Function
```

References

1. Binder, K. (1994). "Phase Transitions in Polymer Blends and Block Copolymer Melts: Some Recent Developments." Advances in Polymer Science **112**: 181-299.
2. Binder, K. (1995). "Surface effects on polymer blends and block copolymer melts: theoretical concepts of surface enrichment, surface induced phase separation and ordering." Acta Polym. **46**(3): 204-25.
3. Binder, K. (1999). "Phase Transitions of Polymer Blends and Block Copolymer Melts in Thin Films." Avances in Polymer Science **138**: 1-89.
4. Binder, K., R. Evans, et al. (1996). "Interface localization transition in Ising films with competing walls: Ginzburg criterion and crossover scaling." Phys. Rev. E: Stat. Phys., Plasmas, Fluids, Relat. Interdiscip. Top. **53**(5-B): 5023-5034.
5. Binder, K., D. P. Landau, et al. (1995). "Thin Ising films with competing walls: A Monte Carlo study." Phys. Rev. E: Stat. Phys., Plasmas, Fluids, Relat. Interdiscip. Top. **51**(4-A): 2823-38.
6. Binder, K., M. Muller, et al. (2001). "Symmetric binary polymer blends confined in thin films between competing walls: Interplay between finite size and wetting behavior." Physical Chemistry Chemical Physics **3**(7): 1160-1168.

7. Binder, K., P. Nielaba, et al. (1997). "Phase coexistence in binary mixtures in thin films with symmetric walls: model calculations for two- and three-dimensional Ising lattices." Z. Phys. B: Condens. Matter **104**(1): 81-98.

8. Boltau, M., S. Walheim, et al. (1998). "Surface-induced structure formation of polymer blends on patterned substrates." Nature (London) **391**(6670): 877-879.

9. Brazhnik, P. K., K. F. Freed, et al. (1994). "Polymer melt near a solid wall." J. Chem. Phys. **101**(10): 9143-54.

10. Budkowski, A., F. Scheffold, et al. (1997). "Surface phase behavior in binary polymer mixtures. III. Temperature dependence of surface enrichment and of wetting." J. Chem. Phys. **106**(2): 719-727.

11. Budkowski, A., U. Steiner, et al. (1992). "The effects of confinement and surface interactions on coexistence in a binary polymer mixture." J. Chem. Phys. **97**(7): 5229-38.

12. Cahn, J. W. (1977). "Critical point wetting." J. Chem. Phys. **66**(8): 3667-72.

13. Cherrabi, R., A. Saout-Elhak, et al. (2000). "Phase separation of polymer blends in solution near adsorbing surface." European Physical Journal E: Soft Matter **2**(1): 91-101.

14. Cherrabi, R., A. Saout-Elhak, et al. (1999). "Phase separation in confined polymer blends." Journal of Chemical Physics **111**(17): 8174-8181.

15. Cohen, S. M. and M. Muthukumar (1989). "Critical wetting in two-component polymer blends." J. Chem. Phys. **90**(10): 5749-55.

16. Cserhati, C., I. A. Szabo, et al. (1998). “Segregation and phase separation in thin films.” Nanostructured Materials **10**(2): 195-204.

17. De Gennes, P. G. (1985). “Wetting: statics and dynamics.” Rev. Mod. Phys. **57**(3, Pt. 1): 827-63.

18. Donley, J. P. and G. H. Fredrickson (1995). “Influence of conformational asymmetry on the surface enrichment of polymer blends. II.” J. Polym. Sci., Part B: Polym. Phys. **33**(9): 1343-51.

19. Flebbe, T., B. Duenweg, et al. (1996). “Phase separation versus wetting: a mean field theory for symmetrical polymer mixtures confined between selectively attractive walls.” J. Phys. II (France) **6**(5): 667-695.

20. Flory, P. J. (1941). J. Chem. Phys. **9**: 660.

21. Fowler, M. E., J. W. Barlow, et al. (1987). “Effect of copolymer composition on the miscibility of blends of styrene-acrylonitrile copolymers with poly(methyl methacrylate).” Polymer **28**(7): 1177-84.

22. Fredrickson, G. H. and J. P. Donley (1992). “Influence of broken conformational symmetry on the surface enrichment of polymer blends.” J. Chem. Phys. **97**(12): 8941-6.

23. Genzer, J. and R. J. Composto (1997). “A self-consistent field study of the wetting transition in binary polymer blends.” J. Chem. Phys. **106**(3): 1257-1263.

24. Genzer, J. and R. J. Composto (1997). “Surface segregation amplification in miscible polymer blends near criticality.” Europhys. Lett. **38**(3): 171-176.

25. Glockner, G. (1979). “On the Behaviour of Styrene-Acrylonitrile Copolymer in Solution - VI.” European Polymer Journal **15**: 727-732.

26. Gutmann, J. S., P. Muller-Buschbaum, et al. (1999). “Influence of the blend compatibility on the morphology of thin polymer blend films.” J. Macromol. Sci., Phys. **B38**(5 & 6): 563-576.

27. Hariharan, A., S. K. Kumar, et al. (1993). “The effect of finite film thickness on the surface segregation in symmetric binary polymer mixtures.” J. Chem. Phys. **99**(1): 656-63.

28. Helfand, E. and Y. Tagami (1971). J. Chem. Phys. **56**: 3592.

29. Higashida, N., J. Kressler, et al. (1995). “Lower critical solution temperature and upper critical solution temperature phase behavior in random copolymer blends: poly(styrene-co-acrylonitrile)/poly(methyl methacrylate) and poly(styrene-co-acrylonitrile)/poly(.epsilon.-caprolactone).” Polymer **36**(14): 2761-4.

30. Huggins, M. L. (1941). J. Chem. Phys **9**: 440.

31. Hunter, R. J. (2001). Foundations of Colloid Science, Oxford University Press.

32. Israelachvili, J. N. (1991). Intermolecular and surface forces, London: Academic Press.

33. Joanny, J. F. and L. Leibler (1978). J. Phys. (Paris) **39**: 951.

34. Jones, R. A. L. (1993). “Effect of long-range forces on surface enrichment in polymer blends.” Physical Review E **47**(2): 1437-1440.

35. Jones, R. A. L., E. J. Kramer, et al. (1989). “Surface enrichment in an isotopic polymer blend.” Phys. Rev. Lett. **62**(3): 280-3.

36. Jones, R. A. L., E. J. Kramer, et al. (1989). “Surface enrichment in polymer blends: simple theory and an experimental test.” Mater. Res. Soc. Symp. Proc. **153**(Interfaces Polym., Met., Ceram.): 133-41.

37. Jones, R. A. L., L. J. Norton, et al. (1991). “Surface-directed spinodal decomposition.” Phys. Rev. Lett. **66**(10): 1326-9.

38. Jones, R. A. L., L. J. Norton, et al. (1990). “The form of the enriched surface layer in polymer blends.” Europhys. Lett. **12**(1): 41-6.

39. Karim, A., T. M. Slawecki, et al. (1998). “Phase-separation-induced surface patterns in thin polymer blend films.” Macromolecules **31**(3): 857-862.

40. Krausch, G., C. A. Dai, et al. (1993). “Interference of spinodal waves in thin polymer films.” Macromolecules **26**(21): 5566-71.

41. Lacombe, R. H. and I. C. Sanchez (1976). “Statistical thermodynamics of fluid mixtures.” J. Phys. Chem. **80**(23): 2568-80.

42. Lee, W.-K., J.-H. Ryou, et al. (1998). Surface mixing morphology in bilayer-polymer films. Polymer Testing. **17:** 167-177.

43. Masson, J. L. and P. F. Green (2000). “Pattern Formation in a Thin Random Copolymer Film: Evolution of an Intermediate Morphology.” Journal of Chemical Physics **112**: 349.

44. Masson, J. L. and P. F. Green (2002). “Hole Formation in Thin Films: A two stage process.” Phys Rev. Lett. **88**: 205504.

45. Masson, J.-L., O. Olufokunbi, et al. (2002). “Flow instabilities in entangled polymer thin films.” Macromolecules **35**: 6992.

46. Muller, M., K. Binder, et al. (2000). “Finite size effects on the phase diagram of a binary mixture confined between competing walls.” Los Alamos National Laboratory, Preprint Archive, Condensed Matter: 1-6, arXiv:cond-mat/0005060.

47. Muller, M., K. Binder, et al. (2000). “Non-monotonous crossover between capillary condensation and interface localisation/delocalisation transition in binary polymer blends.” Europhysics Letters **50**(6): 724-730.

48. Muller, M., K. Binder, et al. (2001). “Phase diagram of polymer blends in confined geometry.” Journal of Molecular Liquids **92**(1-2): 41-52.

49. Muller, M., K. Binder, et al. (2001). “Phase equilibria in thin polymer films.” International Journal of Modern Physics B **15**(13): 1867-1903.

50. Muller, M., L. G. MacDowell, et al. (2001). “Nano-dewetting: Interplay between van der Waals- and short-ranged interactions.” Journal of Chemical Physics **115**(21): 9960-9969.

51. Muller-Buschbaum, P. and M. Stamm (2001). “Film thickness dependence of the domain size in weakly incompatible thin polymer blend films.” Colloid and Polymer Science **279**(4): 376-381.

52. Newby, B.-m. Z. and R. J. Composto (2000). “Influence of Lateral Confinement on Phase Separation in Thin Film Polymer Blends.” Macromolecules **33**(9): 3274-3282.

53. Pandit, R., M. Schick, et al. (1982). “Systematics of multilayer adsorption phenomena on attractive substrates.” Phys. Rev. B: Condens. Matter **26**(9): 5112-40.

54. Pandit, R. and M. Wortis (1982). “Surfaces and interfaces of lattice models: Mean-field theory as an area-preserving map.” Physical Review B **25**(5): 3226-3241.

55. Paul, D. R. and C. B. Bucknall (2000). Polymer Blends Volume 1: Formulation, John Wiley and Sons, Inc.

56. Reiter, G. (1992). “Dewetting of thin polymer films.” Phys. Rev. Lett. **68**(1): 75-8.

57. Reiter, G., A. Sharma, et al. (1999). “Destabilizing effect of long-range forces in thin liquid films on wettable substrates.” Europhysics Letters **46**(4): 512-518.

58. Reiter, G., A. Sharma, et al. (1999). “Thin Film Instability Induced by Long-Range Forces.” Langmuir **15**(7): 2551-2558.

59. Rouault, Y., J. Baschnagel, et al. (1995). “Phase Separation of Symmetrical Polymer Mixtures in Thin-Film Geometry.” Journal of Statistical Physics **80**(5/6): 1995.

60. Ruzette, A.-V. G. and A. M. Mayes (2001). A Simple Free Energy Model for Weakly Interacting Polymer Blends. Macromolecules. **34:** 1894-1907.

61. Sanchez, I. C. and R. H. Lacombe (1976). “An elementary molecular theory of classical fluids. Pure fluids.” J. Phys. Chem. **80**(21): 2352-62.

62. Saout-Elhak, A., M. Benhamou, et al. (1997). “Phase separation in polymer blends near a surface.” J. Phys. II **7**(3): 503-516.

63. Scheffold, F., A. Budkowski, et al. (1996). “Surface phase behavior in binary polymer mixtures. II. Surface enrichment from polyolefin blends.” J. Chem. Phys. **104**(21): 8795-8806.

64. Scheffold, F., E. Eiser, et al. (1996). “Surface phase behavior in binary polymer mixtures. I. Miscibility, phase coexistence, and interactions in polyolefin blends.” J. Chem. Phys. **104**(21): 8786-8794.

65. Schmidt, I. and K. Binder (1985). “Model calculations for wetting transitions in polymer mixtures.” J. Phys. (Les Ulis, Fr.) **46**(10): 1631-44.

66. Scott, R. L. (1952). J. Polym. Sci. **9**: 423.

67. Seemann, R., S. Herminghaus, et al. (2001). “Dewetting Patterns and Molecular Forces: A Reconciliation.” Physical Review Letters **86**(24): 5534-5537.

68. Seemann, R., S. Herminghaus, et al. (2001). “Gaining control of pattern formation of dewetting liquid films.” Journal of Physics: Condensed Matter **13**(21): 4925-4938.

69. Sharma, A. and R. Khanna (1998). “Pattern Formation in Unstable Thin Liquid Films.” Phys. Rev. Lett. **81**(16): 3463-3466.

70. Slep, D., J. Asselta, et al. (1998). “Phase Separation of Polystyrene and Bromo-Polystyrene Mixtures in Equilibrium Structures in Thin Films.” Langmuir **14**(17): 4860-4864.

71. Steiner, U. and J. Klein (1996). “Growth of wetting layers from liquid mixtures.” Phys. Rev. Lett. **77**(12): 2526-2529.

72. Steiner, U., J. Klein, et al. (1994). “Surface phase inversion in finite-sized binary mixtures.” Phys. Rev. Lett. **72**(10): 1498-501.

73. Suess, M., J. Kressler, et al. (1987). “The miscibility window of poly(methyl methacrylate)/poly(styrene-co-acrylonitrile) blends.” Polymer **28**(6): 957-60.

74. Sung, L., A. Karim, et al. (1996). “Dimensional crossover in the phase separation kinetics of thin polymer blend films.” Phys. Rev. Lett. **76**(23): 4368-4371.

75. Tanaka, K., A. Takahara, et al. (1996). “Film Thickness Dependence of the Surface Structure of Immiscible Polystyrene/Poly(methyl methacrylate) Blends.” Macromolecules **29**(9): 3232-9.

76. Tanaka, K., J.-S. Yoon, et al. (1995). “Ultrathinning-Induced Surface Phase Separation of Polystyrene/Poly(vinyl methyl ether) Blend Film.” Macromolecules **28**(4): 934-8.

77. Tang, H., I. Szleifer, et al. (1994). “Critical temperature shifts in thin polymer blend films.” J. Chem. Phys. **100**(7): 5367-71.

78. Vrij, A. and J. T. G. Overbeek (1968). “Rupture of thin liquid films due to spontaneous fluctuations in thickness.” J. Amer. Chem. Soc. **90**(12): 3074-8.

79. Walheim, S., E. Schaffer, et al. (1999). “Nanophase-separated polymer films as high-performance antireflection coatings.” Science (Washington, D. C.) **283**(5401): 520-522.

80. Wang, H. and R. J. Composto (2000). “Hydrodynamic-flow-driven wetting in thin film polymer blends: Growth kinetics and morphology.” Phys. Rev. E: Stat. Phys., Plasmas, Fluids, Relat. Interdiscip. Top. **61**(2): 1659-1663.

81. Wang, H. and R. J. Composto (2000). “Thin film polymer blends undergoing phase separation and wetting: Identification of early, intermediate, and late stages.” J. Chem. Phys. **113**(22): 10386-10397.

82. Wang, H., R. J. Composto, et al. (2001). “Multiple Lateral Length Scales in Phase-Separating Thin-Film Polymer Blends.” Langmuir **17**(9): 2857-2860.

83. Wyart, B. F. and J. Daillant (1990). “Drying of solids wetted by thin liquid films.” CAN. J. PHYS. **68**: 1084-1088.

84. Zhao, W., X. Zhao, et al. (1991). “Neutron and x-ray reflectivity measurements of polystyrene/poly(bromostyrene) (PS/PBrS) interfaces.” Physica B (Amsterdam) **173**(1-2): 43-6.

85. Zhao, X., W. Zhao, et al. (1991). “Determination of the concentration profile at the surface of deuterated polystyrene/hydrogenated polystyrene blends using high-resolution ion scattering techniques.” Macromolecules **24**(22): 5991-6.

86. Zhu, S., Y. Liu, et al. (1999). “Confinement-induced miscibility in polymer blends.” Nature (London) **400**(6739): 49-51.

Vita

Steven Adam Scheer was born on July 2, 1973, in Passaic, New Jersey. With one brother and one sister, he is the son of Matthew and Diana Scheer. He spent his pre teen years in Sussex county New Jersey, and moved to Kansas City, Missouri at the age of 12. He graduated from Kearney Senior High school in May 1991. In Septemeber 1991, he began school at Northeast Missouri State University. He went to school there for three semesters, and then transferred to the University of Missouri at Rolla. In the summer of 1993, he began a co-op with Monsanto Chemical Company. This co-op lasted the duration of his time at Rolla, he spent three semesters working at the phosphate in Carondelet, MO, and three semesters working at the corporate research facility in Creve Couer, MO. He also spent 3 semesters doing undergraduate research with Dr. Daniel Forciniti. He graduated Summa cum Laude in May 1997 receiving a Bachelor of Science in Chemical Engineering. In September 1997 he entered graduate school at the University of Texas at Austin. In October of 1997 he joined Dr. C. Grant Willson's research group. In August of 2001 he completed his Masters of Science in Engineering. He will be employed in the Advanced Logic group at IBM East Fishkill, New York.

Permanent address: 238 Ridge Road, Milton NY 12547

This dissertation was typed by the author.